Finger-Joints for Laminated Beams

Experimental and Numerical Studies of Mechanical Behaviour

Serrano, Erik

1997

Document Version:
Publisher's PDF, also known as Version of record

LUND UNIVERSITY | LUND INSTITUTE OF TECHNOLOGY
Division of Structural Mechanics | Sweden 1997 | Report TVSM–3021

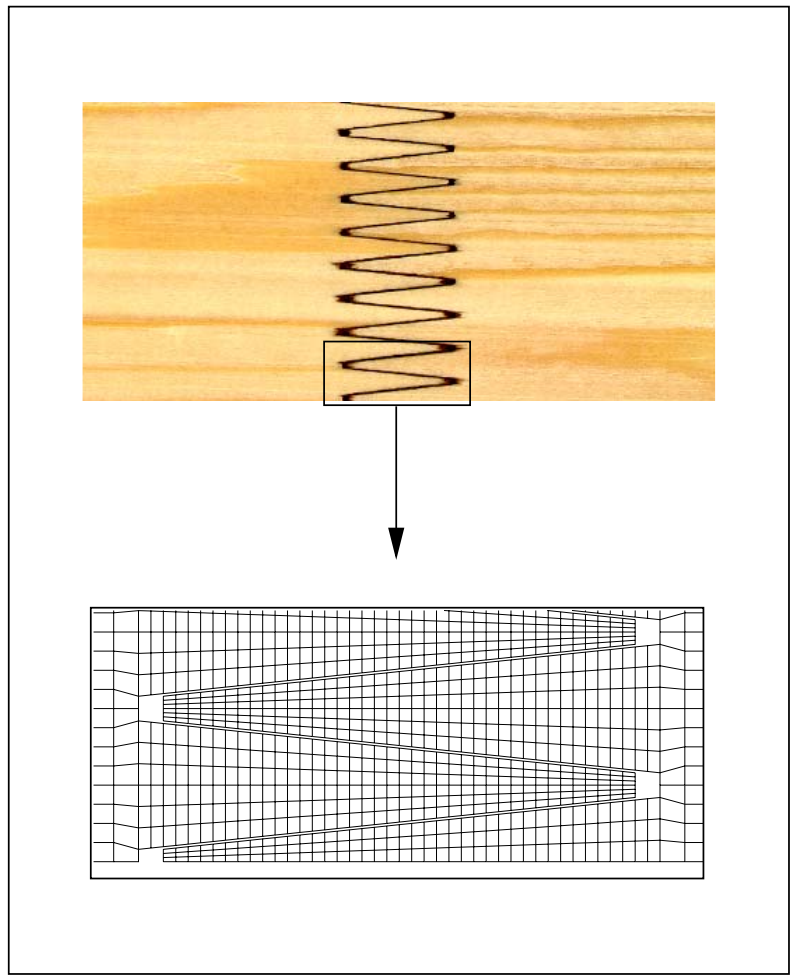

FINGER-JOINTS FOR LAMINATED BEAMS

Experimental and numerical studies of mechanical behaviour

ERIK SERRANO

LUND UNIVERSITY | LUND INSTITUTE OF TECHNOLOGY
Division of Structural Mechanics | Sweden 1997 | Report TVSM-3021
CODEN: LUTVDG / (TVSM-3021) / 1-103 / (1997) | ISSN 0281-6679

FINGER-JOINTS FOR LAMINATED BEAMS
Experimental and numerical studies of mechanical behaviour

ERIK SERRANO

Preface

This licentiate thesis presents results of an ongoing research project at the Division of Structural Mechanics, Lund University. The project, which started in January 1994, has been partly financed by the Swedish Council of Building Research, whose support is gratefully acknowledged.

During the course of my work, I have had the pleasure of being guided through the mysteries of timber engineering, fracture mechanics and finite elements by four highly encouraging supervisors: Adj. Prof. Hans Jørgen Larsen, who initiated the project; Dr. Per Johan Gustafsson, who has been my daily supervisor and introduced me to the area of fracture mechanics; Adj. Prof. Carl-Johan Johansson (Cajo), who has shared with me his experience within the field of timber engineering; and finally Prof. Hans Petersson, former Head of the Division of Structural Mechanics, with his never-ending interest in the modelling of problems related to wood mechanics. All four are highly experienced and internationally esteemed experts within their fields. To have had the opportunity to work with them has been a great honour.

Special thanks to Mr. Bertil Enquist for preparing the test specimens and carrying out the major part of the test programme. Thanks also to Dr. Preben Hoffmeyer, of the Department of Structural Engineering and Materials, Technical University of Denmark, for letting me use the machinery for finger-joint milling.

To all my other colleagues and friends at the Division Structural Mechanics I express my gratitude for their support and companionship. Special thanks are directed as well to Stefan Holmberg for his thorough reading of, and constructive comments on, the manuscript.

Lund, April 1997

Erik Serrano

Abstract

The introduction of laminated timber, glulam being an example, allowed many of the disadvantages associated with solid wood to be overcome. The disadvantages in question are mainly those related to the size and shape limits of structural elements made of solid wood and to the large variability in such material properties of solid wood as strength and stiffness.

In the present thesis, which comprises both experimental and numerical studies, such phenomena like the laminating effect and to some extent the size effect are investigated and discussed using the concept of fracture mechanics.

The experimental part involved the testing of bond line strength, stress vs. deformation and fracture energy of three adhesives (resorcinol-phenol, polyurethane and polyvinylacetate) and tensile testing of finger-jointed laminations. The results from bond line tests were used as input data in a nonlinear fracture mechanics model based on the concept of a fictitious crack. The model was verified by simulating both the bond line tests and the lamination tests. Parameter studies on the influence of bond line characteristics on the strength of finger-joints were also performed, together with analyses of the sensitivity of a finger-joint to defects in the bond line. The influence of finger-jointing pieces of lumber dissimilar in stiffness was also investigated. These parameter studies showed the brittleness of the bond line to be an important parameter in governing the strength of the finger-joint. For brittle resorcinol-phenol adhesive, the approach adopted, one based on nonlinear fracture mechanics, predicted the strength of a finger-jointed lamination to differ considerably from the strength predicted by such classical theories as single point maximum stress theory and perfect elastic-plastic theory. The complete load-displacement response of a finger-joint was determined using a numerical solution procedure that allowed so-called snap-back behaviour to be traced. The behaviour of a laminated beam in bending was also simulated. This showed the laminating effect to partly be explainable on the basis of fracture mechanics.

Keywords: finger-joints, laminated timber, testing, nonlinear fracture mechanics, finite element method, laminating effect.

Notations

Notations are explained where they first appear in the text. For clarity, a list of notations and of the corresponding SI-units is also given here.

Roman letters

$\mathbf{A}$	matrix of strain gauge constants	$[N^{-1}, (Nm)^{-1}]$
A	area	$[m^2]$
Δa	displacement and rotation increments in FE-analyses	$[m, -]$
b	width	$[m]$
COV	coefficient of variation	$[-]$
d	typical size of the structure	$[m]$
E	Young's modulus	$[Pa]$
E_x	Young's modulus in the fibre direction	$[Pa]$
$\mathbf{e}$	vector of strain gauge readings	$[-]$
F_{ult}	ultimate load-bearing capacity	$[N]$
f_f	strength of the material	$[Pa]$
f_m	maximum bending stress	$[Pa]$
f_t	maximum nominal tensile stress in lamination	$[Pa]$
$f_{t,est.}$	estimated maximum nominal stress in lamination according to beam theory	$[Pa]$
G_c	critical energy release rate	$[Nm/m^2]$
G_f	fracture energy	$[Nm/m^2]$
h	height	$[m]$
I	area moment of inertia	$[m^4]$
L	length	$[m]$
l	finger length	$[m]$
l_{ch}	characteristic length	$[m]$
M	bending moment	$[Nm]$
m, n	powers of the strength criteria	$[-]$
N	normal force	$[N]$
ΔP	load increment in FE-analyses	$[N, Nm]$
p	pitch of the finger-joint profile	$[m]$
$\mathbf{q}$	vector of section forces	$[N, Nm]$
R	load-bearing capacity	$[N, Nm]$
$\mathbf{r}$	vector of residuals	$[-]$
s	finger tip gap	$[m]$
T, R, L	tangential, radial and longitudinal direction	$[-]$
w	moisture content	$[-]$

Greek letters

α	ratio of area moments of inertia	$[-]$
β	power in the expression of normalized strength	$[-]$
γ	shape parameter of the stress-slip relationship	$[-]$
δ	displacement	$[m]$
δ_n	normal displacement across the bond line	$[m]$
δ_s	shear displacement across the bond line	$[m]$
δ_h	horizontal displacement parallel to the grain	$[m]$
δ_v	vertical displacement perpendicular to the grain	$[m]$
η	power in the size-effect relationship	$[-]$
ν	Poisson's ratio	$[-]$
ϱ	density	$[kg/m^3]$
σ	normal stress in the bond line	$[Pa]$
σ_{max}	uniaxial normal strength of the adhesive	$[Pa]$
τ	shear stress in the bond line	$[Pa]$
τ_{max}	uniaxial shear strength of the adhesive	$[Pa]$
Φ	vector norm of the residuals	$[-]$
φ	mixed-mode angle	$[-]$
ω	brittleness number	$[-]$

Contents

1. Introduction

1.1 Glued laminated timber and finger-joints

Glued laminated timber (glulam) is often used for large beams in place of solid wood. Glulam is basically what one obtains by glueing several laminations together to produce the cross-section desired. Approximately a hundred years ago, glulam technology was developed in Germany. In Sweden, the production of glulam started in 1919 in Töreboda. Ever since, glulam has played an important role as an alternative to large steel and concrete frameworks. Among its advantages are the high relative strength of the material (strength/density), the ease in working with it and the possibility of choosing almost arbitrary shapes for it, which is very advantageous architecturally. Glulam is a good alternative to concrete and steel for arch and dome structures in particular. The aesthetic value of the naked wooden surface, to be sure, is a matter of taste, yet it is probable that the vast majority of persons find such a surface appealing (Figure 1.1).

Figure 1.1. *Left: With the use of glued laminated timber, spectacular frameworks such as the roofing of this German swimming facility can be produced. Right: Glulam, with its considerable aesthetical value, was chosen for the restoration of this Danish castle (Koldinghus).*

In producing glulam, the lengthwise splicing of the elements, of which the cross-section consists, is of great importance. In the early days of glulam manufacturing, the easiest solution was adopted, that of using so-called butt joints. Later, the overlap or

scarf joint came into use. Today, the glulam industry relies on the finger-joint splicing of laminations (Figure 1.2). The strength of a finger-joint depends on many factors, such as the strength and deformation properties of the adhesive, the strength and stiffness of the surrounding material, and the geometry of the finger-joint. A finger-joint *can*

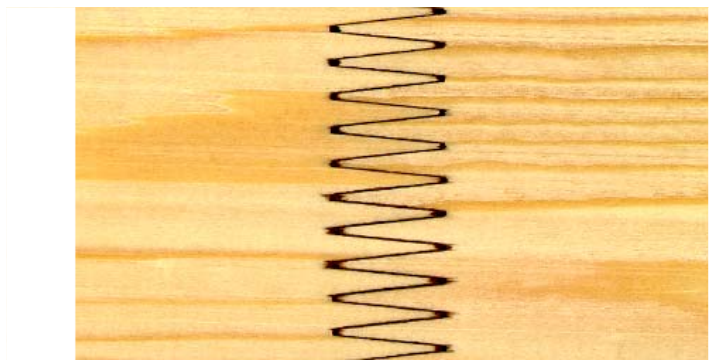

Figure 1.2. *A finger-joint in spruce. Profile I-20 glued with resorcinol.*

represent the weak zone of a lamination, having lesser strength and stiffness than the surrounding material, yet it may also be just as strong as other parts of the lamination containing knots and zones of low density, or even stronger.

Finger-joints are sometimes used to improve the strength of low-quality lumber by being used to replace areas with large knots or other defects. Thus, depending on the quality of the lumber to be finger-jointed, a finger-joint can either reinforce or weaken the lamination.

1.2 Aim of the present work

In this report, work done during the past three years on a research project dealing with laminated wood materials such as glulam is presented. The overall aim of the work here was to contribute to knowledge and methods for the rational modelling, analysis and prediction of the strength of laminated wood materials. In particular the modelling of finger-joints and the influence which finger-joint properties and lamination properties have on the so-called laminating effect were of interest. The strategy was to use the knowledge and experience in the field of experimental and numerical methods for wood adhesive joints inherent in the work of Wernersson [42], based on nonlinear fracture mechanics theory.

The base of the present work can be expressed in terms of the different system levels A-C illustrated in Figure 1.3. The experimental work included the testing of bond lines taken from actual finger-joints and finger-jointed laminations, corresponding to the levels A and B, respectively. Testing bond lines from an actual finger-joint provided the characteristics necessary for numerical simulations. These simulations were verified by testing the finger-jointed laminations. After the numerical model had been verified, it was used to predict the behaviour and specify the characteristics of a finger-jointed lamination, level B. The numerical finger-joint model was also used for parameter studies, including a study of the effect of various defects in the bond line.

Two numerical studies were carried out on glulam beams (corresponding to level C in Figure 1.3) in order to extend knowledge of the laminating effect: a study of the stress distribution in a beam with a small area of low strength and stiffness and a study of the crack propagation along the outermost lamination of a beam. The crack propagation study was performed for various lamination thicknesses.

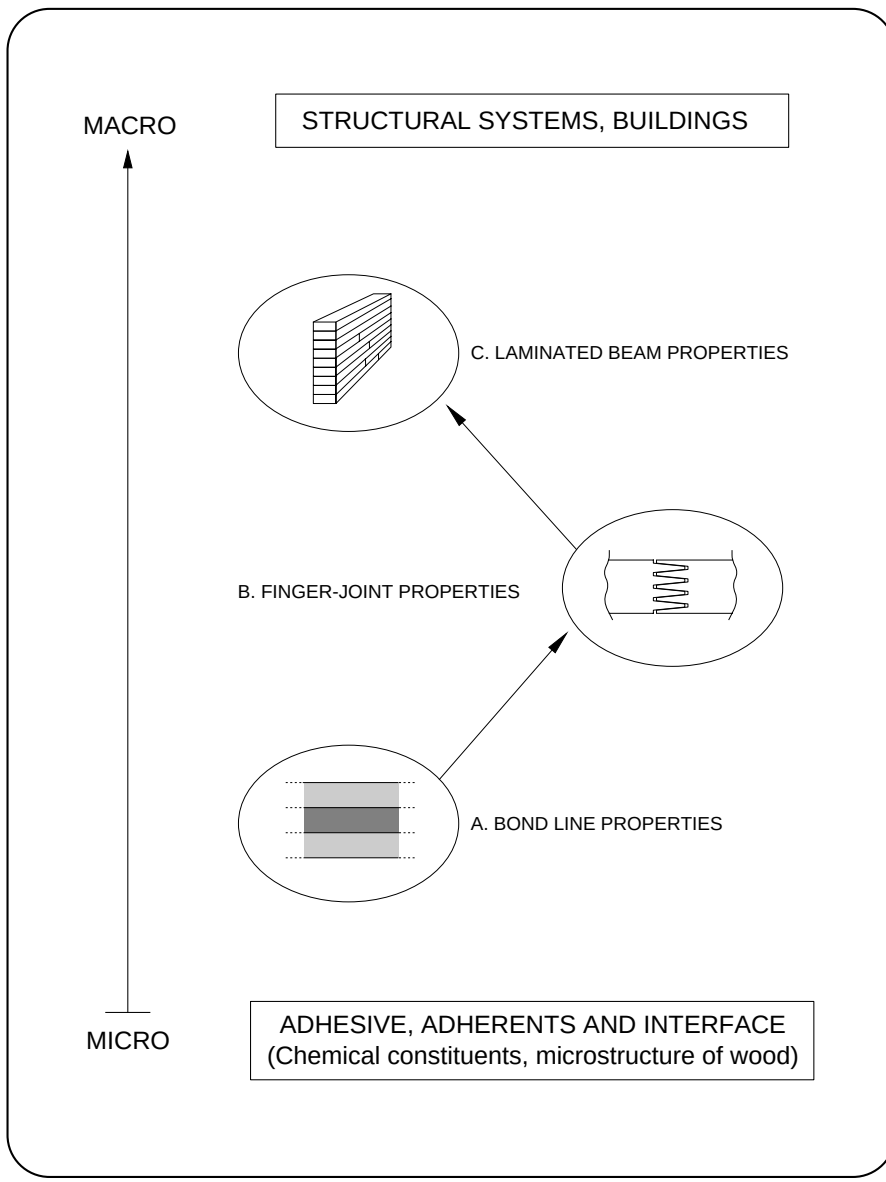

Figure 1.3. *Different system levels. In the present work, the test programme concerned levels A-B, whereas the numerical studies concerned levels A-C.*

1.3 Outline

The report is divided into seven chapters. The work done is presented in the order considered best from the standpoint of presentation. The order is not always the same as that in which the work was done.

Chapter 2 provides an introduction to the area. It includes a brief description of wood, finger-joints and glulam. Various of the phenomena of particular interest in the study are also described, including the laminating effect and the size effect. In addition, a literature survey [35] of tests of glulam strength and of models for calculating glulam strength is referred to and summarized.

Chapter 3 deals with the experimental methods adopted, including sample preparation and test setups, both for the bond line testing and the testing of finger-jointed laminations. The results of these experiments are presented in Chapter 4.

Chapter 5 provides a short introduction to the bond line model used in the present work, a model based on nonlinear fracture mechanics (NLFM), together with an account of the implementation of the model using the finite element method (FEM). The chapter also presents the results of numerical simulations performed in order to verify the bond line model. Verification of the bond line model is based on simulations both of the bond lines tested and of the complete finger-jointed laminations.

Chapter 6 presents a parameter study of the fracture characteristics of a finger-joint. A sensitivity analysis of the influence of bond line defects is included. Simulations of the performance of a laminated beam are reported as well.

Concluding remarks, together with a discussion of future research needs, are presented in Chapter 7.

Certain parts of the work dealt with in this report have been published previously, as a literature review on glulam and finger-joints [35] (in Swedish) and as workshop and conference papers [36, 37, 38].

2. Background and Earlier Work

This chapter presents the background to the present work. The first section contains a brief description of the raw material of interest – wood, followed by certain reflections on today's methods of enhancing the performance of wood through use of wood-based materials. A description of the way of determining the resistance of a structural element as prescribed by the building codes is given at the end of the first section. The second section deals with the product of main interest in this study – glued laminated timber (glulam). A short overview of the production and behaviour of glulam is provided. The phenomena in glulam known as the *laminating effect* and the *size effect* are also discussed. In addition to providing a background to the present work, this chapter also cites various references on the subject of glulam and finger-joints.

2.1 Solid wood and wood-based materials

A short description of wood is given below. For a more complete description reference is made to Kollman & Côté [29], Dinwoodie [13, 14] and Bodig & Jayne [6].

2.1.1 A complex material

Wood is doubtlessly one of the oldest building materials known to man. It has been used in various forms, from tree trunks in pre-historic time to highly engineered materials such as fibre boards, glulam and laminated veneer lumber (LVL) today. The advantages of using wood are well known: it has an attractive appearance, is easy to work with, its strength/weight ratio is high, it has comparatively good heat insulation properties, it is a renewable material, and if exposed to fire it retains its strength for a reasonably long period of time. The disadvantages of wood are also well known: the material properties vary within a very large range, it is an anisotropic material of low strength perpendicular to the grain, and it is sensitive to the exposure to moisture.

The anisotropy of wood can be explained by the structure of the material. Wood is a cellular composite consisting of cellulose, hemicellulose, lignin and extractives. With a deviation of only a few degrees, most wood fibres (90–95%) are oriented in the direction of the tree trunk. In the present work it is assumed that the fibre direction coincides with the direction of the log and with that of boards cut from the log. This direction is referred to as the longitudinal direction and is denoted by L. Two other main directions are the radial (denoted by R) and the tangential (denoted by T). The orientation of the fibres in the L-direction is the main cause of the anisotropy of wood. There are also differences in material properties between the two directions perpendicular to the grain, although these differences are less pronounced. Typical values for Young's modulus in *softwoods* yield ratios of (E_L:E_R:E_T) of (20:1:0.5). The difference between the R- and T-directions is often explained in part by the microfibrils of which the cell walls consist differing in their orientation on the different sides of the cell, and in part by the radially oriented cells, or rays, that are present providing reinforcement in the radial direction.

These ray cells ensure the transport of nutrients in the radial direction. Figure 2.1 shows a piece of wood with the main directions indicated.

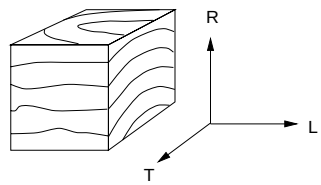

Figure 2.1. *A piece of wood, showing the three directions L, R and T.*

The large variability in strength and in the other parameters is also found within a single log. It can be explained by such anomalies as reaction wood, and by knots, spiral grain and density variation. Differences in climate during the life of a tree is one of various factors that influence the variability of the material properties within a log.

2.1.2 Engineered wood-based materials

To avoid the disadvantages of solid wood, several engineered wood-based materials have been developed over the years. Many of these materials are produced using the same basic concept: cut the solid wood into smaller pieces (sheets, laminations or even fibres) and put them together again by pressing and glueing them, sometimes at temperatures of up to 180°C (fibre-boards). Such materials are termed reconstituted materials. They are more *homogeneous* than solid wood, their material properties such as stiffness and strength not varying as much as in solid wood. If the raw material is disintegrated into fibres or particles which then are randomly oriented in the end product, the result is a material not as strongly orthotropic as solid wood. In such reconstituted materials, the properties of the raw material have been smeared out. In the case of laminated products, this smearing out of the material properties is one of the factors contributing to the so-called *laminating effect*.

2.1.3 Design values

In evaluating the performance of wood-based materials, the large variability in strength and stiffness need to be taken into account if an acceptable level of reliability is to be assured. The present European building code employs the so-called partial coefficient method. In terms of this method, the characteristic value of the parameter in question plays an important role. The characteristic value of the strength, for example, is a value that is a assured with a certain predefined probability. For limit state design 5-percentile values are often employed. This means that the characteristic strength of a component (given as a 5-percentile value) is assured for 95% of the components. If the mean value of the load-bearing capacity is denoted by R_{mean} the characteristic value, R_k, is given by

$$R_k = R_{mean} \cdot (1 - k_{0.05} \cdot COV) \tag{2.1}$$

where COV is the coefficient of variation (known or estimated) for the property examined and $k_{0.05}$ is a factor that depends on the number of samples used to determine

R_{mean} and on whether the COV is known or is estimated. For a perfect Gaussian distribution and a known COV, the factor $k_{0.05}$ is 1.64 (for an infinite number of samples). It is obvious from Equation (2.1) that if the *variability* of an important parameter such as strength or stiffness is *reduced*, the characteristic value used to determine the *design value* will become *higher*.

From the characteristic value, the design value can be calculated. This is usually done by reducing the characteristic value to account for safety regulations, the duration of load, the climate and the size of the structural component.

2.2 Glued laminated timber

2.2.1 General remarks

One way of enhancing the performance of timber is to use glued laminated timber or *glulam*. Glulam is basically the product one gets by glueing together several layers of boards (laminations) so as to build up a desired cross-section. The advantages of glulam are often said to be the following:

- Enhanced strength and stiffness, due mainly to the variation in these parameters being smaller as compared with solid wood.
- Freedom in the choice of cross-sections, lengths and curvatures of the beams.
- Matching of the lamination qualities within the cross-section (strong high-quality laminations being placed in the outermost zones of the cross-section).
- Increased accuracy of dimensions and stability of shape during exposure to variations in moisture.

2.2.2 Production of glulam

The glulam produced in Sweden is composed of 30 to 50 mm thick laminations of *spruce*. The thinner laminations are used for curved beams and the thicker ones for straight beams. The laminations are finger-jointed and are planed prior to being glued together to form the cross-section desired. A commonly used adhesive in Sweden is resorcinol-phenol, both for finger-jointing and for the glueing of laminations. Due to the strong demand for it on the export market (especially to Germany), the use of melamine-urea-formaldehyde (MUF) adhesive has increased in recent years. MUF adhesive has the advantage of being transparent, in contrast to resorcinol-phenol adhesive, which is dark brown. The finger-joints used in glulam manufacturing in Sweden are oriented so that they are visible on the face of the lamination. The most frequently-used finger-joint profile is the so-called I-30 profile. In other countries like Germany and Denmark, the I-20 profile is commonly used. A typical finger-joint with the parameters needed to define its geometry is shown in Figure 2.2. After the laminations have been glued to form a particular cross-section, the beam is planed to obtain the shape desired.

2.2.3 Finger-joints

Over the years there have been many investigations, both experimental and numerical, concerning the behaviour of finger-joints. Experimental work has been carried out

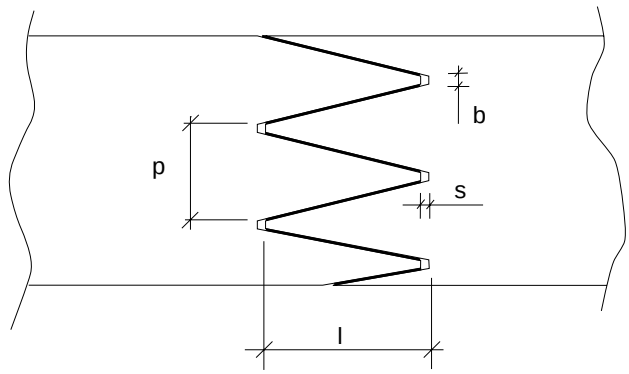

Figure 2.2. *A finger-joint can be defined by 4 parameters: l is the length of the fingers, s is the gap between the tip and the root, p is the pitch and b is the width at the finger root/tip.*

by Selbo [34], Johansson [26, 27, 28], Radovic and Rohlfing [33], Ehlbeck et al. [15] and Colling [8], and numerical investigations by Aicher and Klöck [2, 3], Milner and Yeoh [31] and Wernersson [42].

According to [34] and [8] certain geometrical parameters are particularly important for the strength of finger-joints. In those studies it was shown that the strength of finger-joints increases with the following:

- A larger l/p ratio.
- A lesser finger root/tip width.

Numerical investigations [2, 3] and [31] show that high stress concentrations (stresses in the grain direction) develop in the vicinity of the finger tip/root. In Wernersson [42], the nonlinear behaviour of the bond line is considered, the complete descending branch of the stress-deformation curve being taken into account.

All the numerical investigations cited above have one thing in common, that of their being performed for only a part of a finger-joint, commonly a single finger. In making these calculations, boundary conditions that would apply to a small part in the middle of an infinitely wide lamination are employed. To the author's knowledge, no calculations have previously been made on complete finger-joints, taking the bond line and its nonlinear mechanical properties into account. Such calculations are presented in the present study.

2.3 Behaviour of glulam

2.3.1 Strength

Since wood under compression has a large yield capacity, the bending strength of a glulam beam is often determined by the tensile strength of the outer lamination. Failure often originates in a knot or a finger-joint. A summary of a large number (1767) of bending tests involving glulam beams can be found in Colling [8]. Of the 1767 beams

examined, there were 277 for which the region of maximum bending moment had finger-joints in the outer tension lamination. Of the latter 277 beams, there were 220 (79% of these) that failed in the finger-joints. According to Johansson [28], the finger-joints were of lesser influence: of the 32 beams tested with a finger-joint in the outer tension lamination in the region of maximum bending moment, only 10 (31%) failed due to the finger-joint.

The above applies to failure caused by tensile stress in the direction of the grain. For certain types of notched beams, beams with a hole or curved beams, failure may very well be caused by tension perpendicular to the grain. The two modes of tensile failure (parallel and perpendicular to the grain, respectively) have one thing in common, they are often very brittle and very sudden.

Several methods of predicting the load-bearing capacity of glulam beams in bending have been proposed. One is the so-called I_k/I_g-method given in ASTM [1], which uses a reduction in the moment of inertia due to knots, as a way of taking the strength-reducing effects of knots into account. In 1980 Foschi and Barrett presented a model for the simulation of a glulam beam [18]. This model uses a Monte-Carlo simulation to predict the strength and the distribution of the strength for a number of beams. The so-called Karlsruhe model described by Colling in [8, 9, 10, 11] is based on the ideas of Foschi and Barrett. Another calculation model, PROLAM, was presented in 1985 by Bender et al. in [4] and by Hernandez et al. in 1991 [21].

2.3.2 Size effect

In the late 30's, Weibull [40, 41] presented his theory on the phenomenon of rupture in brittle materials. According to this theory, there is a dependence of the strength on the volume. The reason is that, for a brittle material in which failure is regarded as a "weakest link" failure, the probability of a severe defect is greater in a large volume than in a small. The size effect can be expressed in terms either of mean values or of characteristic values. The difference is obvious if one considers a very large test specimen. According to the Weibull theory, the strength of a very large beam is low. If tests are made on a large number of such beams the variability (expressed as COV) is also low, since a sufficiently large beam will contain a defect that results in the lowest level of strength according to a three-parameter Weibull distribution, for example. Since, according to Equation (2.1) the characteristic value depends on the COV, the characteristic strength of a large beam is approximately the same as its mean strength. The size factor, expressed as the strength of a small beam divided by the strength of a large beam, would then depend on whether use is made of the mean values or of the characteristic values.

The failure of a brittle material in bending is different than failure in pure tension, since bending involves both tension and compression. Thus, the size effect is also dependent on the current stress distribution. A discussion of this topic is found in Colling [7].

Irrespective of whether means or characteristic strength values are used, the size effect or size factor, k_{vol}, is often expressed as:

$$k_{vol} = \left(\frac{V}{V_0}\right)^{\eta}, \ \eta < 0 \tag{2.2}$$

where V is the current volume and V_0 is a reference volume for which the material

strength was determined. Several investigations of the size effect have been carried out over the years for determining the dependence of the strength of beams of solid wood and of glulam on volume. Investigations of this kind on glulam have been carried out by Ehlbeck and Colling [16] and by Solli [39]. Typical values of η have been found to be in the range of -0.1 to -0.4. The size effect is often expressed in terms of a depth or a length factor since beams that are tested according to some standard procedure tend to have a predefined depth to length ratio, typically one of $L/h = 18$. The width of the beam is usually not expected to have any influence. The volume effect as expressed in Equation (2.2) can then be expressed in terms either of beam length or of beam depth.

A complication that arises in discussions of the size effect for solid wood or for glulam is the fact that the raw material is manufactured by nature. If one tries to compare a very large beam with a small one, it is not unlikely that the difference in strength will have arisen from the large beam being from a larger or faster growing tree. Here, the "size effect" could in fact be the effect of comparing different materials.

2.3.3 Laminating effect

Consider a lamination tested in pure tension. If a test of this sort was performed to predict the strength of a glulam beam consisting of laminations of corresponding quality, it would be found that the strength of the beam was higher than what the testing of the laminations would predict. This effect, called the *laminating effect*, can be expressed as a laminating factor, k_{lam}, given by:

$$k_{lam} = \frac{f_{m,beam}}{f_{t,lam}} \tag{2.3}$$

where $f_{t,lam}$ is the tensile strength of the lamination and $f_{m,beam}$ is the bending strength of the beam, evaluated using ordinary beam theory. Examples of such laminating factors are found in the work of Larsen [30], and Falk et al. [17]. Larsen found that for different beam compositions the laminating factor varied from 1.06 to 1.68. The investigation of Falk et al. yielded laminating factors in the range of 1.35 to 1.65.

An expression for the strength of a glulam beam by use of characteristic values, (in MPa), is given by Gehri [19]:

$$f_{m,beam,k} = 12 + f_{t,lam,k} \tag{2.4}$$

Colling and Falk [12] specify the laminating factor based on characteristic values (in MPa) as:

$$f_{m,beam,k} = 6.85 + 1.14 \cdot f_{t,lam,k} \tag{2.5}$$

A similar expression is adopted in the European standard, prEN 1194

$$f_{m,beam,k} = 7 + 1.15 \cdot f_{t,lam,k} \tag{2.6}$$

Due to the difference between the bending strength and the tensile strength of a lamination, the laminating factor as expressed in terms of the bending strength of the lamination, differs from the laminating factor as expressed in terms of tensile strength in Equation (2.3) above. Furthermore, the difference between bending strength and tensile strength is more pronounced for finger-jointed laminations, [17], leading to a laminating factor based on the bending strength that can be less than 1.0. In [17] the laminating

factor based on the characteristic bending strength, i.e $k_{lam} = f_{m,beam,k}/f_{m,lam,k}$, was found to be in the range of 0.70 to 1.15.

The laminating effect has been explained by Foschi and Barrett [18] and Larsen [30] as an effect of the following:

- In a glulam beam the defects are smeared out resulting in a more homogeneous material than solid wood. The probability of a defect's having a serious influence on the strength of the beam is less than it is in a single lamination.
- A single lamination tested in pure tension, will bend due to knots and other anomalies. This is due to the stiffness not being constant over the cross-section of the lamination. If the same lamination was contained in a glulam beam, the rest of the beam would prevent such bending.
- If a lamination that is tested contains knots or other zones of low stiffness, a pure tensile test does not represent the true stress distribution found in a beam that is subjected to pure bending. The adjacent stiffer and stronger laminations would then take up a larger part of the tensile stresses.

Johansson [25] and Hoffmeyer and Bach [24] investigated the possibility of laminating tensile lamination(s). The basic idea is to construct the outermost lamination(s) of a glulam beam using several thin laminations. The results of these two investigations are contradictory. Whereas Johansson found no significant improvement through use of such a procedure, Hoffmeyer and Bach did (the characteristic bending strength of the beams that were tested was improved by 30-50%, depending on the lamination composition). The probable explanation is that in the beams that Johansson tested, only the outermost tension lamination was laminated, whereas in 3 of the 4 compositions Hoffmeyer and Bach tested the two outer laminations were laminated. In addition, the degree to which the laminations were laminated also differed.

3. Experimental Methods

In this chapter the experimental methods employed are presented. First certain general remarks are made concerning the most common ways of testing finger-joints, and thereafter the preparation of the samples is described. In the present test programme tests of two different types were performed. The small-specimen tests were performed to quantify the material parameters needed for modelling the adhesive bond, whereas the large-specimen tests were performed to verify the model. In the next two sections – one for each of the two types of tests, namely bond-line testing and finger-joint testing – the aims of the test programme are considered together with the methods used for evaluating the test results.

3.1 General remarks

3.1.1 Testing of finger-joints

The most common way of evaluating the strength of finger-joints is probably through the flatwise bending of finger-jointed laminations. This method is often preferred in practice, since it is much easier to perform a bending test than a tensile test. In glulam manufacturing in Sweden, the 4-point bending test of laminations is the method most frequently employed. It is notable that the strain (or stress) distribution over the cross-section of the lamination which the most common way of testing finger-joints yields has no resemblance to the distribution found in a lamination within a glulam beam. Since in a glulam beam the beam height is much greater than the thickness of the separate laminations, the outer lamination is subjected to almost pure tension or pure compression, the strain distribution being almost uniform. In the present study, finger-jointed laminations were tested in tension.

3.1.2 Testing for fracture mechanical properties

In order to obtain all the parameters needed in the bond model, stable test performance of the small specimens was called for. The parameters to be obtained are strength, fracture energy and the shapes of the stress-slip relations (σ-δ_n and τ-δ_s-relation). For test performance to be stable, i.e. a test including the complete descending branch of the stress-slip relation, the test setup needs to fulfil certain requirements. When the strength of the material tested is reached, softening begins and a localized failure develops. In order for stability to be achieved, the relaxation of the material surrounding the fracture process zone must correspond to the deformation developing during cracking. Stable test performance of softening materials thus requires displacement control as well as considerable stiffnesses outside the fracture process zone. The stiffness outside the fracture process zone includes the test specimen, its attachment to the testing machine, and the testing machine itself, including the load cells, grips, etc. Another way of expressing the stability requirement is to state that when the material softens, i.e. when the force applied by the testing machine decreases during the increase in

deformation, the strain energy released outside the fracture process zone needs to be smaller than the energy required to extend the fracture zone.

3.2 Sample preparation

3.2.1 From tree to board

The wood used throughout this testing programme is spruce (*Picea abies*). The reason for its selection was that almost all the glulam manufactured in Europe today is made of spruce. The tree from which the specimens were taken was felled in southern Sweden. The tree was carefully marked, so that it would be possible to trace the original position of each of the specimens. The boards used in the manufacturing of finger-joints were taken from less than 10 m above ground level (the tree was approximately 25 m tall) in order to avoid knots insofar as possible and obtain homogeneous wood without the presence of juvenile wood. Each board was taken as far from the pith as possible to reduce the influence of the curvature of the annual rings. This simplifies the numerical simulations since it allows the wood to be treated as an orthotropic material in which the orthotropic directions within the board are constant. This in turn allows analyses to be made in two dimensions, plane stress or plane strain being assumed. The boards were approximately 3 m long and had a cross-section of 120×40 mm^2. The dimensions refer to the cross-section after sawing and drying, but without planing. Figure 3.1 shows how the boards were taken from the log. In order to avoid boundary effects when the finger-joints were glued, the width of the boards was chosen so as to be much larger than the final width of the test specimens. The boards had been stored in a climate of 20°C and 65% RH for over a year prior to the finger-joints being milled. The moisture content of the finger-jointed laminations was 12.6% and the density of the wood at this moisture content was found to be 526 kg/m^3 (mean values of 18 specimens, 2 from each lamination), the coefficients of variation being 0.02 and 0.05, respectively. The density was determined as "wet mass/wet volume".

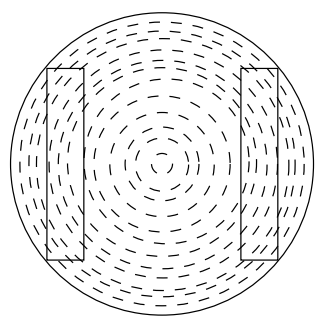

Figure 3.1. *The boards were taken from as far from the pith as possible so as to reduce the influence of the curvature of the annual rings and avoid juvenile wood.*

3.2.2 Finger-jointing

To produce finger-joints, each board was cut into 4 samples of approximately 0.75 m length. Each of these samples was cut into two halves, each half being given the desired finger profile (I-20) in a milling machine. The geometry of this profile is given, as shown in Figure 2.2, by the parameters l, s, p and b, which were 20 mm, 0.6 mm, 6.2 mm and 1.0 mm, respectively. The finger profile was visible on the *face* of the board.

An adhesive commonly used in manufacturing finger-joints for glulam in Sweden is resorcinol-phenol (RP). This adhesive has the disadvantage, however, of being dark brown. Due to demands of the export market, a transparent adhesive, melamine-urea-formaldehyde (MUF), has been used the last few years years. Recently, new one-component polyurethane adhesives have been developed as well. These are available in light "wood-alike" colours.

For the investigation it was decided that three different types of adhesives would be tested:

- 2-component resorcinol–phenol "RP" (Casco Nobel nr 1711+2620).
- 2-component polyurethane "PUR" (Casco Nobel nr 1899+1821).
- Polyvinylacetate "PVAc" (Casco Nobel nr 3326).

The decision to test PUR and PVAc was due to the RP-adhesive being very brittle. PVAc-adhesive is very ductile, the brittleness of the PUR-adhesive lying somewhere between that of RP and of PVAc. The three glues tested thus represent a large range in terms of brittleness.

Before the two halves of the board were glued together again, the one half was rotated 180° around its length axis. This made it possible to obtain an almost perfect match of the material in the vicinity of the finger-joint when the finger-jointed board, after curing, was cut lengthwise into two test samples. One sample could then be used for testing the entire lamination and the other for testing the bond line. Due to this matching procedure, the curvature of the annual rings of the two jointed board-halves do not match. In testing the laminations, however, the effect of this mismatch is small if the curvature of the annual rings is likewise small. This mismatch of annual ring curvature is shown in Figure 3.2, but for purpose of clarity without the finger-joints.

The adhesive was applied using a piece of lumber in which the same finger profile was milled in one end. A pneumatic piston was used in glueing the samples together again. The force of the piston on the finger-jointed lamination was controlled by the air pressure. A normal force on the lamination corresponding to a mean compressive stress of about 0.5 MPa was employed. If a higher compressive stress is used, there is the risk of the wood splitting at the finger roots.

The samples were stored in a controlled climate (20°C, 65% RH) for approximately 6 months prior to the testing of the finger-jointed laminations (the bond lines were tested approximately 6–10 months after the laminations were tested). When the samples had cured, they were planed to a uniform thickness (35-40 mm) and then split lengthwise as shown in Figure 3.2.

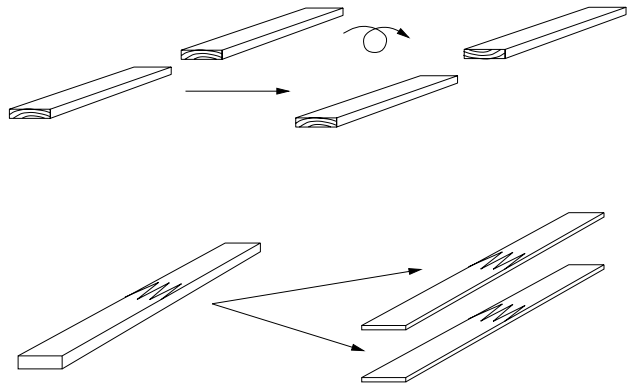

Figure 3.2. *One half of the sample was rotated 180° before being glued to the other half, so as to obtain a good match of the material in the vicinity of the finger-joint. For clarity, the finger-joints are not shown in the upper half of the figure. The finger-jointed sample is split lengthwise into two pieces after curing.*

3.3 Bond line testing

3.3.1 Purpose

The purpose of testing the bond line of the finger-joints was to quantify the bond line material parameters to be used in the numerical modelling of the joint. The parameters the model contains are the following:

- The tensile- and the shear strength of the bond line, denoted σ_{max} and τ_{max}, respectively.
- The shape of the stress–displacement curves in normal- and shear-deformation loading (including the descending branch from maximum stress to complete failure).

These parameters determine the behaviour of the bond line in the model. The testing of the bond line is not pure material testing since several materials are involved: the adhesive, the adherents and the interface between the adhesive and adherents. A model describing the behaviour of the bond line must take into account the coupling between normal (peel) stress and shear stress. If the model is assumed to correctly describe this coupling, it is only necessary to perform tests in pure mode I and in pure mode II. However, if the bond line model is to be calibrated for this coupling effect, one needs to perform several tests in mixed mode as well. The coupling effect assumed in the present numerical calculations is described in Chapter 5.

3.3.2 Test setup

The test specimens were taken from boards that matched the specimens for lamination testing. This assured that the glueing of the bond line was done in the same way for the

small specimens as for the large ones (complete finger-jointed laminations). One should note that the grain direction was not parallel to the bond line. For the finger profile tested the difference is about 6° (1:10.5). This may seem irrelevant at a first glance. However, since the adherents are strongly orthotropic, with a stiffness ratio of about 1:20 in the two directions in the plane of the specimen, the small grain-to-bond-line angle was of certain importance. The deviation in grain was not actually measured in the present study, the grain direction being assumed throughout the study to coincide with that of the board. The specimens used in the experiments were selected with care with regard to avoiding knots and deviations in the grain. A small deviation in the grain, say of less than 5°, is always possible, however.

The testing of the bond line behaviour was carried out in a bi-axial testing machine. The test setup is shown schematically in Figure 3.3.

The testing machine consists of two cross heads that can be controlled by stroke deformation or by force. A camera and a frame grabbing computer are also connected to the testing machine. Using the pictures taken of the specimen during the test, it is possible to measure by means of image processing the deformations that have taken place in the vicinity of the bond line. The specimen was attached to a bi-axial load cell measuring horizontal and vertical load. The test specimen had a glued area of 30 mm^2. The bond line was 3 mm long in the direction considered (Figure 3.3). This short length of the bond line assures a relatively uniform stress distribution, which is crucial for simplicity in evaluating the test results. The stress distribution was verified by finite element simulations, see Chapter 5. The specimens were attached to the testing machine by glueing them to the steel surfaces as indicated in Figure 3.3.

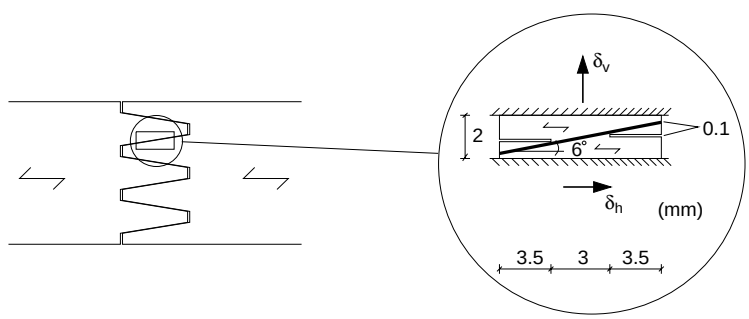

Figure 3.3. *Specimen for bond line testing. The bond line direction in the specimen deviates by approximately 6° from the grain direction. The glued area is 30 mm^2. The specimen is 10 mm in depth. δ_h and δ_v indicate the horizontal and vertical relative displacements, respectively.*

3.3.3 Methods of evaluation

The displacements and loads recorded were the relative shear and the normal displacements between the two steel parts to which the specimen was glued and the corresponding horizontal and vertical loads. This global load-displacement relation obtained was transformed to a stress–relative displacement curve for the bond line. This was done by subtracting the flexibility of the surrounding material and dividing

the forces applied by the glued area, a uniform stress distribution over the bond line thus being assumed. The bond line tests were performed in a manner aimed at resembling the loading present in a finger-joint. The loading directions are thus expressed in relation to the wood fibres, rather than in relation to the bond line. The constitutive relation for the bond line, however, is expressed in terms of relative motion, parallel and perpendicular to the bond line. The stress–relative displacement curves are therefore transformed to the directions parallel to the bond line and perpendicular to it, respectively. The stress-relative displacement curves are then approximated by tri-linear relations for input in the model, see Chapter 5.

3.4 Finger-joint testing

3.4.1 Purpose

The purpose of testing the finger-jointed laminations was to verify the numerical model described in Chapter 5. Through use of three types of adhesive differing markedly in their mechanical properties, the model could be verified for a wide range of bond properties. To be able to describe the behaviour of a tension lamination in a glulam beam it is necessary to test under "beam alike" conditions. As mentioned earlier, one explanation for the laminating effect is that it is an effect of the test results evaluation, arising from the simultaneous bending of the specimen. In testing a lamination it is essential, therefore, to either assure pure centric tension of the specimen *or* measure the bending moment that would occur if uniform tensile deformation was enforced. One way of preventing the specimen from developing curvature is to use a short specimen which is clamped to the testing machine.

3.4.2 Test setups

Half of the finger-jointed board was used for the testing of complete finger-joints. The board was cut to a final width of 70 mm and was planed to a thickness of 10 mm. The total length of the specimens was approximately 420 mm. Specimens were equipped with ten strain gauges each, four on each wide face side 20 mm from the finger root, and two on the edges. An LVDT-transducer measuring along a length of 150 mm was mounted on each face of the specimen. Measuring deformation using the LVDTs yielded mean values for strain over a large part of the specimen. The placing of strain gauges and transducers is shown in Figure 3.4.

In performing a test under clamped conditions, so that the conditions will resemble those of a lamination in a glulam beam, it is useful to measure the bending moments that can occur. The strain gauges mounted on the specimens provide this information. If tests are only performed under clamped conditions, a problem arises. If it is *assumed* that ordinary beam theory applies (i.e. that plane sections remain plane during deformation) and that the modulus of elasticity is constant over the cross-section it is a straightforward task to determine the bending moments. Because of variations in the modulus of elasticity, as well as knots and other anomalies, however, it is not obvious that this can be done. In order to avoid such uncertainties in evaluation of the test results, it was decided to conduct two introductory tests in the elastic region so as to calibrate the strain gauges for section forces occurring when testing to failure. A four-point bending test in flatwise bending followed by a centric tensile test without

clamping or bending, was carried out. For sake of simplicity, it was decided to not perform any edgewise bending tests in the elastic region, since the test specimens were very thin in relation to their width, making it difficult to perform a four-point bending test. The two introductory tests just referred to were performed with estimated maximum stresses of approximately 7.5 and 15 MPa for the bending test and tensile test respectively. Following these tests, each specimen was tested to failure in tension under clamped conditions. The three test setups are shown schematically in Figure 3.5.

Steel plates were glued to the ends of the specimens, Figure 3.6, to prevent the wood from being crushed in the test under clamped conditions. A 10 mm hole through which a dowel was placed was drilled in each of the steel plates. The tensile test in the elastic region was performed by connecting a steel wire to the dowel placed in each end of the specimen. This assured that no bending due to eccentric loading would occur. A detail of the test specimen with the dowel, the steel plates and the steel wire is shown in Figure 3.6.

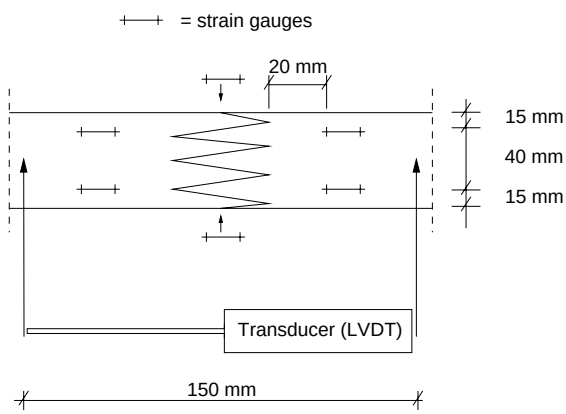

Figure 3.4. *The specimens were equipped with 10 strain gauges and 2 transducers (LVDT).*

3.4.3 Methods of evaluation

For each of the two introductory tests performed on each specimen, the strain gauges gave constants representing strain values [μstr] per section force [N or Nm]. Eight such constants, one for each strain gauge on the face of the specimen, were determined for each section force. The strain gauges on the edges of the specimens were not included in the evaluation, since these strain gauges were placed on the bond line of the finger-joint, yielding large deformations during the tests. The flatwise bending tests were used to calibrate the strain gauges for the flatwise bending moment, whereas the tensile tests were used to calibrate with respect to normal force *and* to edgewise bending. The calibration for edgewise bending was performed by assuming ordinary beam theory to be applicable, the strain gauge constant , determined by the tension test, being multiplied by the area of the cross-section and then divided by (I/c), where I is the moment of inertia of the cross section for edgewise bending and c is the distance from the neutral axis to the strain gauge. From the information provided by the 8 strain

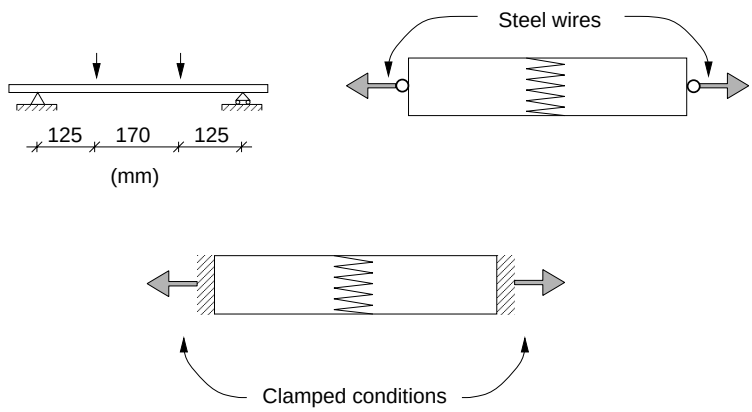

Figure 3.5. *Three different tests were performed on each specimen.*

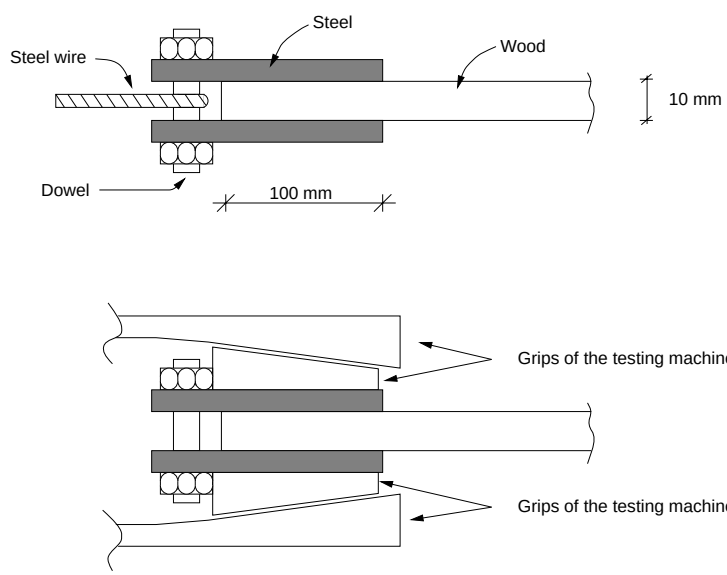

Figure 3.6. *Detail of the specimen in finger-joint testing. A steel wire was attached to the dowel for the introductory pure centric tension test (upper half). The testing machine used for the tests under clamped conditions had wedge-shaped grips (lower half).*

gauges, it was possible to determine the section forces of interest (normal force, two shear forces and two bending moments) in the way described above. The shear forces could be determined by evaluating the bending moments at two different locations on the specimen since, due to equilibrium requirements, the bending moments must be constant or vary linearly. The shear forces, or more specifically the variations in the bending moments in the specimens, were found to be very small, however. This implies the bending moments to be nearly constant. Therefore all 8 strain gauges were used to determine only one set of section forces, these representing the section forces at the mid-section of the lamination, where the finger-joint is located.

For each specimen, a set of constants can be arranged in a matrix, $\mathbf{A}$, of dimensions 8×3, each row representing the influence of the three section forces (one normal force and two bending moments) on a gauge reading, these section forces being representative for the mid-section of the lamination. Thus

$$\mathbf{A}\mathbf{q}_0 = \mathbf{e}_0 \tag{3.1}$$

where $\mathbf{q}_0 = [N \;\; M_{flat} \;\; M_{edge}]^T$ is a 3×1 vector containing the section forces and $\mathbf{e}_0$ is a 8×1 vector containing the gauge readings. Each row in this system of equations thus represents the reading for a certain strain gauge for a load case involving normal force, flatwise bending and edgewise bending, respectively.

In performing the tensile test under clamped conditions the measured gauge readings, $\mathbf{e} = [e_1 \;\; e_2 \ldots e_8]^T$, are used in Equation (3.1), yielding:

$$\mathbf{A}\mathbf{q} = \mathbf{e} \tag{3.2}$$

which is an over-determined system of equations. If a trial solution $\mathbf{q}^*$ to Equation (3.2) is introduced, the residual $\mathbf{r}$ can be expressed as

$$\mathbf{r} = \mathbf{A}\mathbf{q}^* - \mathbf{e} \tag{3.3}$$

The solution sought should minimize the residual in some vector norm. One suitable norm is the L_2-norm of the residual, which is equal to the sum of squares of the components in $\mathbf{r}$, i.e.

$$\Phi = \mathbf{r}^T\mathbf{r} = (\mathbf{A}\mathbf{q}^* - \mathbf{e})^T(\mathbf{A}\mathbf{q}^* - \mathbf{e}) \tag{3.4}$$

Thus the solution sought is equivalent to minimizing Φ, yielding

$$\frac{\partial\Phi}{\partial q_i^*} = 0, \qquad i = 1, 2, 3 \tag{3.5}$$

In index notation this yields

$$\frac{\partial\Phi}{\partial q_i^*} = \frac{\partial(r_j r_j)}{\partial q_i^*} = 2r_j\frac{\partial r_j}{\partial q_i^*}, \qquad j = 1, 2, 3, \ldots, 8 \tag{3.6}$$

with

$$\frac{\partial r_j}{\partial q_i^*} = \frac{\partial}{\partial q_i^*}(A_{jk}q_k^* - e_j) = A_{jk}\delta_{ki} = A_{ji} \tag{3.7}$$

which is valid for constant $\mathbf{A}$. Making use of Equations (3.7) and (3.6) in Equation (3.5) then yields

$$(A_{jk}q_k^* - e_j)A_{ji} = 0 \quad \Leftrightarrow \quad A_{ji}A_{jk}q_k^* = A_{ji}e_j \tag{3.8}$$

In matrix form, this equation is written as

$$\mathbf{A}^T\mathbf{A}\mathbf{q}^* = \mathbf{A}^T\mathbf{e} \tag{3.9}$$

This system of equations is an ordinary one in which the number of unknown variables is the same as the number of equations. Accordingly, a possible solution is given by

$$\mathbf{q}^* = (\mathbf{A}^T\mathbf{A})^{-1}\mathbf{A}^T\mathbf{e} \tag{3.10}$$

This solution is equivalent to the least square fit of the test data to the calibrated constants of the strain gauges. The solution (Equation (3.10)) is calculated for every sample in time during the test to failure under clamped conditions. It thus gives the sectional forces as a function of time. During calibration of the strain gauges, it was assumed that the relations between sectional forces and measured strains were linear. Furthermore, it was assumed that this linear relation is independent of the section forces. It is not required, however, that the stiffness in different parts of the specimen be equal. In addition, for the evaluation of the flatwise bending and tension, it is not required that ordinary beam theory be valid.

4. Experimental Results

4.1 Bond line tests

4.1.1 General remarks

The results for the small-specimen tests are presented in this section. The tests were performed in order to obtain input data to the material model of the bond line. Therefore, the diagrams showing stress–relative displacement curves refer to the main directions relative to the bond line (i.e. parallel and perpendicular to it) since these are the directions used in the constitutive relations. The corresponding stresses are the shear stress and the normal stress in the bond line. The forces and displacements recorded during the tests were however related to the directions parallel and perpendicular to the grain. Figure 4.1 shows the definition of positive normal stress, σ, and positive shear stress, τ, and the corresponding relative displacements, δ_n and δ_s, respectively together with the relative displacements that were recorded, δ_h and δ_v.

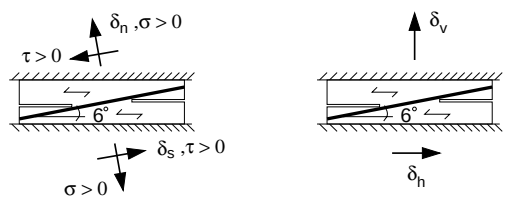

Figure 4.1. *Left: Definition of positive normal stress, σ, and positive shear stress, τ and corresponding relative displacements, δ_n and δ_s, respectively. Right: The forces and displacements recorded during testing related to the directions denoted δ_h and δ_v.*

Three small specimens per lamination were cut out from 9 finger-jointed laminations altogether (three for every type of adhesive), matching the 9 laminations from the large specimen tests. The three small specimens originating from the same lamination were then tested in three different deformation modes. If a lamination glued with a certain type of adhesive is considered to be independent of the other two laminations bonded with the same adhesive, in total 27 *different* tests were performed (3 directions, 3 laminations/adhesive, 3 adhesives). If each adhesive is considered to belong to the same group, however, 3 repetitions were performed for three loading directions and three types of adhesive. By treating the tests as being 27 different ones, it was possible to examine whether any correlation between bond line strength/fracture energy and finger joint strength existed. Since no such correlation was found, the bond line tests were treated as being performed on three different adhesives with 3 repetitions for each.

The three loading paths used in the tests were related to the grain direction of the specimen. The displacements δ_h and δ_v of the bi-axial testing machine were set to be parallel to the grain, perpendicular to the grain and 2:1 to it (parallel:perpendicular),

respectively. Since the bond line direction is somewhat different from the grain direction this results in slightly different paths with respect to bond line directions (approximately 9.5:1, 0.105:1 and 1.57:1 $\delta_s : \delta_n$). These three modes of testing are henceforth denoted as the shear-deformation test, the normal-deformation test and the mixed-mode test, respectively. In order to describe the constitutive relations of the bond lines, *uniaxial* strengths are needed. The uniaxial strengths σ_{max} and τ_{max} were estimated from the test results, using an interaction formula of the type

$$\left(\frac{\sigma}{\sigma_{max}}\right)^m + \left(\frac{\tau}{\tau_{max}}\right)^m = 1 \tag{4.1}$$

where σ_{max} and τ_{max} were determined using a least square fit of the test results. In Equation (4.1), σ and τ denote the normal and shear strength of the bond line for the current mode of loading. The strength of the bond line is defined as the point at which either σ or τ starts to decrease.

The power m was set to 2.0, 1.0 and 1.5 for the RP, PUR and PVAc adhesives, respectively. For all the small-specimen tests, the stroke rate of the testing machine was chosen to give approximately the same time to failure as for the lamination test, i.e. a few minutes. This resulted in stroke rates of 0.001–0.0002 mm/s for the different adhesives. In the tests performed, the stroke rates were constant for each type of adhesive. The stroke rates chosen for the PVAc-adhesive were determined, however, by a trial and error approach before the main series was tested. In a single test of the PVAc at a stroke rate equal to 1/10 of that adopted for the main series, the strength of the bond line was reduced by approximately 40%. Such reduction, although smaller in magnitude, accords with the results for PVAc reported in [42].

The fracture energies were calculated as the total work done during the course of loading. This work can be expressed as:

$$G_f = \int_\Gamma \sigma d\delta_n + \int_\Gamma \tau d\delta_s \tag{4.2}$$

Γ being the deformation path leading to complete separation of the bond line. The normal stress σ and the shear stress τ were calculated assuming a uniform stress distribution over the fracture area. The deformations δ_n and δ_s were calculated by transforming the deformations measured by LVDTs in the vicinity of the specimen to a coordinate system coinciding with the bond line directions.

4.1.2 RP-adhesive

Since the resorcinol-adhesive was found to be very brittle, certain difficulties concerning the stability of the test arose. A total of 16 tests needed to be performed in order to achieve the 9 stable tests presented. The stress-displacement curves for the RP-adhesive tests are shown in Figures 4.2–4.4. For the shear-deformation test, normal tensile stresses perpendicular to the bond line developed due to the slope of bond line relative the grain orientation. It is noteworthy that after maximum shear stress had been reached in the shear-deformation tests, compressive stresses perpendicular to the bond line developed. This can be explained by the constraint on the deformation of zero displacement in the normal direction for shear-deformation testing. It is remarkable, however, that for normal-deformation testing, maximum shear stress developed long after the maximum normal stress was reached. Although the results for

the shear-deformation tests appear almost unstable, the descending part of the stress-displacement curves was in fact recorded during 10-20 seconds, using several samples ranging from maximum load to approximately 3 MPa. The strengths for the small RP-specimens, together with a quadratic ($m = 2$ in Equation (4.1)) interaction used to estimate the uniaxial strengths, are given in Figure 4.5. The quadratic interaction yields a *uniaxial* shear strength of 19.3 MPa and a *uniaxial* normal strength of 6.5 MPa. The fracture energies for the three deformation modes tested were found to be 1250, 560 and 440 J/m^2 for the shear, mixed and normal deformation mode, respectively.

4.1.3 PUR-adhesive

The polyurethane adhesive was much more ductile than the resorcinol adhesive, and the response obtained with it showed certain tendencies of nonlinear deformations prior to peak stress. The stress-displacement curves for the three modes of loading are shown in Figures 4.6–4.8. As can be seen in Figure 4.9, for $m = 1$, the fit for strength was fairly good, implying the interaction to be linear. The fracture energies for the three deformation modes tested were found to be 740, 420 and 470 J/m^2 for the shear-, mixed- and normal-deformation modes, respectively.

4.1.4 PVAc-adhesive

The PVAc-adhesive was much more ductile than the RP-adhesive and there were no tendencies to instability when the tests were performed. Prior to peak stress, a tendency of a nonlinear plastic hardening deformation was evident. The stress–relative displacements obtained for the 9 tests are shown in Figures 4.10–4.12. The strength of the bond line for the three different loading combinations was fitted in terms of Equation (4.1) to an interaction in which $m = 1.5$, resulting in a better fit than with the quadratic interaction employed for RP-adhesive. The strengths obtained in the nine different tests, together with the fit to the interaction formula, are shown in Figure 4.13. The fracture energies for the three deformation modes that were tested, as given by Equation (4.2), were found to be 2080, 1280 and 1380 J/m^2 for the shear, mixed and normal deformation mode, respectively. One should note that, since the PVAc-adhesive showed considerable plastic or nonlinear behaviour prior to peak stress, the fracture energy values reported, as defined by Equation (4.2), include the pre-peak-stress work-of-fracture.

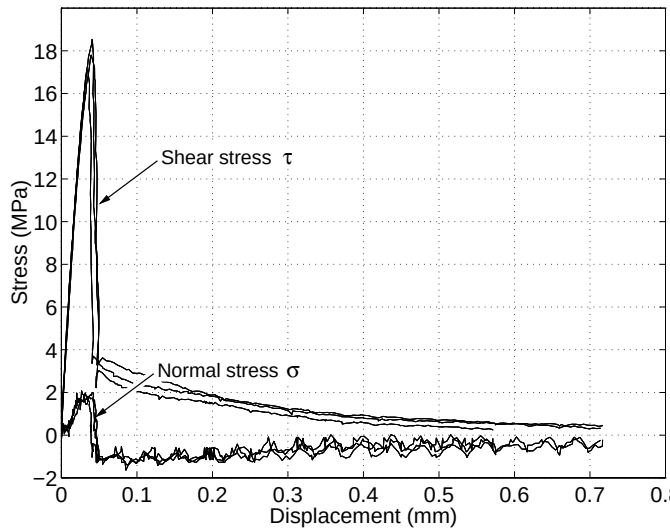

Figure 4.2. *Shear and normal stress versus shear displacement δ_s for RP-adhesive in shear-deformation testing.*

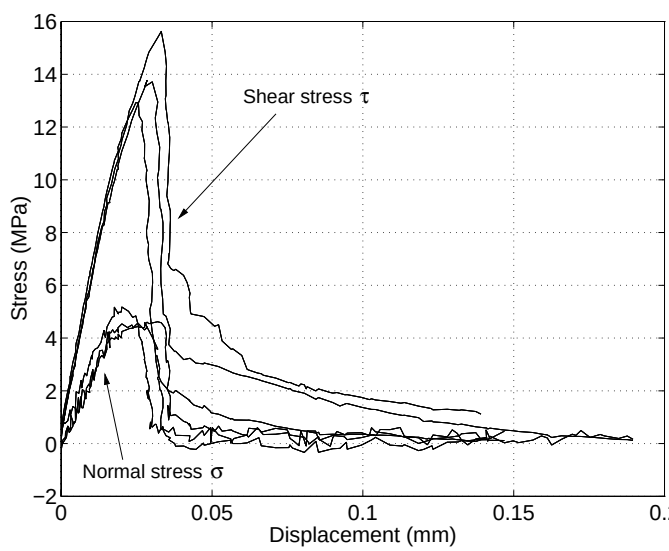

Figure 4.3. *Shear and normal stress versus shear displacement δ_s for RP-adhesive in mixed mode testing.*

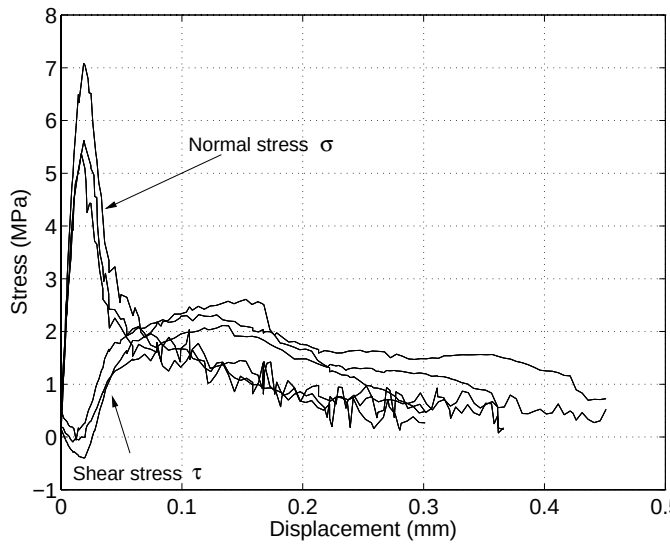

Figure 4.4. *Normal and shear stress versus normal displacement δ_n for RP-adhesive in normal-deformation testing.*

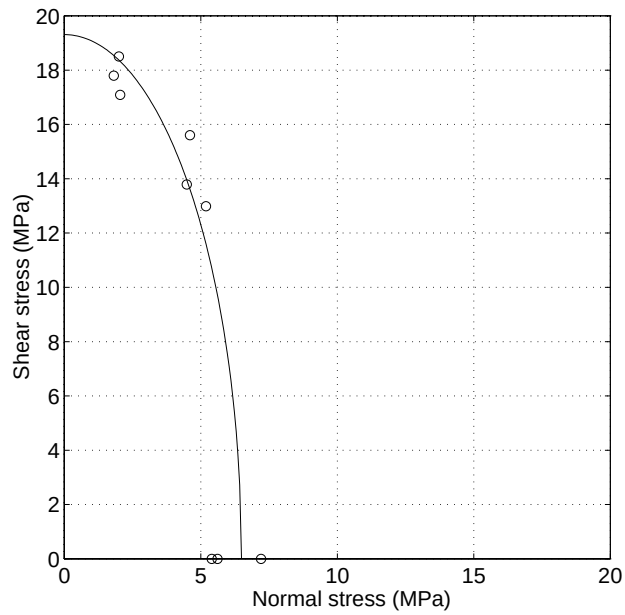

Figure 4.5. *Fit of test data (circles) to a quadratic interaction formula corresponding to Equation (4.1) with $m = 2.0$ (solid line). RP-adhesive.*

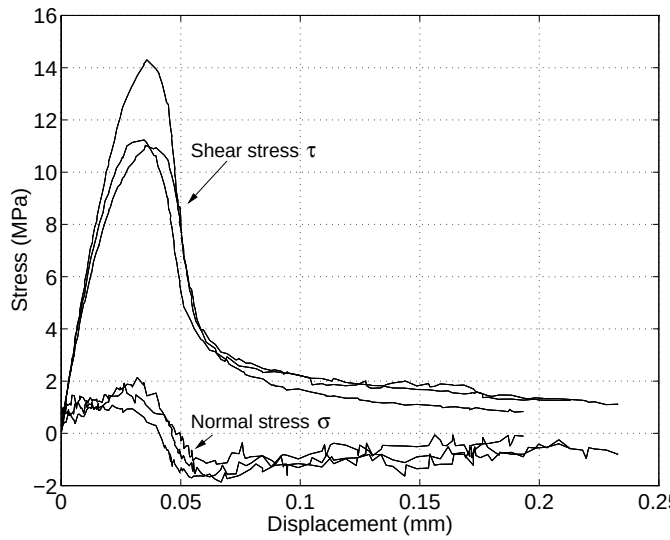

Figure 4.6. *Shear and normal stress versus shear displacement δ_s for PUR-adhesive in shear-deformation testing.*

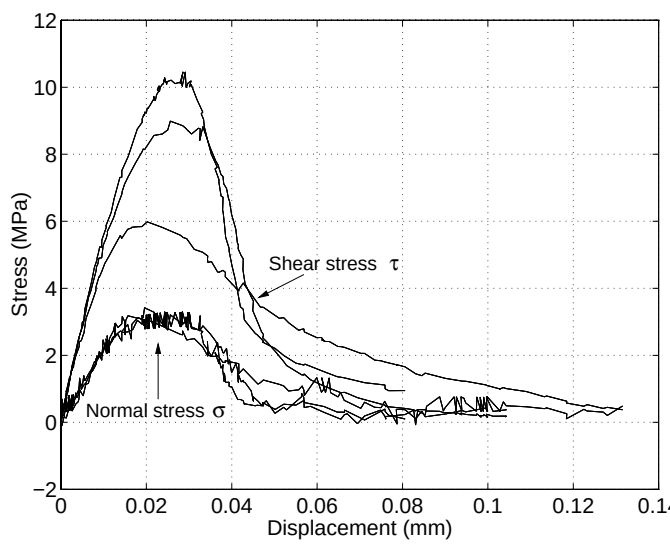

Figure 4.7. *Shear and normal stress versus shear displacement δ_s for PUR-adhesive in mixed mode testing.*

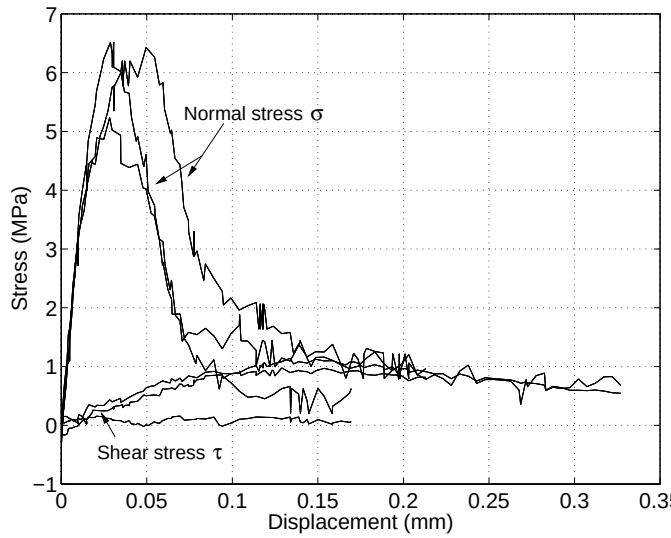

Figure 4.8. *Normal and shear stress versus normal displacement δ_n for PUR-adhesive in normal-deformation testing.*

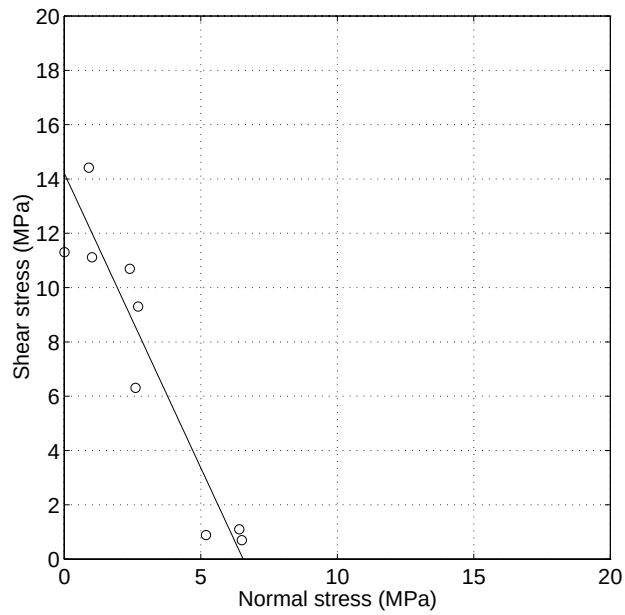

Figure 4.9. *Fit of test data (circles) to a linear interaction formula corresponding to Equation (4.1) with $m = 1.0$ (solid line). PUR-adhesive.*

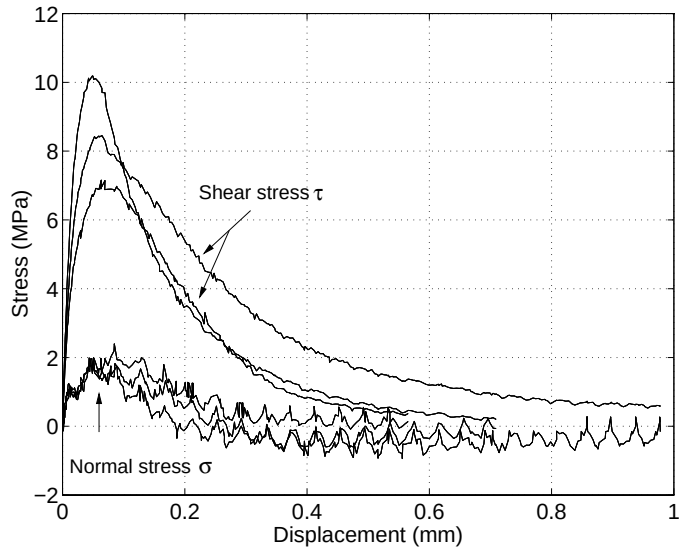

Figure 4.10. *Shear and normal stress versus shear displacement δ_s for PVAc-adhesive in shear-deformation testing.*

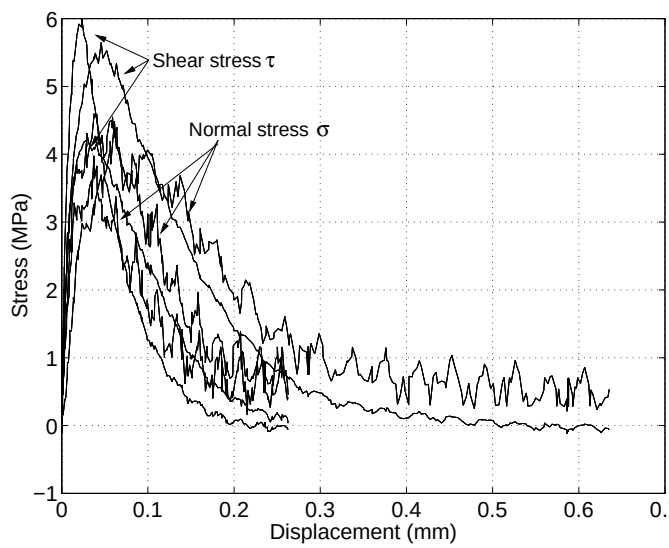

Figure 4.11. *Shear and normal stress versus shear displacement δ_s for PVAc-adhesive in mixed-mode testing.*

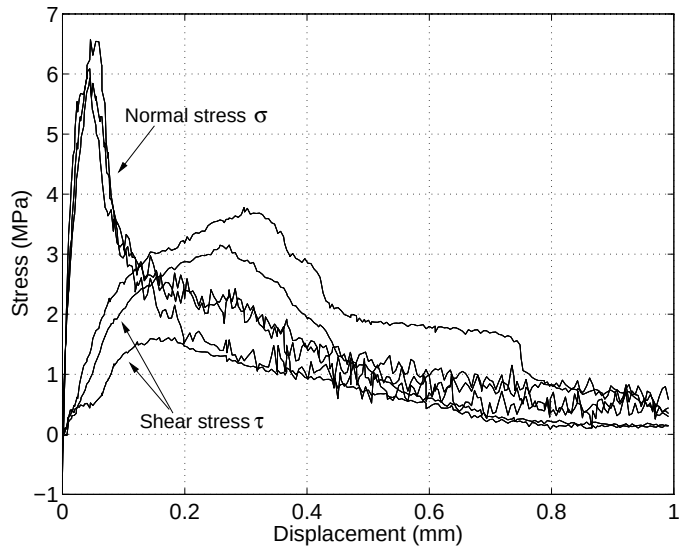

Figure 4.12. *Normal and shear stress versus normal displacement δ_n for PVAc-adhesive in normal-deformation testing.*

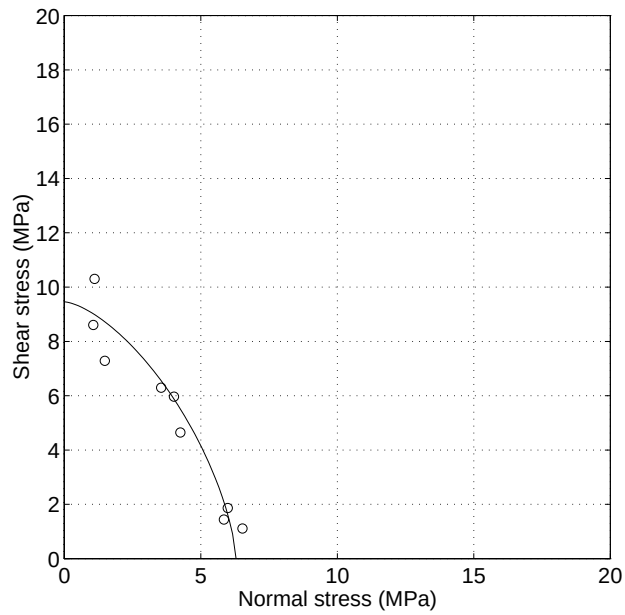

Figure 4.13. *Fit of test data (circles) to interaction formula corresponding to Equation (4.1) with $m = 1.5$ (solid line). PVAc-adhesive.*

4.2 Tensile strength of laminations with finger-joints

4.2.1 General remarks

Results of testing the finger-jointed laminations are presented in the following. The tests were performed using the test setups described in Chapter 3. As indicated earlier, three types of adhesive were tested: RP, PUR and PVAc.

The results are given in diagram form as the estimated stress at certain points in the cross-section versus the measured mean stress, i.e. (measured normal force)/(cross-section area). The estimate is obtained by first evaluating the normal force and bending moments according to the method described in the previous chapter, expressing the section forces according to conventional beam theory then as stresses. It is illustrative to express the loading in terms of stresses in this way, despite this not being necessary, the use of beam theory indeed involving an approximation. The corner points of the cross-section of the specimen were chosen as the points for evaluating the stresses. According to beam theory, the maximum normal stress due to bending and to tension occurs at one of these points provided that, as assumed here, the modulus of elasticity is constant over the cross-section. The corners are enumerated from 1 to 4, see Figure 4.14.

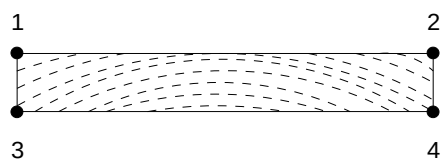

Figure 4.14. *The corner points 1–4 of the cross-section.*

The curves 1–4 in the diagrams correspond to these corner points. The curve without any label represents to the mean value of curves 1–4. This mean value of the estimated stresses should be the same as the measured mean stress. As can be seen in the diagrams this is also the case, indicating the method of evaluating the strains by calibrating the strain gauges for two other load cases and then combining these, being successful.

The specimens are denoted according to their original position in the log, such as: *Gxyz*, where G is a code for the species in question (*Picea abies*), x is the code for the level at which the log was cut from the tree, y is the code for the distance from the pith, and z is the code for the distance from the root-end within the log in question.

The modulus of elasticity can be evaluated in a number of ways, on the basis of the introductory bending and tensile tests using either strain gauge or transducer readings, or on the basis of the test to failure under clamped conditions. In the following, the moduli of elasticity of the specimens as measured by the strain gauges during the flatwise bending tests are given. In Appendix A, a more comprehensive compilation of the measured moduli of elasticity, including the moduli of elasticity for separate halves of the specimens is provided.

Besides using measurement of strain, the modulus of elasticity can be estimated in an approximate manner on the basis of density using a regression formula. One such formula is that given by Johansson in [28]:

$$E = \rho^{1.577} \tag{4.3}$$

where the density ρ is the oven-dry density (dry weight/volume at 12% moisture content, kg/m^3) of the material and E is the modulus of elasticity in MPa. According to Johansson, [28], this regression formula yields a good fit for Swedish spruce (*Picea abies*). The densities measured for the different specimens are listed in Appendix A.

4.2.2 RP-glued finger-joints

The three laminations glued using resorcinol-phenol all failed completely along the fingers. The failure was mainly in the wood in the vicinity of the bond line, there being a large amount of wood fibres at the fracture surfaces. The measured strengths (normal force/area) were 46.8, 56.3 and 50.3 MPa for specimens G15a, G15b and G15c, respectively. The moduli of elasticity for the specimens were calculated on the basis of the introductory flatwise bending tests, yielding stiffnesses of 16500, 16500 and 17700 MPa, respectively, for the three specimens. Figure 4.15 shows specimen G15a after failure. The results of the tests to failure are shown in Figures 4.16–4.18.

4.2.3 PUR-glued finger-joints

Two of the three laminations glued with polyurethane failed completely along the fingers. The failure in these cases was mainly in the wood in the vicinity of the bond line, there being a large amount of wood fibres at the fracture surfaces. The third specimen, G33c, failed along 9 of 11 fingers and along a crack from the fingers to the support. This specimen is shown in Figure 4.19. The measured strengths (normal force/area) were 40.0, 41.6 and 44.7 MPa for specimens G33a, G33b and G33c, respectively. The corresponding moduli of elasticity of the specimens were calculated on the basis of the introductory flatwise bending tests, yielding stiffnesses of 16600, 17200 and 18000 MPa, respectively, for the three specimens. The results of the tests to failure are shown in Figures 4.20–4.22.

4.2.4 PVAc-glued finger-joints

Two of the three specimens of finger-joints glued with PVAc failed completely along the bond line of the fingers (G13c and G13d) while the third specimen (G14a) failed partially along the fingers and partially in the solid wood. Figure 4.23 shows the partial finger failure of the specimen denoted as G14a. The measured strengths (normal force/area) were 32.0, 33.6 and 35.0 MPa for specimens G13c, G13d and G14a, respectively. The corresponding moduli of elasticity were calculated on the basis of the introductory flatwise bending tests, yielding stiffnesses of 17600, 17700 and 13600 MPa, respectively, for the three specimens. It is notable that the specimen G14a, taken from a different position in the log, showed considerably less stiffness. As mentioned above, the failure of this specimen also differed from that of the other two specimens. The results of the tests to failure are shown in Figures 4.24–4.26.

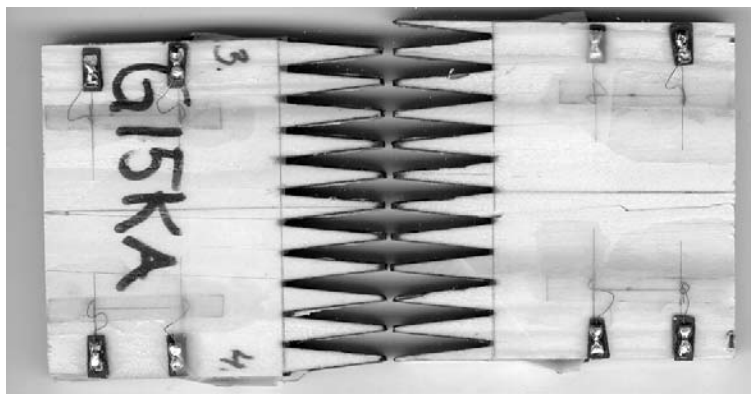

Figure 4.15. *Failure of specimen G15a, RP-adhesive.*

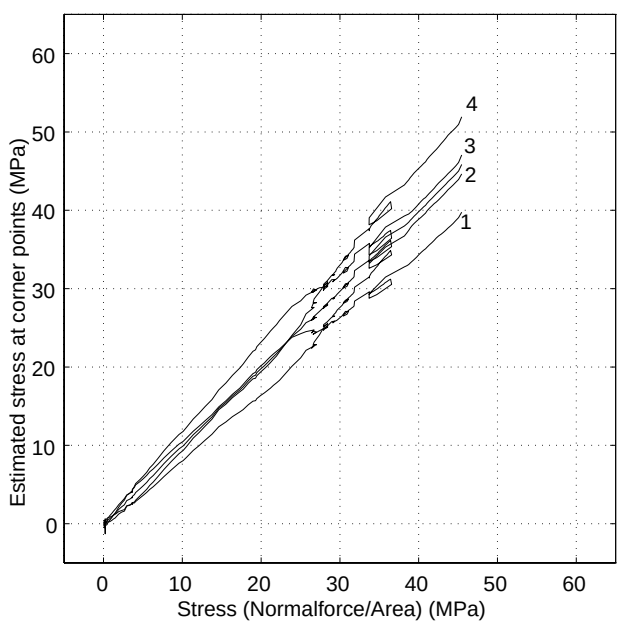

Figure 4.16. *Results for sample G15a, RP-adhesive.*

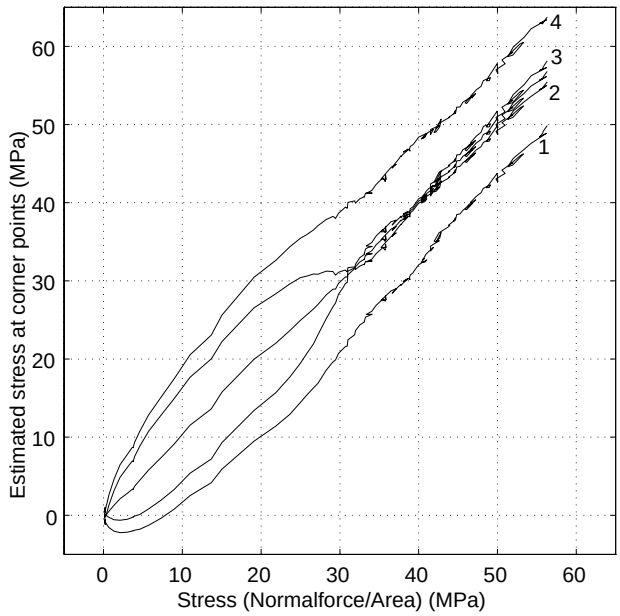

Figure 4.17. *Results for sample G15b, RP-adhesive.*

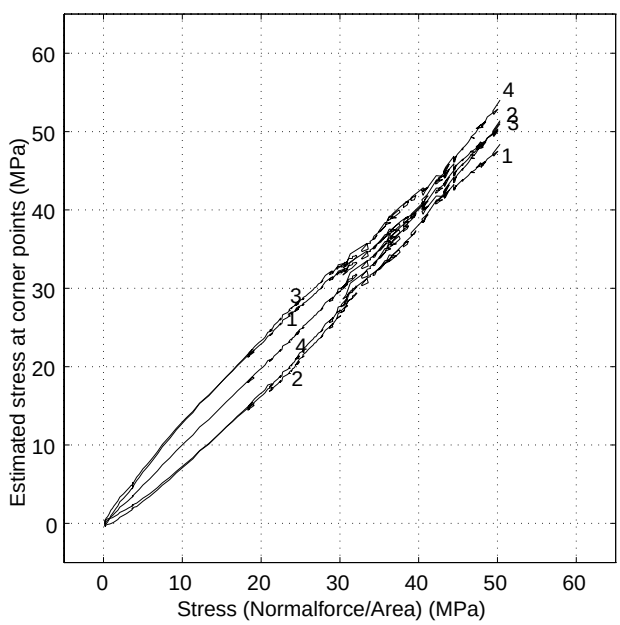

Figure 4.18. *Results for sample G15c, RP-adhesive.*

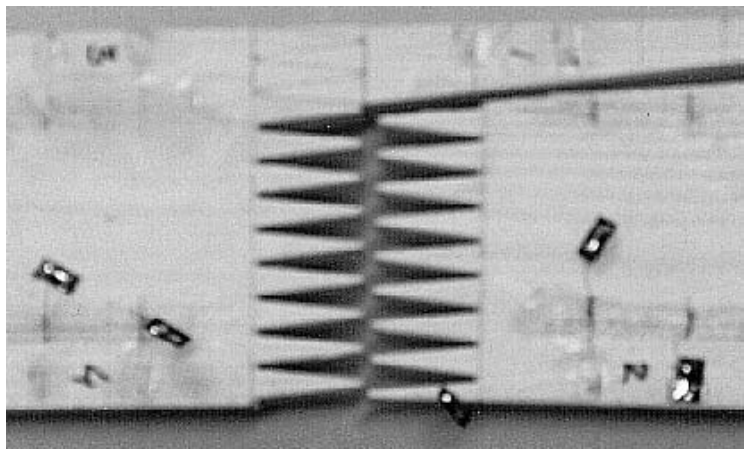

Figure 4.19. *Failure of specimen G33c, PUR-adhesive.*

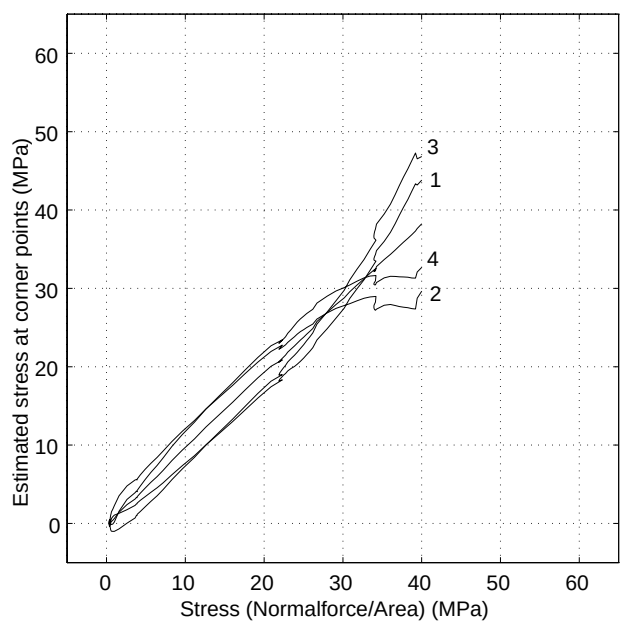

Figure 4.20. *Results for sample G33a, PUR-adhesive.*

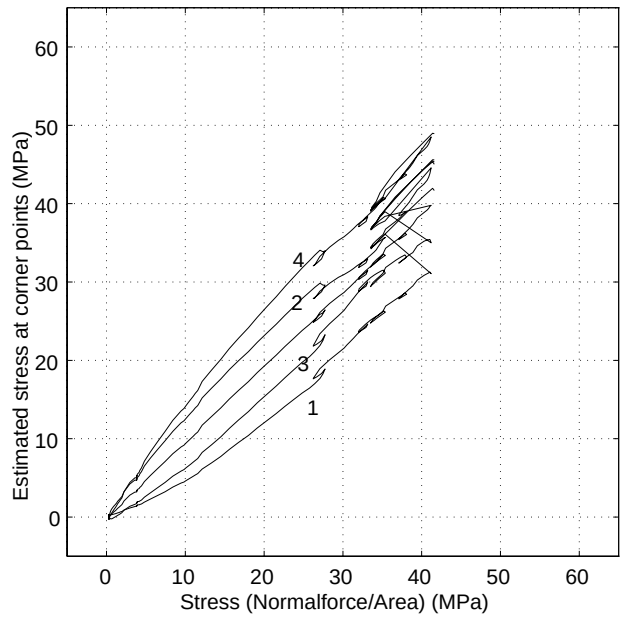

Figure 4.21. *Results for sample G33b, PUR-adhesive.*

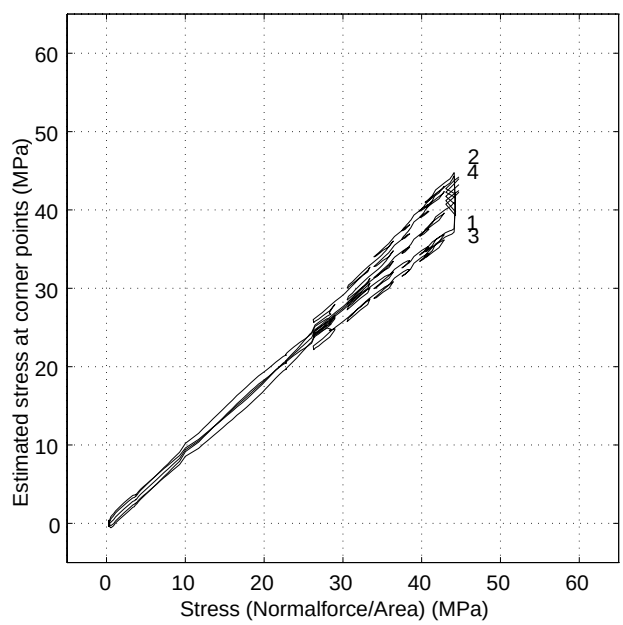

Figure 4.22. *Results for sample G33c, PUR-adhesive.*

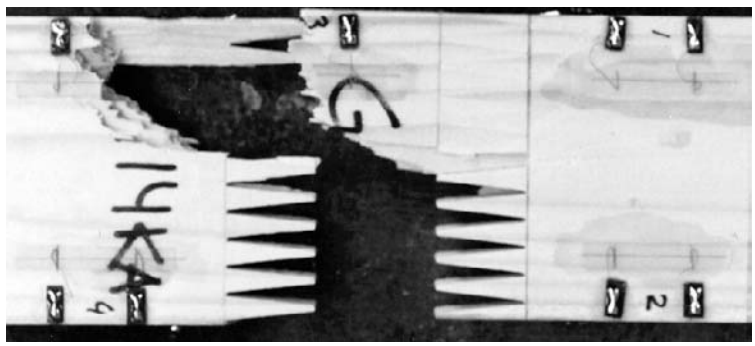

Figure 4.23. *Failure of specimen G14a. PVAc-adhesive.*

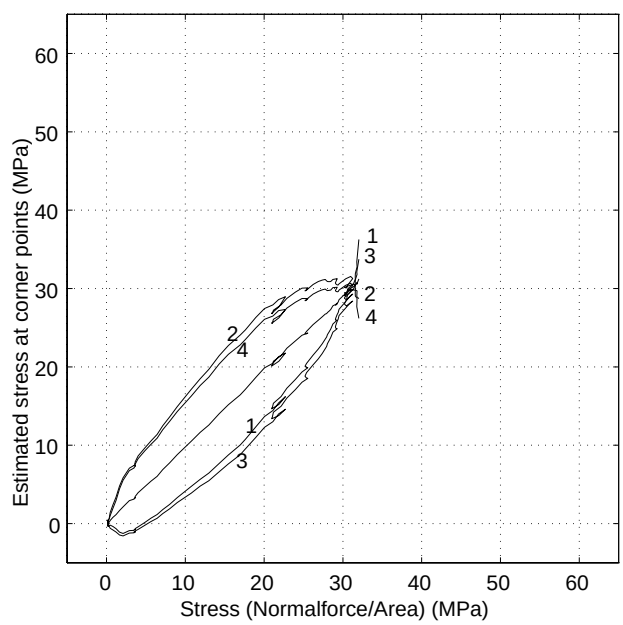

Figure 4.24. *Results for sample G13c, PVAc-adhesive.*

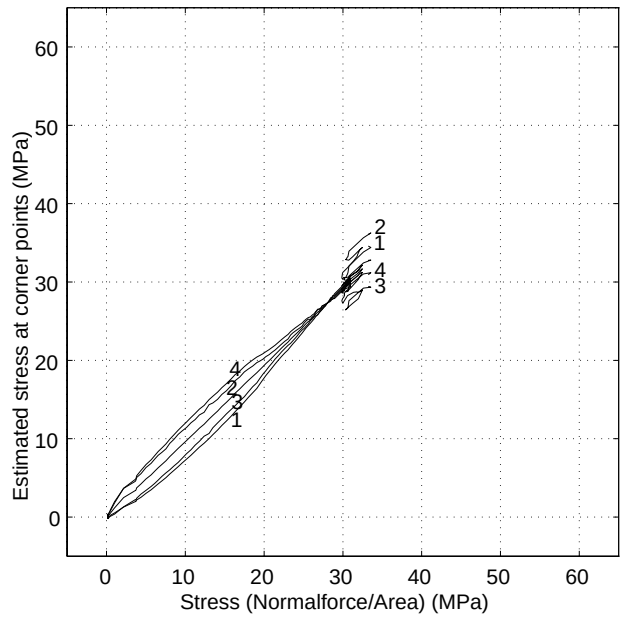

Figure 4.25. *Results for sample G13d, PVAc-adhesive.*

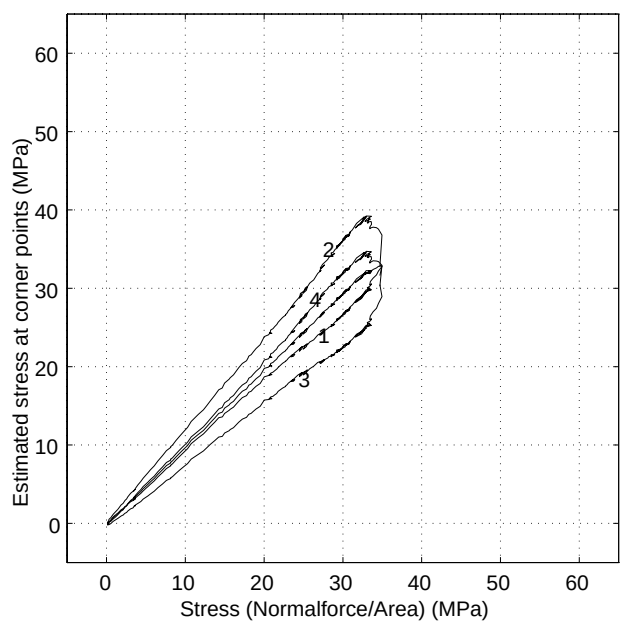

Figure 4.26. *Results for sample G14a, PVAc-adhesive.*

4.3 Compilation of test results.

A summary of the test results, indicating the strengths and fracture energies of the adhesives as obtained in the small-specimen tests, together with the measured and estimated strengths of the finger-jointed laminations is presented in Table 4.1. The uniaxial strengths of the bond lines are estimated using the interaction formula in Equation (4.1). This equation is also shown as a solid line in Figures 4.5, 4.9 and 4.13, respectively.

The specimens used in finger-joint testing were selected with great care and were subjected to thorough documentation in terms of strain measurement during the testing. Three different types of adhesive were used so that distinct differences in mechanical behaviour would be present. The test results showed very little scatter, each type of adhesive yielding strengths of the finger-joints within a distinct (unique) interval. From the introductory bending tests performed on each of the large specimens, the mean value of the longitudinal modulus of elasticity as estimated from strain gauge measurements was found to be 16800 MPa. The density of the wood, in turn, was found to be 526 kg/m^3 at 12.6% moisture content, as reported in the previous chapter. This corresponds to an oven dry density of approximately ("dry mass/wet volume") 467 kg/m^3, corresponding to a modulus of elasticity of $E = 467^{1.577} = 16200$ MPa in terms of Equation (4.3). This deviates by about 4% from the mean value as estimated from the strain gauge measurements.

Table 4.1. *Uniaxial strengths of the bond lines (τ_{max} and σ_{max}) according to Equation (4.1). The fracture energies ($G_{f,I,II,mixed}$) are evaluated using Equation (4.2). For the finger-joint strengths (f_t), the index est. refers to estimated maximum stress according to beam theory. The moduli of elasticity, E, are based on the strain gauge measurements made during the flatwise bending tests (mean of three specimens). Units are MPa and J/m^2.*

	RP-adhesive	PUR-adhesive	PVAc adhesive
τ_{max}	19.3	14.2	9.46
σ_{max}	6.50	6.55	6.29
$G_{f,I}$	440	470	1380
$G_{f,II}$	1250	740	2080
$G_{f,mixed}$	560	420	1280
f_t	51.2	42.1	33.5
$f_{t,est.}$	56.6	46.7	37.2
E	16900	17200	16300

An important outcome of the tests performed is visualized in Figure 4.27. The figure shows the finger-joint strength in relation to the shear strength of the bond line. In addition to the individual strength of the 9 laminations tested, the mean value for

each type of adhesive is also indicated (+). The dashed curve represents a least square fit of the mean values to an expression of the type $y = kx^{\alpha}$.

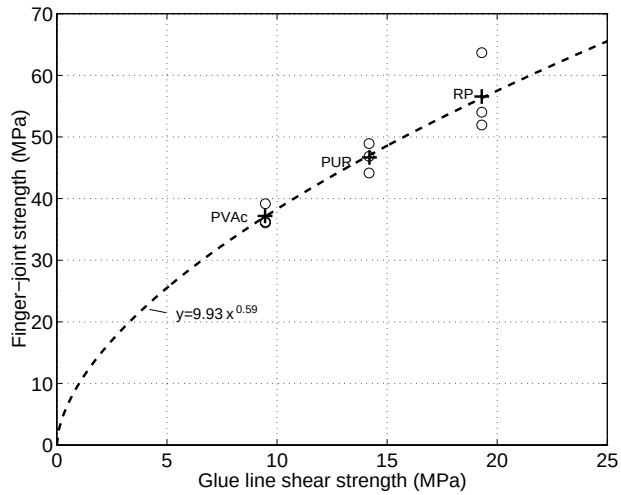

Figure 4.27. *Finger-joint strength versus shear strength of adhesive. The mean value for each adhesive is indicated by '+'. The dashed line is a least square fit of $y = kx^{\alpha}$ to the mean values.*

To clarify the differences in material response, "hand-drawn" mean curves of the stress-displacement relations for the shear-deformation and normal-deformation tests are shown in Figures 4.28 and 4.29.

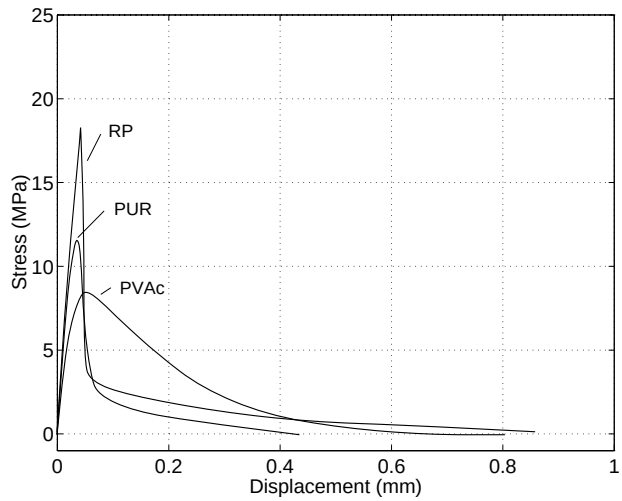

Figure 4.28. *Shear stress versus shear displacement. Mean curves for different adhesives in shear deformation testing.*

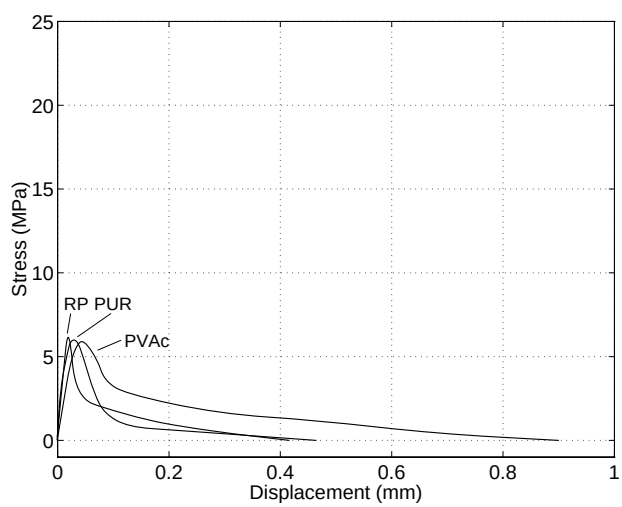

Figure 4.29. *Normal stress versus normal displacement. Mean curves for different adhesives in normal deformation testing.*

5. Model Verification

This chapter provides a background to the numerical studies that were carried out and deals with the numerical simulations performed for verifying the bond line model. First, a short description of the bond line model as developed by Wernersson [42] is presented, together with its finite element implementation. The bond line model and its finite element implementation is described in greater detail in [42].

Simulations of both the small bond line specimens and the large finger-joint specimens that were carried out are reported in the sections that follow. The small-specimen simulations were mainly performed so as to verify the assumption of uniform stress distribution adopted during the evaluation. The large-specimen simulations were performed in order to verify the applicability to the analysis of finger-joints of the present bond line model.

5.1 A nonlinear model for adhesive bonds

Wernersson [42] presents a mixed mode cohesive crack model for analysis of adhesive bonds. The model takes into account the descending branch of the stress–displacement curves for both shear stress and normal stress in the bond. Furthermore, the model takes into account the coupling between normal stress and shear stress in the bond line where shear strength decreases when normal stress is acting simultaneously and vice versa. Emphasis is placed on severe stress states in which a tensile normal stress acts across the bond line. In the case of compressive normal stress, the bond line is assumed to act as a linear elastic medium and there to be no reduction in shear strength. The model is based on an expansion of the uniaxial stress–displacement relations. All relations are derived for the case of plane stress, any Poisson's effects within the bond line being neglected.

5.1.1 Constitutive relations

Let the relative displacement across the bond line be denoted by δ_n and δ_s for opening-normal and shear deformations, respectively. The constitutive relation of the bond line is given then by the functions

$$\sigma = \sigma(\delta_n) \tag{5.1}$$

for pure opening deformation (causing normal stresses only) and

$$\tau = \tau(\delta_s) \tag{5.2}$$

for pure shear deformation (causing shear stresses only).

In the model these functions were chosen originally as being multi-linear and at the same time linear elastic to maximum stress.

The bond line model is similar in some respects to such cohesive crack models as the fictitious crack model, [23], used for the analysis of solid materials assumed to be homogeneous, although it also differs in some ways. The present modelling involves

at least two different materials, the adherents and the adhesive. In the equilibrium equations, the influence of bond line thickness is neglected, no account being taken of the normal stresses in the plane of the bond line, despite the non-zeros thickness of the bond line. Unlike a cohesive crack model, the deformation across the bond line here is not zero before and at peak stress. The "pre-peak-stress" deformation generally includes both an elastic part and a nonlinear plastic part. In the present calculations, the "pre-peak-stress" performance is modelled, however, by a linear elastic relation. This implies that in "pre-peak-stress" states the behaviour is inadequately modelled if nonlinearity is of importance. This could in particular be the case with the PVAc and PUR-adhesives.

In order to define the constitutive relations for mixed mode loading, the uniaxial properties for pure normal and shear stress are expanded in the δ_n–δ_s–plane. The state of deformation is given by the components δ_n and δ_s or alternatively, in polar coordinates, by the radial displacement δ and the mixed mode angle φ, defined as:

$$\delta = \sqrt{\delta_n^2 + \delta_s^2} \tag{5.3}$$

$$\varphi = \arctan\left(\frac{\delta_s}{\delta_n}\right) \tag{5.4}$$

The stress–displacement relation is assumed to retain its piecewise linear shape for radial paths, but vary smoothly with the mixed mode angle φ. The radial distances δ_k, which define the transition from one linear part, k, to the next, $k+1$, are defined by a relation of the type

$$\left(\frac{\delta_{n,k}}{\delta_{n_0,k}}\right)^m + \left(\frac{\delta_{s,k}}{\delta_{s_0,k}}\right)^n = 1 \tag{5.5}$$

where the indices (n_0, k) and (s_0, k) relate to the uniaxial response for normal and shear stress, respectively. In the present study the powers m and n in (5.5) are set to $m = n = 2$ (RP-adhesive), $m = n = 1.0$ (PUR-adhesive) and $m = n = 1.5$ (PVAc-adhesive), yielding a quadratic and linear interaction for the RP and PUR-adhesives, respectively. For each linear part, k, of the constitutive relation, it is necessary to define the stresses σ_k, σ_{k+1}, τ_k and τ_{k+1} at the beginning and the end of the interval. These stresses are related to the corresponding uniaxial stress by the relation

$$\sigma_k = \sigma_{0,k}\frac{\delta_1 \cos\varphi}{\delta_{n_0,1}} \tag{5.6}$$

$$\tau_k = \tau_{0,k}\frac{\delta_1 \sin\varphi}{\delta_{s_0,1}} \tag{5.7}$$

The relations describing the constitutive behaviour of the bond line involve coupling effects, normal stress thus depending not only on the opening deformation but also on the shear deformation. This is realistic for the softening region. In the first region (the elastic "pre-peak-stress" region), the normal and shear stresses are assumed to be uncoupled. In this subspace of the δ_n–δ_s–plane, the constitutive relations are identical to the uniaxial relations as given in (5.1) and (5.2), yielding the relations

$$\sigma(\delta_n, \delta_s) = f(\delta_n) \tag{5.8}$$

$$\tau(\delta_n, \delta_s) = g(\delta_s) \tag{5.9}$$

the functions f and g being linear functions of δ_n and δ_s, respectively. For the case of $m = n$, these relations are valid for δ's for which

$$\delta \leq \left[\left(\frac{\cos\varphi}{\delta_{n0,1}} \right)^m + \left(\frac{\sin\varphi}{\delta_{s0,1}} \right)^m \right]^{(-1/m)} \tag{5.10}$$

this being derived from Equation (5.5) by replacing $\delta_{n,k}$ and $\delta_{s,k}$ by $\delta_n (= \delta\cos\varphi)$ and $\delta_s (= \delta\sin\varphi)$, respectively.

The definition of the non-softening region given in Equation (5.10) corresponds, for the case of $m = 2$, to a stress-based failure criterion often used for mixed mode linear elastic analysis

$$\left(\frac{\sigma}{\sigma_{max}} \right)^2 + \left(\frac{\tau}{\tau_{max}} \right)^2 = 1 \tag{5.11}$$

also known as the Norris criterion. Equation (5.5) can be derived from a criterion of this type since in the elastic region, the normal and shear stresses are proportional to the deformations δ_n and δ_s, respectively.

5.1.2 Finite element implementation

The bond line model described in the previous section was implemented in a commercial finite element code [22] as a special purpose element. The element is defined by two nodes, one on each side of the bond line. For practical reasons (related to pre-processing) the elements are always used in pairs, however, resulting in a 4-node element without any coupling between its two ends. The constitutive relations which form the basis of the bond line model are based on a total formulation. In order to perform general nonlinear analyses the constitutive relations are reformulated to incremental form, the stiffness matrix of the element representing the tangent stiffness, calculated by differentiating the constitutive relations numerically. In addition to the tangential stiffness, the contributions of the element to the equations of equilibrium, to be solved at each node associated with a given element, have to be calculated. These nodal forces are calculated as the stress multiplied by the area of influence for each pair of nodes, this area being half the distance between two pairs of nodes, times the width of the bond line. In using the special purpose element, the user must specify, along with geometric and connectivity data, the break points on the uniaxial piecewise linear stress-displacement curves and the powers m and n as defined in Equation (5.5).

5.2 Simulation of small test specimens

5.2.1 General remarks

The results of the bond line tests, evaluated as described in Chapter 3, were verified by means of FE-analyses. The results of the tests, in terms of the uniaxial stress-slip behaviour of the bond line, were used as input to the analyses. Such analyses should yield load-displacement responses close to those recorded during the tests of the corresponding specimens. Possible significant deviations between the recorded and calculated curves would indicate either that the assumptions made during evaluation of the test recordings might not be valid or that the simplified piecewise linear description of the stress-slip curve could be too crude an approximation.

In order to take account of the plastic deformations occurring in the bond line, the total deformation across the bond line at peak stress was modified for the PVAc and PUR-adhesives. This modification was made as an iterative procedure, the input in terms of the stress-slip relations being modified successively so as to obtain results as close as possible to those recorded during testing. Although such an approach is by no means neutral, it is a way of satisfying the simplifying assumptions made, such as the assumed linear elastic behaviour of the bond line prior to peak stress.

5.2.2 Input for bond line model

The uniaxial piecewise linear relations that were used as input in the bond line model are shown for the three different adhesives in Figures 5.1–5.3. Tri-linear relations were used for all the adhesives since this was considered to provide a reasonably good fit to the test results. The powers m and n that define the coupling between normal stress and shear stress in terms of Equation (5.5) were selected (where for all cases $m = n$) as 2.0, 1.0 and 1.5 for the RP, PUR and PVAc-adhesives, respectively (cf. Figures 4.5, 4.9 and 4.13). For the RP-adhesive, the initial stiffness was very high as compared with the other adhesive types tested. The RP-adhesive was also the only adhesive showing very little plastic (nonlinear) deformations, or none at all, prior to peak stress.

Since the RP-adhesive was very brittle, resulting in a non-uniform stress distribution at peak load, 10% higher values for the uniaxial strength were adopted here than reported in previous chapter. This increase was found to provide good agreement between the test results and FE-simulations of the small specimen. Accordingly, uniaxial strengths of 21.2 and 7.1 MPa were adopted for the RP-adhesive, for pure shear and for normal mode failure, respectively. The stress distribution at peak load for the shear deformation test involving RP-adhesive, as calculated in the FE-analysis, is shown in Figure 5.4. Note that the deformations in Figures 5.1–5.3 do not include the deformations in the wooden adherents whereas the deformations recorded in the experiments (Figures 4.28-4.29) do.

5.2.3 Comparison between simulations and tests

FE-simulations of the tests involving small specimens were carried out using the uniaxial responses given in Figures 5.1–5.3. The material outside the bond line was modelled as being linear elastic and orthotropic and in a state of plane stress. The engineering constants were chosen (x denoting fibre direction) as $E_x = 16800, E_y = E_x/30 = 560, G_{xy} = E_x/16 = 1050$ MPa, $\nu_{xy} = 0.45$. The value of E_x stems from the introductory flatwise bending tests and the stiffness relations are based on [5]. For the material outside the bond line, 4-node isoparametric plane stress elements were employed. The finite element mesh in an undeformed state is shown in Figure 5.5. The upper and lower boundaries of the model were prescribed so as to remain plane during deformation, thus resembling the glueing of the specimen to the testing machine. Figures 5.6, 5.7 and 5.8 show results of FE-analyses that were performed. For the normal-deformation test (see Figure 5.7), the simulation result differs considerably in terms of the horizontal force. The tests showed that the bond line at pure normal deformation gives rise to a shear force. This shear force is not predicted by the current bond line model. Another interesting phenomenon visible in Figure 5.7 is the fact that the maximum horizontal force occurred long after maximum vertical force was reached. Such non-simultaneous softening in mode I and II has been reported for solid wood by Wernersson [42].

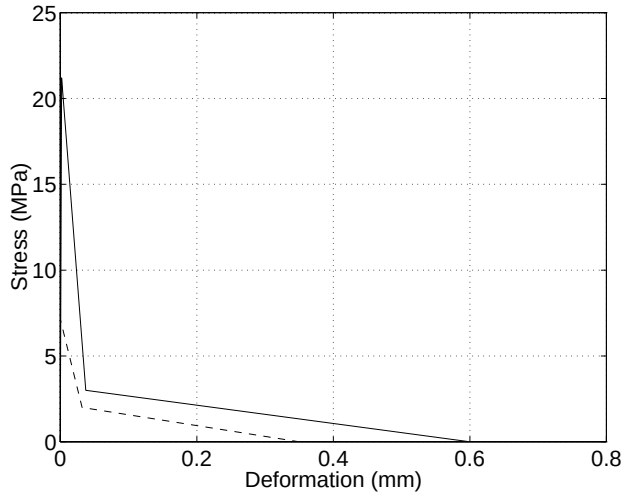

Figure 5.1. *Uniaxial input used for RP-adhesive in FE-simulations. The solid line corresponds to pure shear deformation, the dashed line to pure normal deformation.*

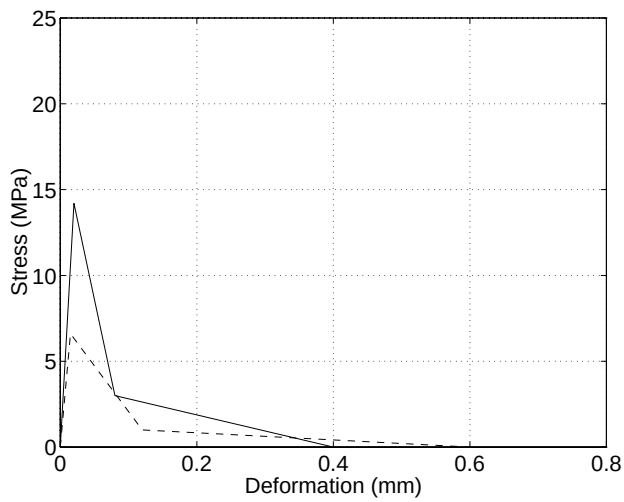

Figure 5.2. *Uniaxial input used for PUR-adhesive in FE-simulations. The solid line corresponds to pure shear deformation, the dashed line to pure normal deformation.*

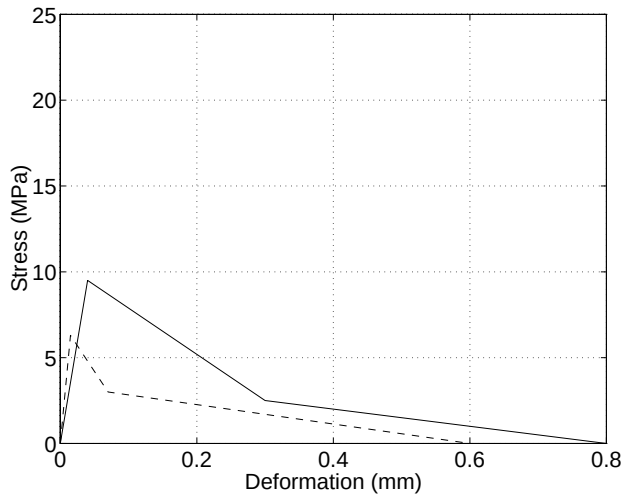

Figure 5.3. *Uniaxial input used for PVAc-adhesive in FE-simulations. The solid line corresponds to pure shear deformation, the dashed line to pure normal deformation.*

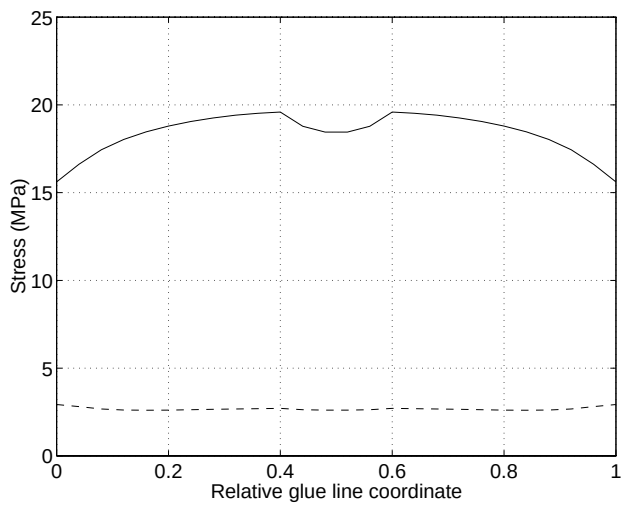

Figure 5.4. *Stress distribution at peak load for a small RP-glued test specimen as analysed by finite elements. The solid line represents shear stress and the dashed line normal stress.*

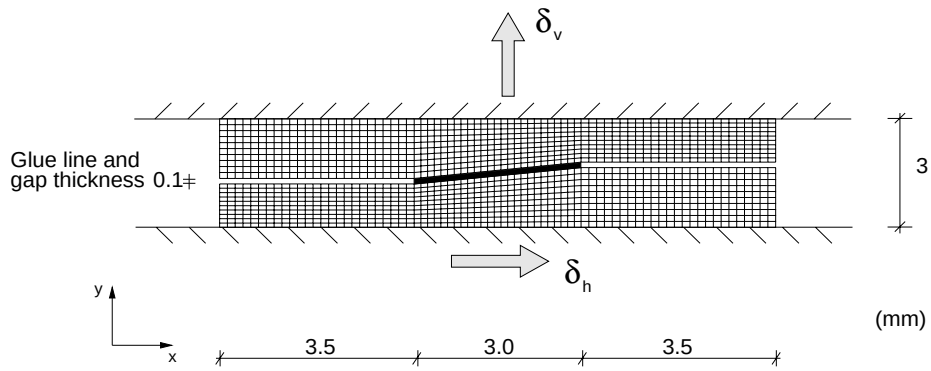

Figure 5.5. *Finite element mesh used to verify results of the small specimen tests. The dark area represents the bond line, modelled using 25 elements. Simulations were performed to simulate the shear-deformation tests, the normal-deformations tests, and the mixed mode tests.*

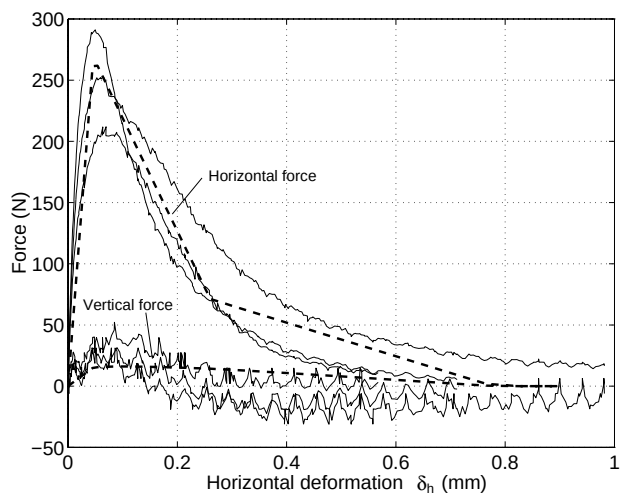

Figure 5.6. *Comparison of results of FE-simulation (dashed lines) with results of tests of the small test specimens (solid lines) for PVAc-glued bond in shear-deformation testing ($\delta_v = 0$). The forces relate to the directions defined as δ_h and δ_v in Figure 5.5.*

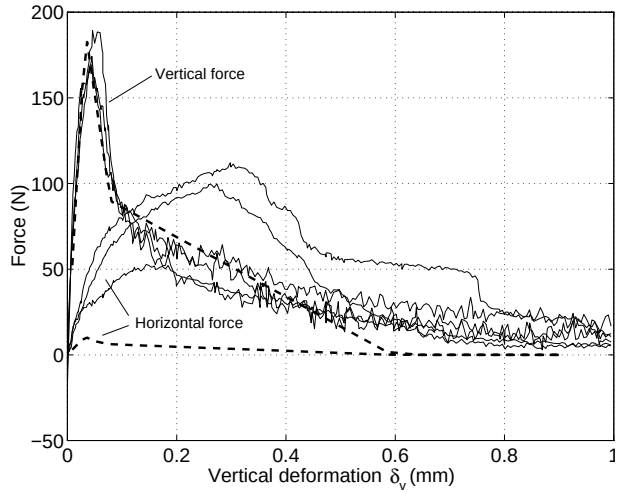

Figure 5.7. *Comparison of results of FE-simulation (dashed lines) with results of tests of the small test specimens (solid lines) for PVAc-glued bond in normal-deformation testing ($\delta_h = 0$). The forces relate to the directions defined as δ_h and δ_v in Figure 5.5.*

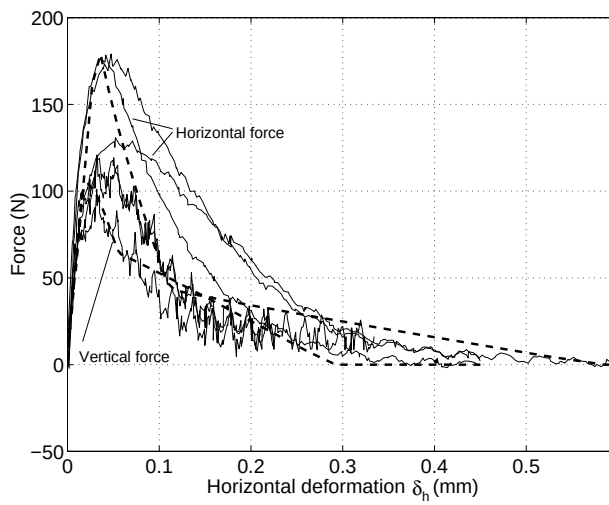

Figure 5.8. *Comparison of results of FE-simulation (dashed lines) with results of tests of the small test specimens (solid lines) for PVAc-glued bond in mixed mode testing ($\delta_h/\delta_v = 2$). The forces relate to the directions defined as δ_h and δ_v in Figure 5.5.*

5.3 Simulation of large test specimens

The results of the small specimen tests reported in the previous chapter provided input data to the bond line model. On the basis of the large specimen tests it was possible to estimate the modulus of elasticity in the fibre direction. The wood was assumed to be an orthotropic, linear elastic material having the following engineering constants (x denoting fibre direction): $E_x = 16800, E_y = E_x/30 = 560, G_{xy} = E_x/16 = 1050$ MPa, $\nu_{xy} = 0.45$. The value of E_x stems from the introductory flatwise bending tests and the stiffness relations are based on [5]. A finite element model of the large test specimens was constructed using these material data for the bond line and for the wood. The FE-model, shown in Figure 5.9, consists of about 10500 elements, of which 836 are bond line elements. Each bond line element is 0.5 mm long and 0.1 mm thick. There are about 10900 nodes altogether. Use was made of 4-node isoparametric plane stress elements for the material outside the bond line. A lamination is 421 mm long, 68.2 mm wide and 10 mm thick.

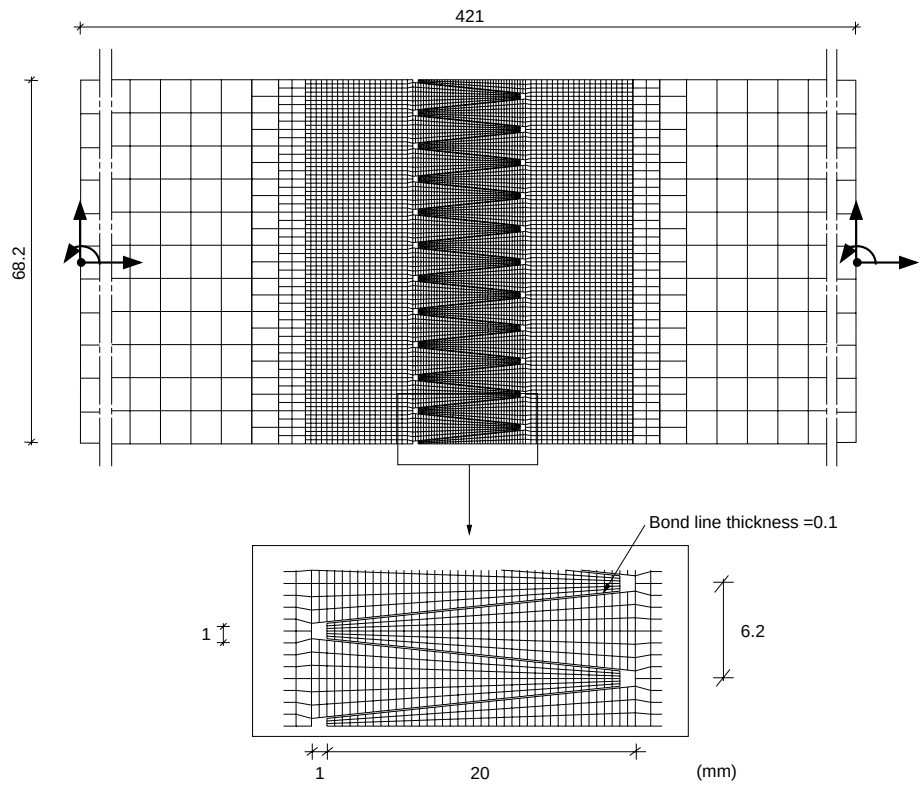

Figure 5.9. *FE-model used in the simulation of large-specimen tests.*

The loading was applied by prescribing the horizontal displacements at the nodes at the two ends of a lamination. These nodal displacements were assigned values corresponding to horizontal displacement and rotation of the ends of the lamination, the plane end-sections being assumed to remain plane during deformation. This loading results in a combined state of normal force and bending moment (edgewise bending). The bending was intended to resemble the bending that occurred in the tests. Since,

geometrically, the bond line represents a very small part of the model its influence on the global response in terms of the total elongation of the lamination is very small and negligible. From zero to maximum load, the global response of the lamination is thus an almost perfect straight line. The local performance in the vicinity of the finger-joint, which determines the load-bearing capacity of the lamination, is markedly nonlinear, however. Despite the strongly nonlinear performance of the bond line, from a global perspective the failure appears to be very sudden and brittle.

5.3.1 RP-glued finger-joint

The end rotation applied to the RP-glued finger-joint corresponds to an eccentricity of normal force that is almost constant during the entire course of loading (0.6 mm) and to a ratio of formal bending stress ($M/\left(bh^2/6\right)$) to normal stress (N/A) of 0.05. The end rotations applied are equivalent to a 0.003 rad. rotation of each end per 2 mm total elongation of the specimen. Using as input the results of the small specimen tests, the most stressed bond line was found to reach the maximum stress at approximately 25% of maximum global load. In other words, a conventional maximum stress failure criterion would underestimate the load-bearing capacity of the finger-jointed lamination by about 75%. The ultimate load was found to be 51.9 kN, equivalent to a mean normal stress of 76.1 MPa. Due to the small eccentricity of the load that was applied, the maximum nominal stress at the edge was still larger: 79.9 MPa. The results of the simulation of the RP-glued finger-joint are shown in Figures 5.10–5.12.

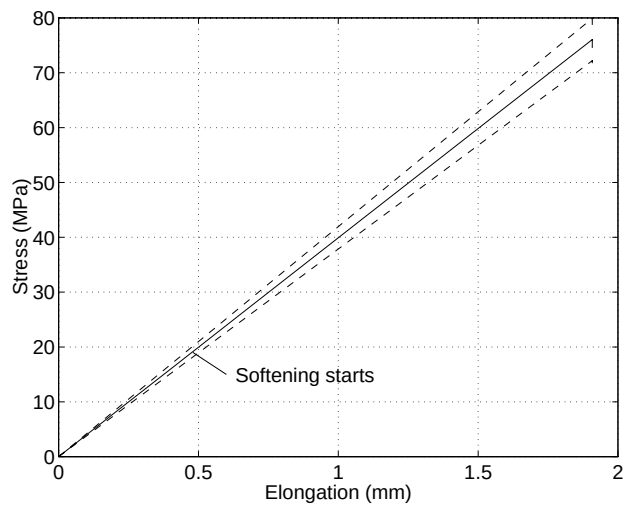

Figure 5.10. *Stress versus total elongation of finger-jointed lamination glued with resorcinol. The solid line shows the mean stress in the cross-section and the dashed lines show the stress at the edges.*

It is of interest to note that at peak load approximately 1/3 of the bond length at the outermost finger has started to soften (become partly damaged). It is instructive to compare the total elongation of the lamination at maximum load with the elongation

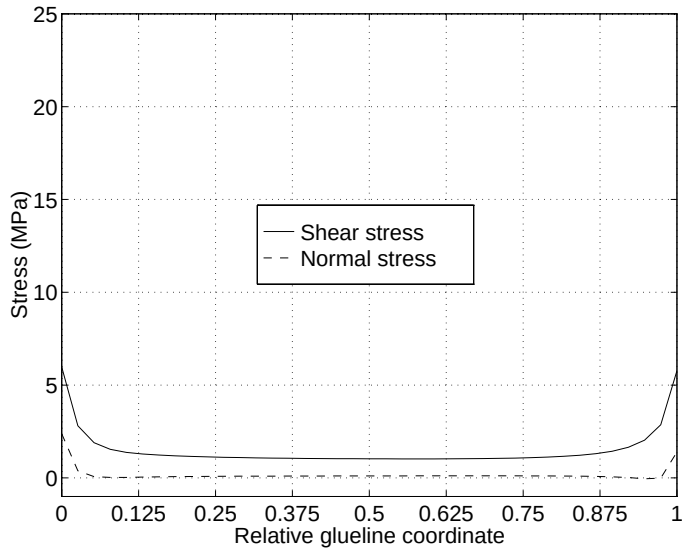

Figure 5.11. *Stress distribution in the outermost bond line of a resorcinol finger-joint at 10% of maximum load (elastic state).*

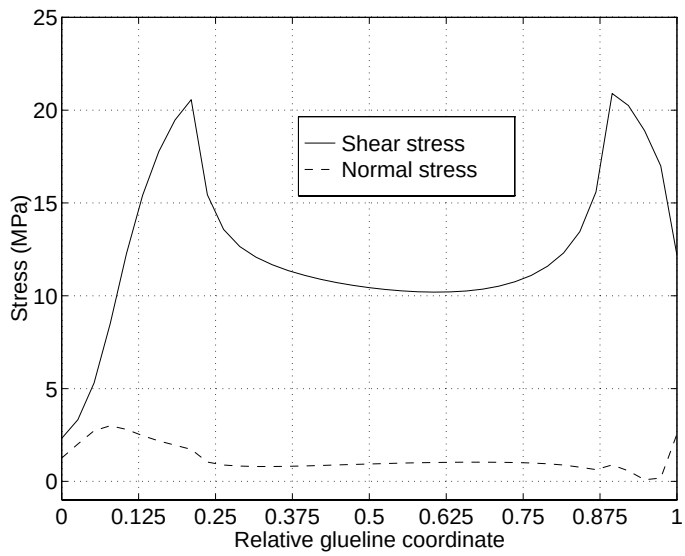

Figure 5.12. *Stress distribution in the outermost bond line of a resorcinol finger-joint at maximum load.*

predicted for a solid lamination by ordinary beam theory i.e.

$$\delta = \frac{L}{EA} \cdot P_{ult} = \frac{421}{16800 \cdot 68.2 \cdot 10} \cdot 51.9 \times 10^3 = 1.907 \ mm \tag{5.12}$$

The FE-analysis indicated the total elongation of the finger-jointed lamination to be 1.919 mm at maximum load. The deviation from this is less than 1%.

5.3.2 PUR-glued finger-joint

The PUR-glued finger-joint was also analysed using the results of the small specimen tests as input. The large specimen tests indicated certain eccentricity to occur during testing. The finger-joint was thus given an end rotation, one about twice that given the RP-glued finger-joint, or in other words a rotation of each end-section of 0.006 rad. per 2 mm of total elongation of the lamination. The ultimate load-bearing capacity of the finger-joint was found to be 37.8 kN, corresponding to a mean normal stress of 55.4 MPa. Due to the eccentricity given, the maximum nominal stress in the cross-section of the lamination was 61.1 MPa. Figures 5.13–5.14 present the results of these simulations in terms of stress distribution along the mostly stressed bond line. At peak load, approximately 35% of the outermost bond line had started to soften. Figure 5.15 shows a contour plot of the longitudinal stress at maximum global load. The maximum local stress parallel to the grain is approximately 110 MPa, which is in the same range as the expected strength of the clear wood in the longitudinal direction. According to the calculations, the mostly stressed bond line element reached maximum stress at approximately 60% of the global maximum load. Thus, a linear elastic, maximum stress failure criterion would underestimate the load-bearing capacity by 40%. Although the bond line behaviour is strongly nonlinear, the global response in terms of stress versus elongation is not. Just as for the RP-adhesive, this is due to the bond line representing geometrically only a very small part of the complete lamination.

5.3.3 PVAc-glued finger-joint

A PVAc-glued finger-joint was simulated using the same eccentricity as for the PUR-glued finger-joint. The ultimate global load was found to be 35.2 kN, corresponding to a mean normal stress of 51.6 MPa. The maximum nominal stress in the cross-section was 56.8 MPa. At approximately 65% of the global maximum load, the mostly stressed bond line element reached maximum stress and started to soften. The results of the simulations are presented in Figures 5.16 and 5.17, showing the stress distributions in an elastic state and at the maximum global load, respectively. For this very ductile adhesive, the outermost bond line in the finger-joint had softened along almost its entire length at peak load.

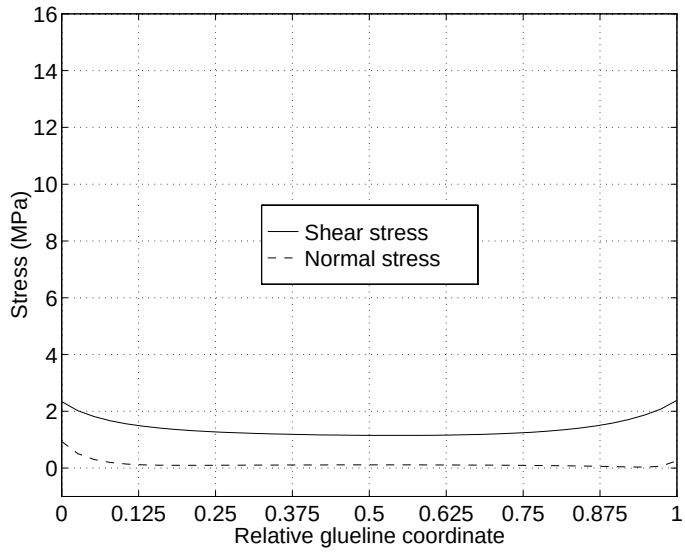

Figure 5.13. *Stress distribution in the outermost bond line of a PUR finger-joint at 15% of maximum load (elastic state).*

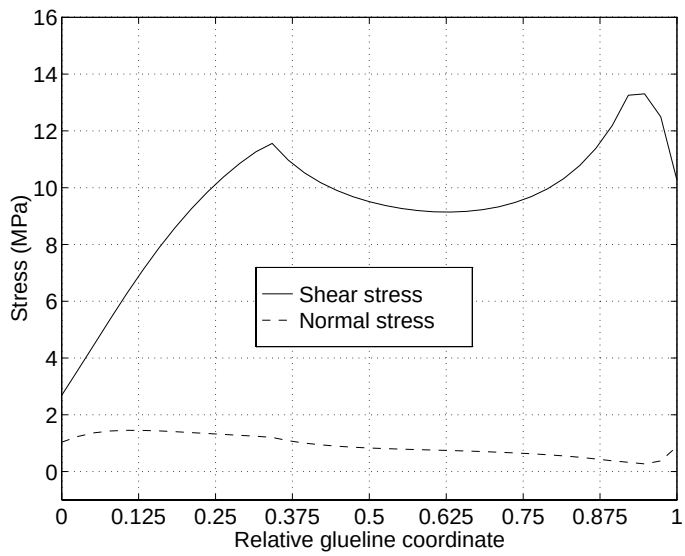

Figure 5.14. *Stress distribution in the outermost bond line of a PUR finger-joint at maximum load.*

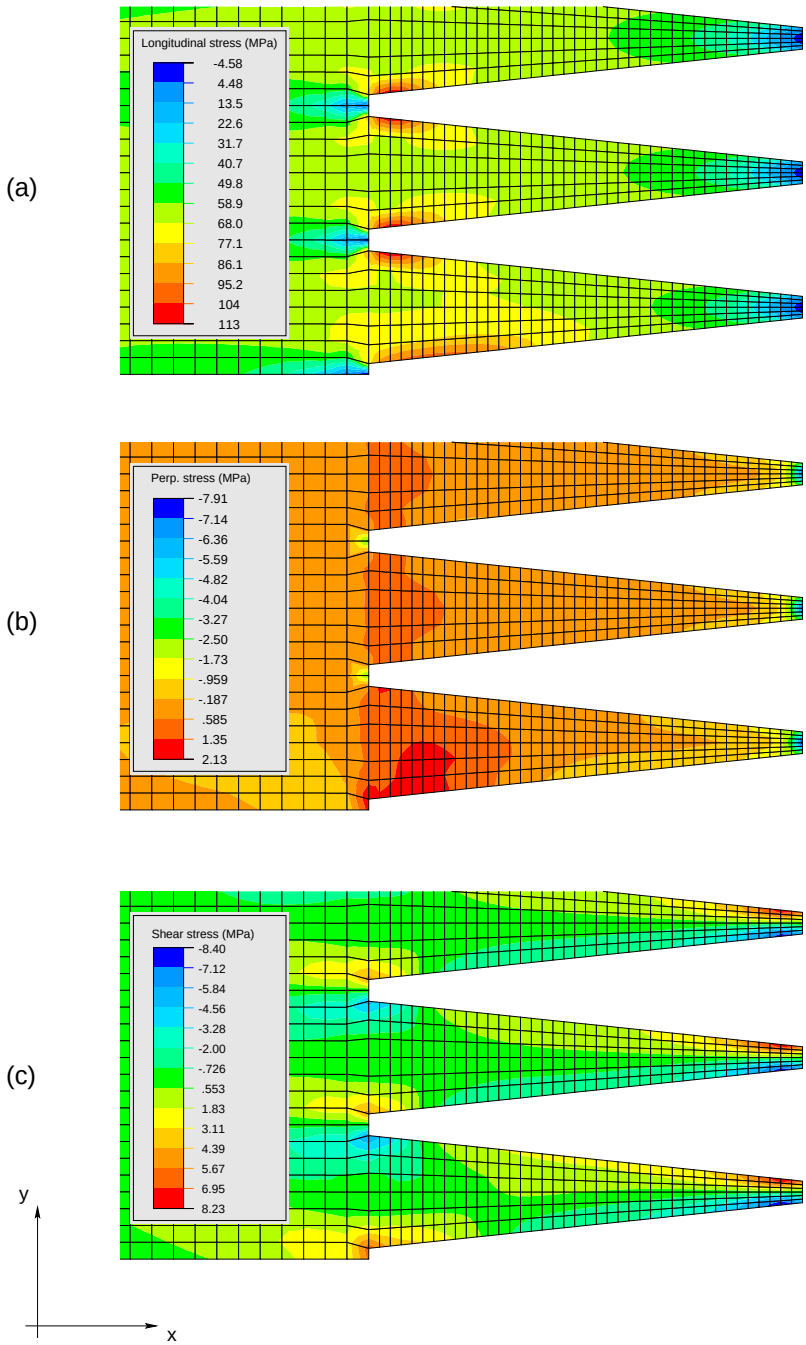

Figure 5.15. *Stress distributions at maximum load for a PUR-glued finger-joint. a–c show σ_{xx}, σ_{yy} and σ_{xy}, respectively (x denotes the fibre direction).*

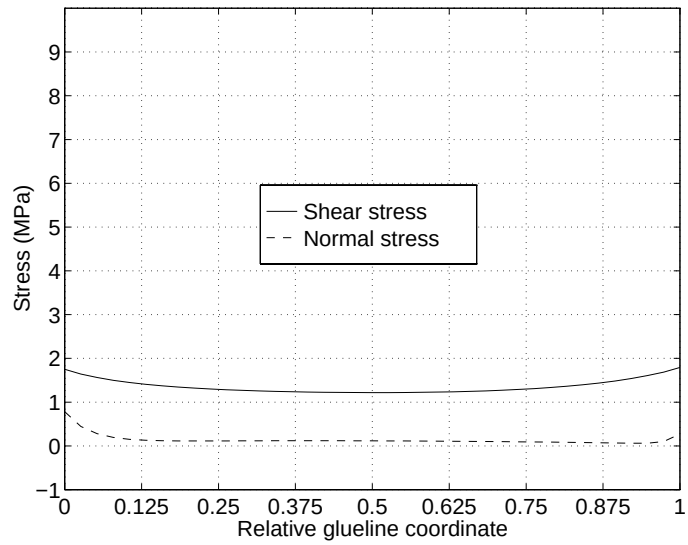

Figure 5.16. *Stress distribution in outermost bond line of PVAc finger-joint at 15% of maximum load (elastic state).*

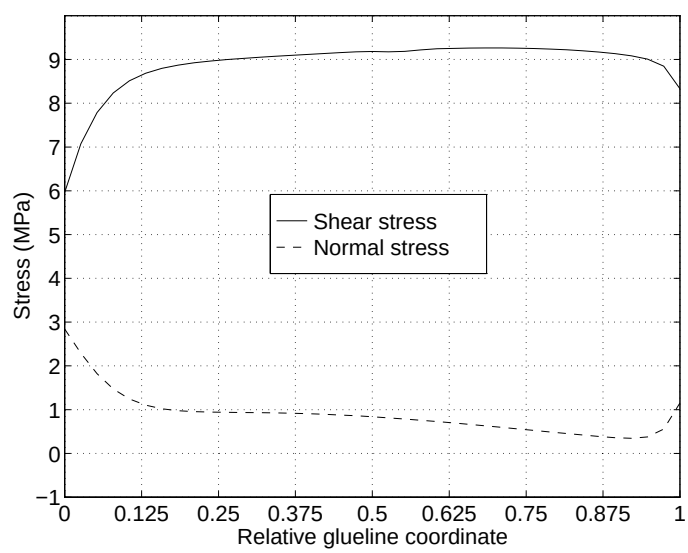

Figure 5.17. *Stress distribution in the outermost bond line of a PVAc finger-joint at maximum load.*

5.3.4 Simulation of pure tensile tests

As indicated in Chapter 4, the simultaneous bending of the lamination resulted in the maximum stress in the lamination present at failure being approximately 10% higher than the mean stress (see Table 4.1). Thus, if a tensile test is evaluated by measuring the mean stress only, e.g. by measuring the normal force, an apparent laminating factor will arise. By performing simulations of *pure tensile* tests this phenomenon can also be verified using the numerical model. The results of these simulations are summarized in Table 5.1. The results indicate that the load-bearing capacity of a lamination is indeed determined by the maximum formal bending stress in the cross-section rather than by the corresponding mean stress.

Table 5.1. *Maximum formal bending stress in cross-section at failure (MPa). The values for "bending" correspond to the simultaneous bending that occurred in the tests. The values for "no bending" correspond to a perfect pure tensile test.*

Adhesive	Bending	No bending
RP	79.9	79.9
PUR	61.1	61.0
PVAc	56.8	55.5

5.3.5 Comparison between simulations and tests

In order to facilitate the comparison between the simulations and the tests Table 5.2 gives a summary of the test results and the calculated strengths of the finger-joints. In this table, the test results refer to the estimated maximum stress in the cross section at failure according to the method of evaluation described in Chapter 3. This strength is denoted $f_{t,est.}$. For each adhesive, three different calculated strengths are also given. The strength denoted $f_{t,NLFM}$ is the strength predicted using the nonlinear bond line model. This strength corresponds to the ultimate loads previously reported in this chapter. The strength values denoted $f_{t,brittle}$ correspond to the load applied at the instant for which the strength of the bond line is reached in the mostly stressed bond line element. These values were reported previously in this chapter. Finally, the strength values denoted $f_{t,plastic}$ were calculated assuming the stress distribution along the fingers being completely uniform, and the ratio of normal stress to shear stress being equal to the slope of the finger-joint (0.105). In addition, the interaction formula given in Equation (4.1) was used with $m = 2.0$, 1.0, 1.5 for the RP, PUR and PVAc-adhesives, respectively. The strengths calculated in this manner closely correspond to the strengths predicted by a fully nonlinear analysis using the present bond line model and assuming the fracture energy to be infinitely large.

The simulations using the nonlinear bond line model give values that overestimates the strength of the finger-joint by 30–50%. The simulations based on this model, however, predict the strength of a finger-joint with approximately the same accuracy irrespective of the brittleness of the bond line. The strength prediction based on

maximum local stress ($f_{t,brittle}$), yield values that differ considerably for the brittle RP-adhesive whereas the value for the PVAc-adhesive coincides with the test result. The predictions based on a perfectly elastic-plastic bond line overestimates the strengths by 50–120%, the estimate again being the poorest for the RP-adhesive and better for the more ductile joints. The NLFM-approach can be said to be accurate although badly calibrated, whereas the two other approaches are not so accurate and, if correctly calibrated for one type of adhesive, only valid for a narrow range of brittleness of the adhesive. A model based on nonlinear fracture mechanics (NLFM), such as the one employed in this study, can be regarded as a unifying theory that includes the brittle failure at zero fracture energy and the perfect plastic failure as special cases. If such a model is correctly calibrated it will yield more accurate results than the results obtained by using a brittle or a perfectly plastic material model.

Table 5.2. *Comparison between tests and calculations of maximum formal stress in cross-section at failure (MPa).*

Adhesive	$f_{t,est.}$	$f_{t,NLFM}$	$f_{t,brittle}$	$f_{t,plastic}$
RP	56.6	79.9 (+41%)	20 (-65%)	125 (+121%)
PUR	46.7	61.1 (+31%)	37 (-21%)	72 (+54%)
PVAc	37.2	56.8 (+53%)	37 (-0.5%)	57 (+53%)

A probable explanation for the strength level prediction using NLFM being poor, is in terms of size effect due to variability in strength of the bond line (Weibull effect). The small test specimen results, which the simulations are based on, involved the testing of bond lines 3 mm in length. The total length of the bond line in the finger-joint is approximately 420 mm, i.e 140 times larger. A calibration of the bond line model using a lower strength than the one recorded in the small specimen tests is therefore well motivated, but since no data was available on the magnitude of the size effect (Weibull effect) in bond lines, this was not done. From the numerical results presented in Chapter 6 it is evident that even a single and small defect in the bond line can reduce the strength of the finger-joint significantly. Another explanation for the poor prediction using NLFM, is the uncertainties in the stiffness properties not measured in the present study. Although perhaps not of decisive influence, the stiffness relations assumed in the simulations of $E_x/G_{xy} = 16$ can of course also have some influence on the results. As studied in Chapter 6, differences in stiffness between the two adherents may influence the results.

6. Parameter Study and Numerical Examples

6.1 Parameter study of finger-joint

6.1.1 General remarks

A parameter study of factors affecting the load-bearing capacity of finger-joints was carried out. In this study the FE-model shown in Figure 5.9 was employed. The computational results are presented using the results for the RP-glued joint in a combined state of normal force and an edgewise bending moment as a reference case. All FE-simulations except the study presented in Subsection 6.3.1 were performed using the nonlinear fracture mechanics model described in Chapter 5.

Since the maximum local elastic stress in the bond line is already very high at a low external loading of the lamination, the behaviour of the bond line after peak stress is obviously crucial. The softening of the bond line can develop in a stable manner only as long as the elastic energy released can dissipate into the fracture process zone(s). The most obvious parameter to vary is thus that of the fracture energy. The strength of the bond line and the stiffness of the wood are other parameters of interest. The latter two parameters are perhaps the most obvious for a non-fracture mechanics approach. In performing a parameter study of say the fracture energy, one can proceed in a number of ways. If the normalized stress-deformation curves are kept unchanged, however, a parameter study can be performed in a simple manner. From nonlinear fracture mechanics using the fictitious crack model, it is a well established fact that the ultimate normalized strength of a structure is a function of two parameters only, the so-called brittleness number ω and a parameter γ that describes the shape of the stress-deformation relation [20]. The brittleness number ω is the ratio of the size of the structure to the characteristic length, l_{ch}, of the material in question, i.e.

$$\omega = d/l_{ch} = \frac{df_f^2}{EG_f} \tag{6.1}$$

where d is a measure of the size of the structure, E denotes the stiffness of the material, G_f its fracture energy and f_f its strength. A large brittleness number indicates that a linear elastic fracture mechanical approach is appropriate, whereas a small brittleness number indicates that an approach based on the assumption of a perfectly plastic material is useful. The influence of the brittleness on the load bearing capacity can be studied by nonlinear fracture mechanics using the fictitious crack model, for example. A comprehensive study of this sort can be found in the work of Gustafsson [20].

The normalized strength, $F_{ult}/(d^2 f_f)$, is a function of the brittleness of the structure, $df_f^2/(EG_f)$:

$$\frac{F_{ult}}{d^2 f_f} = \mathcal{F}(\frac{df_f^2}{EG_f}) \tag{6.2}$$

where $\mathcal{F}$ denotes an unknown function. Using a power function to approximate $\mathcal{F}$ yields

$$\frac{F_{ult}}{d^2 f_f} = C_0 \left(\frac{d f_f^2}{E G_f} \right)^{\beta} \quad \beta \leq 0 \tag{6.3}$$

where C_0 and β are constants. This is often a good approximation, at least if the variation in brittleness is small. Rearranging Equation (6.3) gives

$$\frac{F_{ult}}{d^2} = C_0 \; d^{\beta} f_f^{(2\beta+1)} E^{-\beta} G_f^{-\beta} \tag{6.4}$$

For the case of linear elastic fracture mechanics (LEFM) it can be shown that $\beta = -0.5$, resulting in

$$\frac{F_{ult}}{d^2} = C_0 \; d^{-1/2} E^{1/2} G_f^{1/2} = C_0 \sqrt{\frac{E G_f}{d}} \tag{6.5}$$

which is the square root size effect predicted by LEFM. For the case of $\beta = 0$, Equation (6.4) becomes

$$\frac{F_{ult}}{d^2} = C_0 \; d^{\,0} f_f E^0 G_f^0 = C_0 f_f \tag{6.6}$$

which corresponds to the load-bearing capacity being determined using a stress-based failure criterion.

In addition to studying the influence of brittleness, a series of simulations was performed in order to investigate the sensitivity to defects in terms of bond line voids.

Finally, a study of the effect of finger-jointing two pieces of lumber of dissimilar stiffness is presented. Such a study is of relevance since wood is a material with large variability in its material properties.

6.1.2 Large variations of brittleness

A parameter study of the influence of the brittleness ω on the load-bearing capacity of finger-joints was carried out. The different values of ω were obtained by changing the fracture energy of the material and letting the dimensions of the finger-joint be constant. Here, $\omega = (d\tau_{max}^2)/(EG_{f,II})$, with $d = 68.2$ mm, $\tau_{max} = 21.2$ MPa and $E = 16800$ MPa. The results obtained at very large brittleness numbers ω are somewhat uncertain. This is due to the fracture process zone (FPZ) being smaller for larger values of ω, resulting in too coarse an FE-mesh for the stress gradient present at these very large brittleness numbers. To avoid this and make the parameter study mesh-independent, element sizes should be chosen in relation to the size of the FPZ, a finer mesh thus being used for larger values of ω. The results of this parameter study are shown in Figure 6.1, where the dashed line indicates the somewhat uncertain values at high brittleness numbers.

6.1.3 Small variations of brittleness

A parameter study concerned with smaller variations in the fracture energy (± 25 and $\pm 50\%$) was also performed through changing the fracture energy for one mode at a time. Such variations provide valuable information on which mode of fracture is the governing one at failure. The results of these simulations are shown in Figure 6.2. The major outcome is that the energy contribution of mode I fracture to the load-bearing capacity is almost negligible. In the case of both the mode I and mode II

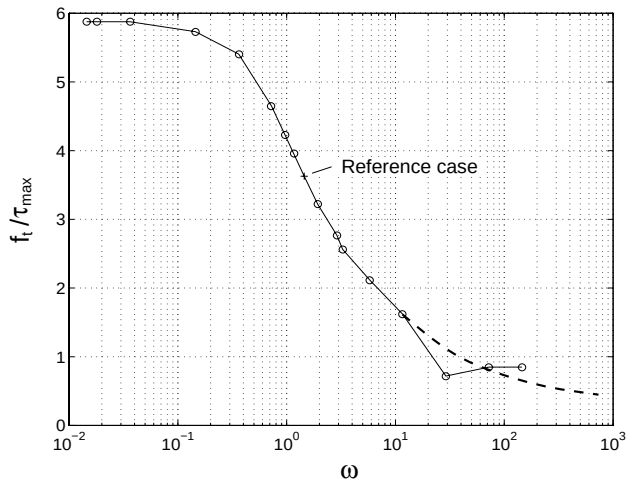

Figure 6.1. *Variation in normalized load-bearing capacity (f_t/τ_{max}) of a finger-jointed lamination (RP-adhesive) at different brittleness numbers (ω). f_t is the nominal maximum stress in the lamination according to ordinary beam theory, τ_{max} is the strength of the bond line (shear strength) and ω is the brittleness of the lamination as given by Equation (6.1).*

fracture energies being changed, a 1.0% change was found to cause approximately a 0.4% change in finger-joint strength. According to Equation (6.4), this corresponds to $\beta = -0.4$. This, in turn, corresponds to a 0.2% change in finger joint strength per 1.0% change in bond line strength. This prediction was confirmed by numerical simulations.

6.1.4 Defects in the bond line

In this study, two types of defects in the RP-bond line were simulated. First, various bond line elements were removed from the outermost, most highly stressed bond line only, followed by simulations of defects in the bond line at every finger tip of the finger-jointed lamination. The different types of defects are shown schematically in Figure 6.3. The results of the simulations are summarized in Table 6.1. The table shows that, for defects of small-size there is no decisive difference between the behaviour for a single defect at *one* finger tip and that for there being defects at *each* finger tip. There are 11 fingers in each half of the finger-joint. Each bond line is approximately 19 mm long, the bond lines thus having a total length of approximately $2 \cdot 11 \cdot 19 = 420$ mm altogether. Already with a single defect 1 mm in length, the reduction in strength is approximately 8%. It is very likely that defects of this magnitude are always present. This is the case for a brittle adhesive like the resorcinol. For ductile joints the failure takes place at almost uniform stress distribution, so that in the limiting case for a perfectly plastic bond line, the strength reduction will be proportional to the reduction in total bond length. This would for the finger-joint geometry studied, result in a $4 \cdot 11/420 = 10.5\%$ reduction in strength for defects of 1 mm length at each finger tip.

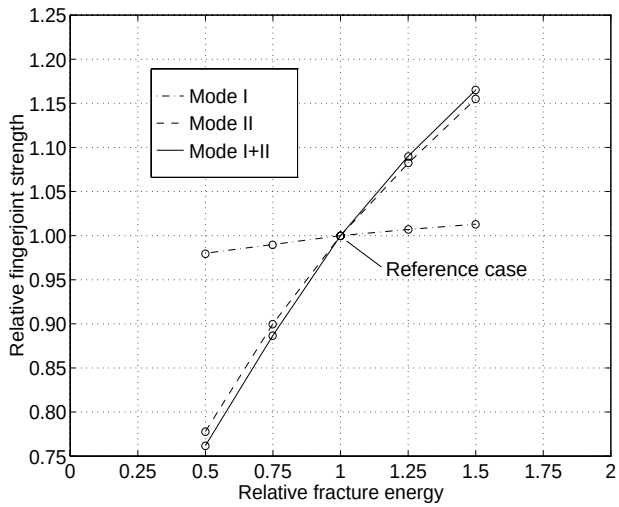

Figure 6.2. *Finger-joint strength as a function of fracture energy. The strength and fracture energies are normalized with respect to the reference case. A 1% change in both mode I and II causes approximately a 0.4% change in finger-joint strength.*

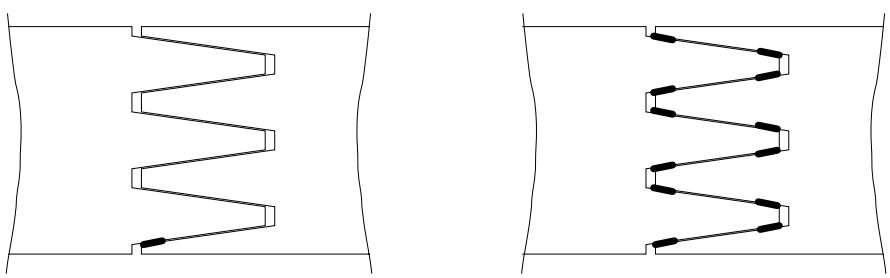

Figure 6.3. *Two types of defects were simulated: one defect at the outermost bond line only (left) and defects at every finger tip (right).*

Table 6.1. *Influence of defects in the bond line(s) on the strength of a finger-joint. The strengths of the finger-joints, f_t, are given in relation to the strength in the reference case, $f_{t,0}$.*

Size of defect (mm)	1 defect $f_t/f_{t,0}$	Defects at every finger $f_t/f_{t,0}$
0.50	0.960	0.956
1.00	0.923	0.913
2.01	0.860	0.830
4.02	0.767	

6.1.5 Finger-jointing pieces of dissimilar stiffness

In the reference case for this parameter study, it is assumed that the two pieces of lumber to be joined are exactly alike in stiffness. Since wood is a material showing large variability in its material properties, however, it is very likely that the two pieces are, in fact, dissimilar in stiffness. Thus, a series of analyses was performed in which the stiffness of one half of the finger-jointed lamination was varied. Since the reference value for the stiffness is rather high, $E_x = 16800$ MPa, this study was performed by letting one half of the finger-jointed lamination consist of a material with *lower* stiffness. The relations between the stiffness parameters in the different directions were kept unchanged so that (x denotes fibre direction): $E_x/E_y = 30, E_x/G_{xy} = 16$, $\nu_{xy} = 0.45$. If the stiffness of the two pieces to be finger-jointed is the same, the stress distribution along a finger is almost symmetric (cf. Figure 5.11), at least for the fingers in the middle of the lamination. However, if the two pieces differ in stiffness, the stress distribution is changed. This could readily lead to that a stiffness reduction in only one half of the finger-joint being more severe than a reduction in stiffness in the complete finger-joint.

A series of analyses involving reduced stiffness in the left and in the right half of the model, respectively, was performed using the FE-model shown in Figure 5.9. The reduction in the stiffness parameters was 20, 40 and 60%, respectively, corresponding to a modulus of elasticity in the fibre direction of 13440, 10080 and 6720 MPa. Since the stress distribution in the outermost bond line is not exactly symmetric, the case of the left side having a lesser stiffness is the more serious one. This can be explained by looking at Figure 5.12. From the figure it is evident that the left half of the bond line is more severely stressed than the right half. Now if the stiffness of the left half of the lamination is lower than that of the right half, the stresses transferred by the bond line are concentrated to the left half even more, resulting in the load-bearing capacity of the finger-joint being lowered. The results of the parameter study are summarized in Table 6.2. It should be noted that the simulations involving dissimilar stiffness in the two halves were made assuming the failure of the finger-joints to take place in the bond line and not in the wood itself. Since the strength of wood can be assumed to be correlated to its stiffness, it is possible, however, that large stiffness variations tend to lead to wood failure. This was not included in the present study.

Table 6.2. *The influence of finger-jointing pieces of dissimilar stiffness. The reduction in strength in percent compared with the reference case is also given.*

E_{left}/E_0	E_{right}/E_0	f_t	$\Delta f_t[\%]$
1.0	1.0	79.9	0
0.8	1.0	69.3	-13
0.6	1.0	57.5	-28
0.4	1.0	46.7	-42
1.0	0.8	75.4	-6
1.0	0.6	61.9	-23
1.0	0.4	47.2	-41
0.8	0.8	73.4	-8
0.6	0.6	65.3	-18
0.4	0.4	54.6	-32

6.2 Numerical example – strain softening of finger-joints

6.2.1 General remarks

In order to use the results of a finger-joint simulation in subsequent analyses of a glulam beam it is necessary to evaluate the force-elongation relation of the joint. If the behaviour of the joint is known, the approach adopted for the bond at the bond line level, can be used at lamination level as well, by replacing the finger-joint in a glulam beam by nonlinear elements. The characteristics of such nonlinear elements would include the descending branch of the force-elongation relation of the finger-joint. However, as mentioned in connection to the simulations of lamination behaviour, the response of a complete finger-joint is unstable and the failure is sudden and brittle from a global point of view. This can be dealt with in several ways when numerical simulations are performed: by including inertia effects, by simulating a smaller part of the lamination and thereby building up less strain energy at peak load, and finally by using a solution technique that allows snap-back behaviour to be traced. The latter two approaches were used here for calculating the complete force-elongation relation of the finger-jointed laminations.

6.2.2 The complete force-elongation response of a finger-joint

By analysing only a small part of the finger-joint, in the manner that Wernersson describes [42], less strain energy is built up in the model, the problem thus becoming easier to solve numerically. By assuming that, due to symmetry, only a small part in the middle of a wide lamination needs to be analysed, the number of elements can be reduced considerably. The FE-model employed and the assumed symmetry conditions are shown in Figure 6.4. Each boundary is assumed to retain its initial plane shape without rotating. This means that the upper and lower boundaries in Figure 6.4 are kept parallel but that the distance between them is free to change during the analysis. Each boundary node is free to move in a direction tangential to the boundary. In the model, use is made of polar symmetry. This means that the displacements at the nodes along a polar-symmetry line, on either side of the point of symmetry, are equal but opposite.

To enable the results to be compared with those obtained in the simulations of the large specimens, the same mesh was used. Furthermore, the so-called Riks algorithm was employed in the analysis, [22]. This is an arc-length method making it possible to trace snap-back behaviour. Figure 6.5 shows the basic idea of arc-length methods in the one-dimensional case. Instead of making equilibrium iterations at a certain load level, as is done for the case of Newton-Raphson schemes (ΔP, Δa_i), the load-displacement vector is swept following some pre-defined hyperplane or hypersphere in load-displacement space until equilibrium is reached (ΔP_i, Δa_i).

The results of the FE-analyses of the three different adhesives are shown in Figures 6.6–6.8. The diagrams, showing the response of the finger-joints in pure tension, are given as normal stress, f_x in Figure 6.4, versus elongation of the finger joint. The strengths of the finger-joints were found to be 88.2, 68.8 and 55.6 MPa for the RP, PUR and PVAc-adhesives, respectively. For the large model of the complete finger-joint, these values were 79.9, 61.0 and 55.5 MPa, respectively (see Table 5.1, "no bending"). The simplified model thus overestimates the strengths by 10% and 13% for the RP and PUR-adhesives, respectively, whereas the PVAc-glued finger-joint, due to

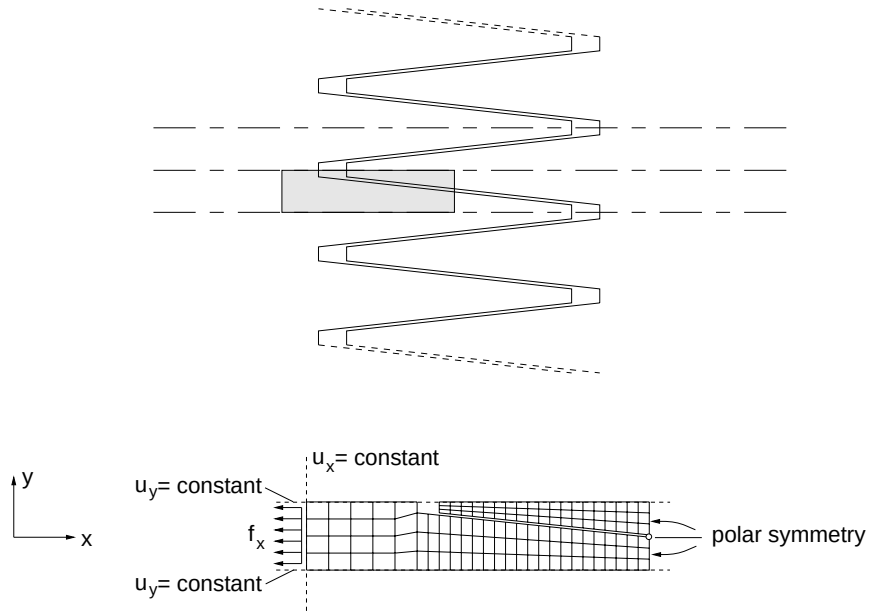

Figure 6.4. *Upper: By analysing only a small part of the finger-joint (the shaded area) the number of elements can be reduced considerably. Lower: The rather coarse mesh used in analyses of the complete load-elongation response of a finger-joint is the same as used in analyses of the large test specimens.*

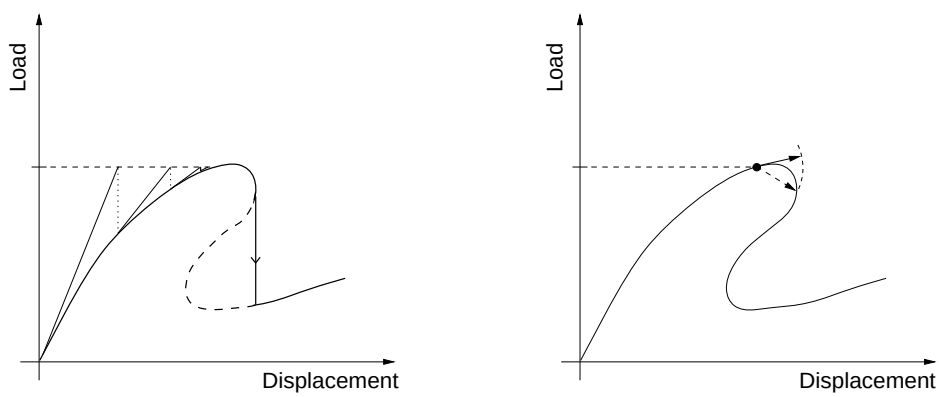

Figure 6.5. *Left: In using a Newton-Raphson scheme the iterations within each increment are made to a certain load. Right: The basic idea of arc-length methods is to sweep the load displacement vector until equilibrium is reached.*

its extremely ductile behaviour, is almost insensitive to the simplification made. The failure of the PVAc-glued finger-joint takes place at almost uniform stress distribution in the complete finger-joint, whereas the other types of adhesives give stress distributions that differ for the outermost fingers compared with the fingers in the middle of the lamination. In Figures 6.6–6.8, the responses of the finger-joints as calculated by the FE-program are denoted by a solid line. An equivalent response of a finger-joint is indicated by dashed lines. This equivalent response is calculated, reducing the elongation through subtracting the elastic deformation of a solid wooden member of the same length as the finger-joint that is analysed. Such an equivalent response can be used in a simplified model of a finger-joint by letting the joint be represented by nonlinear springs of zero initial length. These spring elements are then assigned stress–elongation responses equal to those indicated by the dashed lines in Figures 6.6–6.8. This approach is indicated in Figure 6.9. From the FE-analyses it is also possible to calculate the critical length of the different finger-joints. Here, the critical length means the length at which the response becomes unstable, i.e the descending branch of the stress-elongation response is vertical. For the three adhesives tested, these critical lengths were found to be 0.75 mm, 12.7 mm and 86.6 mm for the RP, PUR and PVAc-adhesive, respectively. Thus it is only the PVAc-glued joint that has a critical length larger than the finger-joint itself.

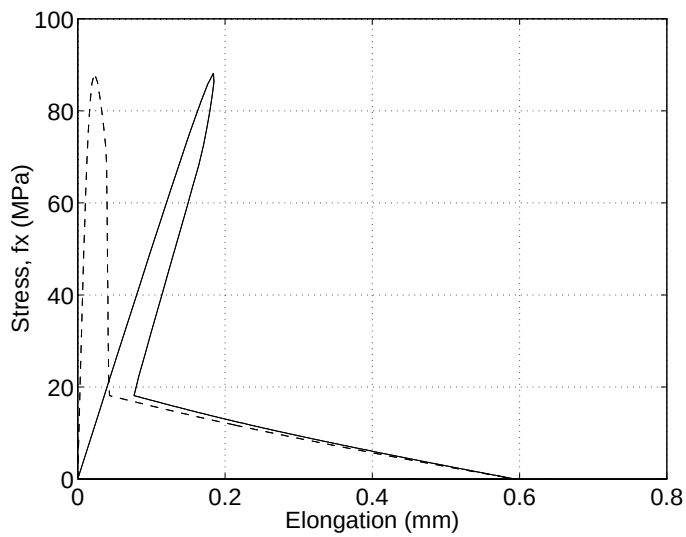

Figure 6.6. *Response of a RP-glued finger-joint. The solid line is the result of the FE-simulation. The dashed line is calculated by subtracting from this the elastic deformation of a solid wooden member of the same length as the finger-joint.*

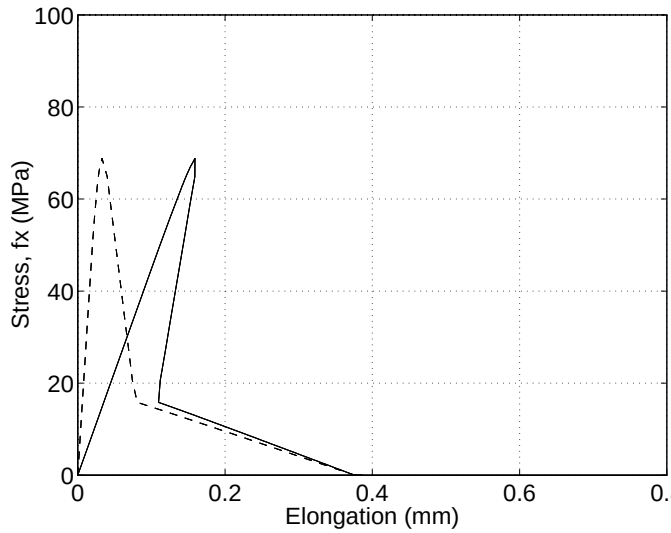

Figure 6.7. *Response of a PUR-glued finger-joint. The solid line is the result of the FE-simulation. The dashed line is calculated by subtracting from this the elastic deformation of a solid wooden member of the same length as the finger-joint.*

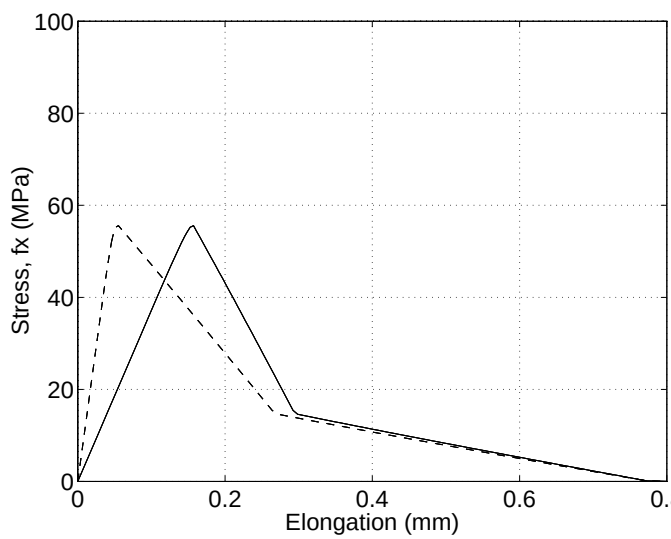

Figure 6.8. *Response of a PVAc-glued finger-joint. The solid line is the result of the FE-simulation. The dashed line is calculated by subtracting from this the elastic deformation of a solid wooden member of the same length as the finger-joint.*

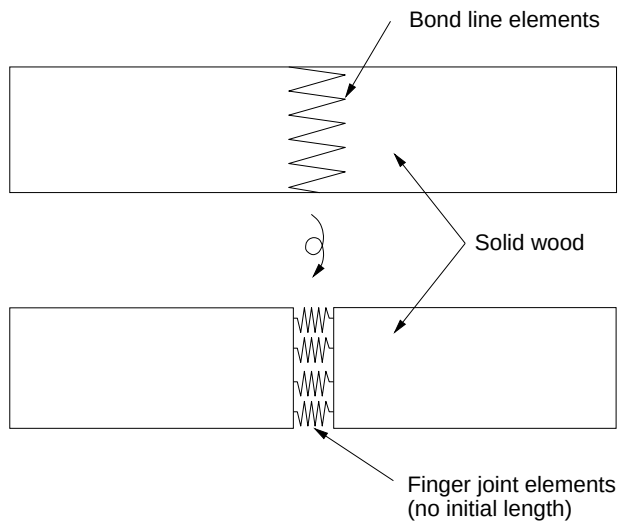

Figure 6.9. *A possible approach to simplifying the modelling of finger-joints. Instead of using a large number of bond line elements and a complicated geometry, equivalent elements representing the finger-joint response can be employed. The response of such elements is given in Figures 6.6–6.8 by the dashed curves. The figure is schematic, since no stiffness in the direction perpendicular to the lamination is indicated.*

6.3 Numerical examples - laminated beam behaviour

Two types of simulations of laminated beam behaviour are presented here. The first is a linear elastic analysis of a beam subjected to a pure bending moment, using varying stiffness parameters. These analyses were carried out in order to study the influence of stiffness variation on the stress distribution in a beam. The second type of laminated beam simulations concerns the nonlinear behaviour of the bond line of the outermost lamination. These simulations were performed in order to study the possibility of predicting the laminating effect by use of a fracture mechanical approach.

6.3.1 Influence of stiffness variation on stress distribution

In analysing a beam of non-homogeneous cross-section, an assumption commonly made is that plane sections perpendicular to the beam axis remain plane and perpendicular when the beam is deformed. This assumption leads to the well-known result of a piecewise linear stress distribution over the cross-section of a glulam beam consisting of laminations differing in their modulus of elasticity. According to these assumptions, a zone of lower stiffness would be subjected to stresses of lesser magnitude, in line with the reduction in stiffness. It is often claimed that such a "weak" zone (e.g. a knot or a finger-joint) of lower stiffness, and probably thus of lower strength too than adjacent material, would be subjected to stresses of smaller magnitude and would therefore not have so strong effect on global beam strength. The present analysis shows that a low stiffness zone is not necessarily relaxed in the way described above.

The load-case analysed is that of a glulam beam subjected to pure bending. The linear elastic analysis is performed using plane stress, 4-node, finite elements. At the boundaries where the bending moments are applied, plane sections of the beam are assumed to remain plane during loading. The beam is 315 mm in height, (7 laminations, each 45 mm thick) 600 mm in length and 100 mm in width. There is assumed to be a zone of lower stiffness in the outer tension lamination. The weak zone is 45 mm in height, its length varying from 7.5 mm to 600 mm in the different analyses. The finite element mesh used in the analyses is shown in Figure 6.10. In the weak zone, all the stiffness parameters are reduced by the same percentage, the surrounding material being assigned the engineering constants of E_x=12000 MPa, E_y=400 MPa, G_{xy}=600 MPa, and ν_{xy}=0.53.

Two types of analyses were performed. In the first series of analyses, the length of the weak zone was varied from its being of the same length as the beam (600 mm) to its being of the length of two finite elements in the fine-meshed area (7.5 mm), see Figure 6.10. In these cases, the stiffness parameters E_x, E_y and G_{xy} in the weak zone were assumed to be reduced by 25%. In the second series of analyses, the influence of varying the stiffness reduction was investigated. The weak zone, 30 mm in length, was reduced in stiffness by 25, 50, 75 and 100%, respectively. In both types of analyses, the height of weak zone was taken to be the same as the lamination thickness, i.e. 45 mm.

Results

The results of the finite element analyses are shown in Figures 6.11–6.14. Figure 6.11 shows the influence of the length of the weak zone on the stress distribution in the mid-section. As expected, when the weak zone is as long as the beam, the stress

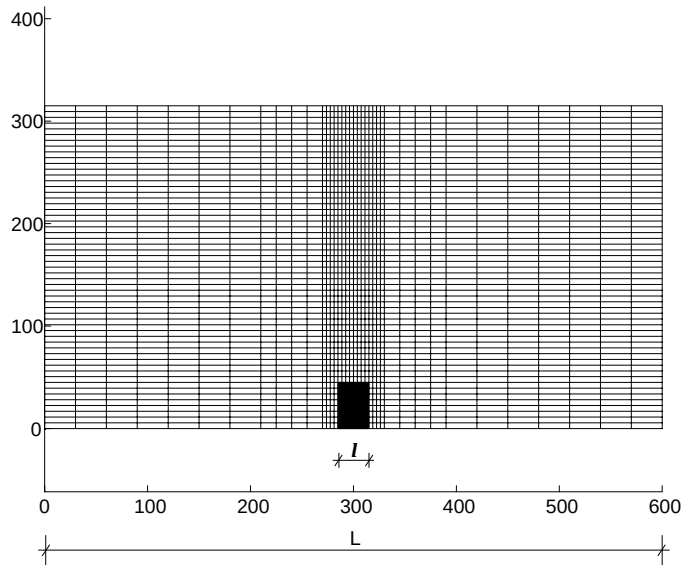

Figure 6.10. *Finite element mesh. The dark area is the weak zone, having a length in this case of 30 mm.*

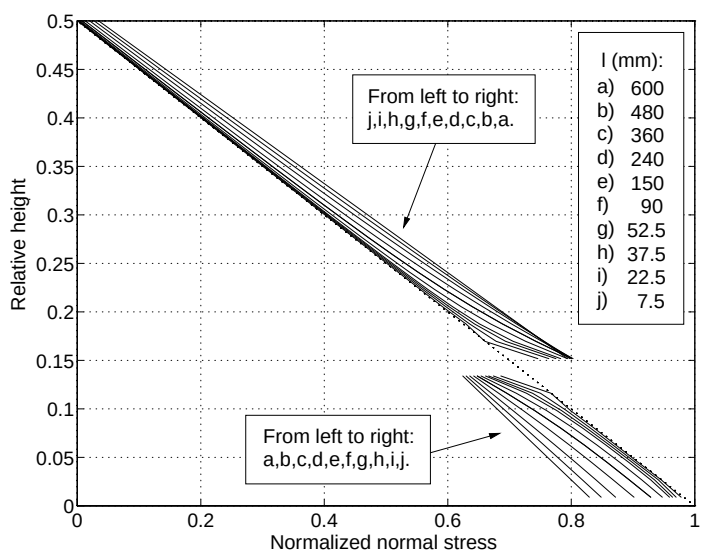

Figure 6.11. *Influence of the length of the weak zone on the stress distribution in the mid-section in the case of a stiffness reduction of 25% in the weak zone.*

distribution is indeed piecewise linear, in accordance with beam theory. A reduction in the extension of the weak zone results in a redistribution of the axial stresses. In the limiting case, as the length of the weak zone approaches zero, the stress distribution is found to approach the linear one expected in a homogeneous cross-section. According to beam theory, the length of the weak zone should not affect the stress distribution at all. Figure 6.12 shows the stress distribution in the mid-section of the beam for a

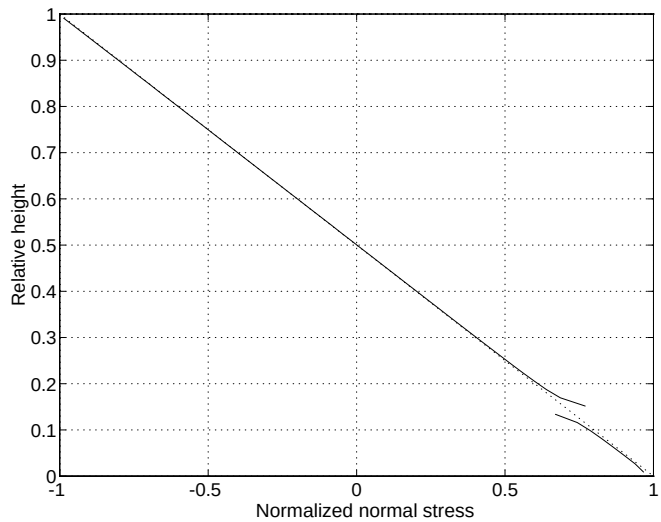

Figure 6.12. *Stress distribution in the mid-section of the beam for a length of the weak zone of 30 mm. The stiffness reduction is 25%.*

length of the weak zone of 30 mm. The reduction of the stresses in the weak zone is very local. In Figure 6.13 the influence on the axial tensile *force* (i.e. the mean stress in the outermost lamination) in the weak zone is shown. In the case of a weak zone 30 mm in length, the axial force is reduced by only about 3% for a stiffness reduction of 25%. In Figure 6.14 the influence of the stiffness reduction on the stress distribution in the mid-section is shown. The four curves represent a 25, 50, 75 and 100% reduction in stiffness, respectively. As expected, for a 100% reduction in stiffness, the stresses in the weak zone are zero, since the weak zone then represents a hole or a notch.

The analyses suggest that the simple assumption that a local reduction in stiffness and strength has only minor influence on beam strength is *not* valid for small zones such as knots and finger-joints. Since the stress reduction in a small zone is far from proportional to the stiffness reduction, the stress is closer to the strength of the material in a small weak zone than one would expect by intuition.

6.3.2 Laminating effect as predicted by fracture mechanics

Consider a glulam beam consisting of several layers of laminations, each having the same thickness Δh, Figure 6.15. The load case studied is that of a beam subjected to a pure bending moment. In the outer tension lamination, the beam contains a weak

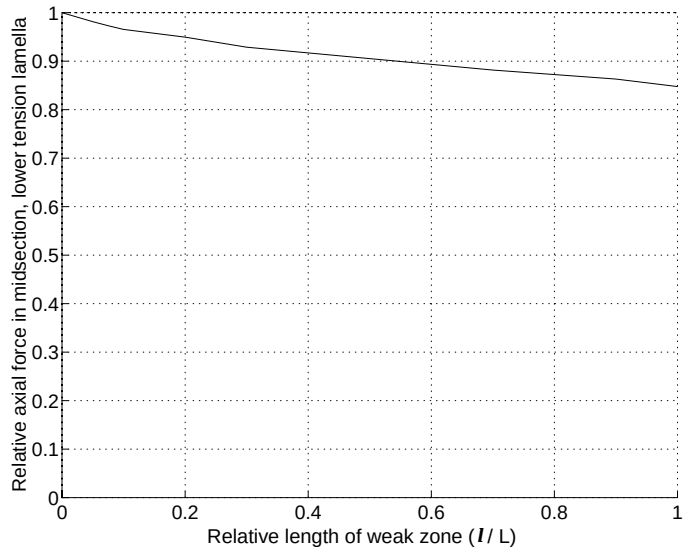

Figure 6.13. *Influence of the length of the weak zone on the axial tensile force in the outermost lamination. The stiffness reduction is 25%.*

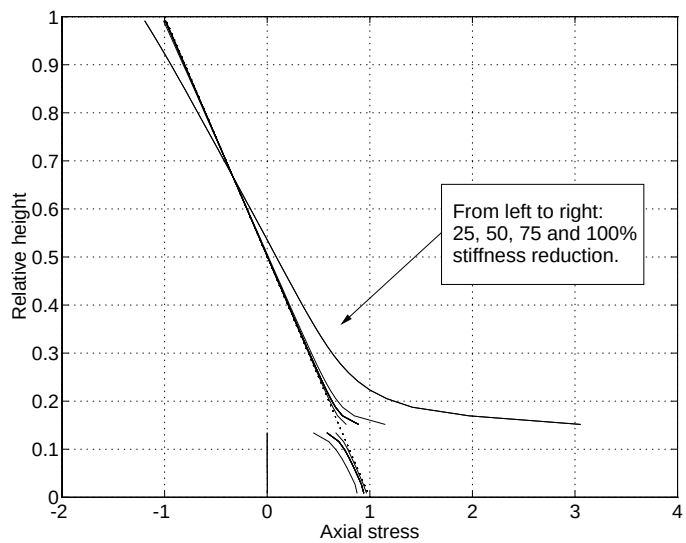

Figure 6.14. *Influence of the magnitude of stiffness reduction on the stress distribution in the mid-section. The curves represent 25, 50, 75 and 100% stiffness reduction, respectively. The weak zone has a length of 30 mm.*

zone representing e.g. a knot or a finger-joint. *If* the weak zone has failed and the beam still has load-bearing capacity left, its subsequent behaviour may be governed by crack propagation in the direction of the beam. The grain direction is assumed to coincide with the length axis of the beam. This situation is illustrated in Figure 6.15

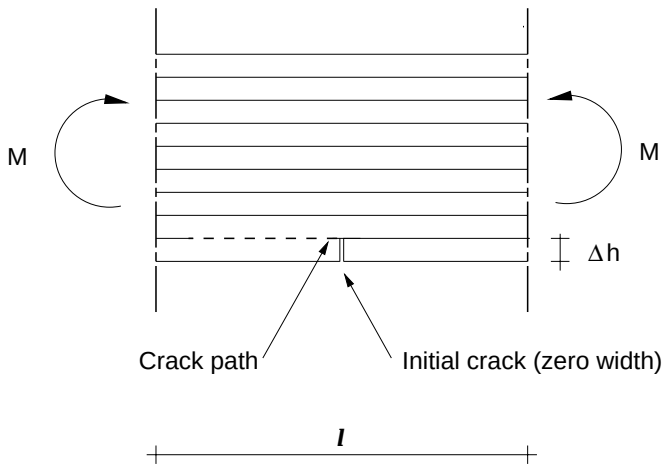

Figure 6.15. *A laminated beam with an initial crack of a length equal to the lamination thickness. The dashed line represents the crack path at crack propagation.*

Based on the assumptions of *linear elastic* fracture mechanics (LEFM), Petersson [32] derived an expression for the critical bending moment, M_c, at which a crack will propagate:

$$M_c = \sqrt{\frac{2 \cdot G_c \cdot b \cdot E \cdot I}{1/\alpha^3 - 1}} \tag{6.7}$$

where E denotes the modulus of elasticity in the fibre direction, G_c the fracture energy at crack propagation (the energy required to extend the crack a unit area), I the moment of inertia of the beam ($bh^3/12$, b is the beam width and h its height) and α the ratio $(h - \Delta h)/h$. To use Equation (6.7), the fracture energy must be known. However, since the fracture energy for wood varies from approximately 200–400 J/m^2 for pure mode I to about three times this value for pure mode II, the current mixed mode state must be known for an accurate choice of the value of G_c to be made. However, if the mode I value of G_c is used with (6.7) what is obtained is a lower bound and often a fairly accurate approximation.

If a more sophisticated analysis is desired, one needs not only to calculate the current degree of mixed mode at crack propagation, but also to take account of the effect of the gradual development of the fracture zone and its non-zero size. A nonlinear fracture mechanics approach such as that used in the present work allows this to be solved. To verify Equation (6.7), a series of finite element analyses were performed using the bond line model described in Chapter 5.

The case studied is that of a beam of height $h = 450$ mm and length $l = 1600$ mm, cf. Figure 6.15, subjected to a pure bending moment, assuming the plane end-sections

to remain plane during deformation. Since the analyses were performed taking the symmetry of the problem into account, only half of the beam in Figure 6.15 needed to be analysed. To investigate the laminating effect, five different lamination thicknesses Δh were studied, namely 50, 25, 12.5, 6.25 and 3.125 mm. In each case the length of the initial crack was assumed to be equal to the lamination thickness, as indicated in Figure 6.15. The finite element mesh used for the case of a 12.5 mm thick lamination is shown in Figure 6.16. The elements along the crack path are 0.8 mm long in the fine meshed area.

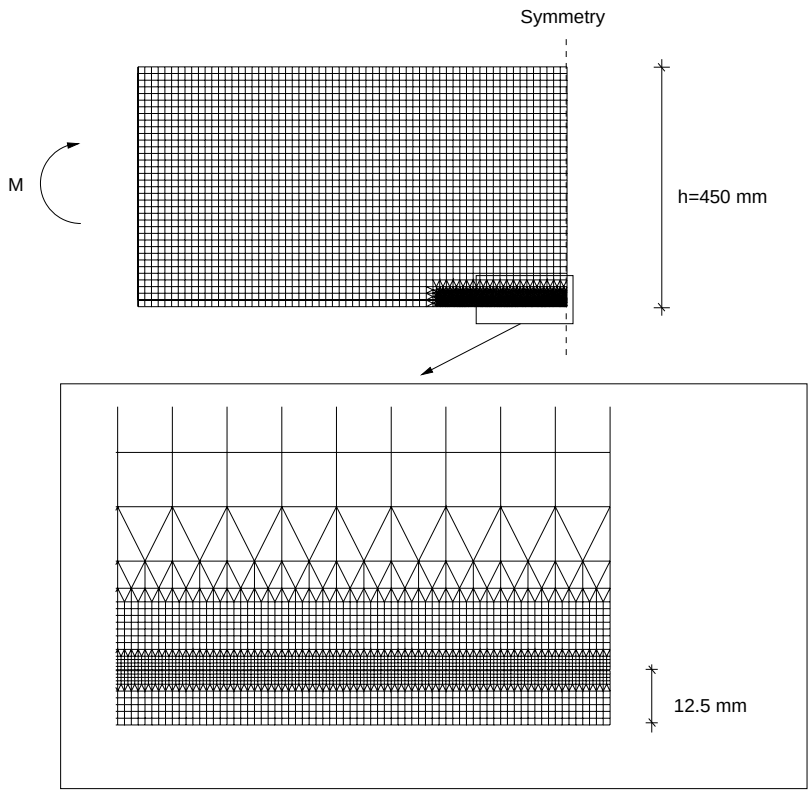

Figure 6.16. *Mesh used in finite element analysis. The mesh shown was used for a lamination thickness and an initial crack length equal to 12.5 mm. The bond line along which crack propagation is assumed to take place is in the middle of the fine-meshed area.*

The bond line data was chosen in accordance with the values given by Wernersson in [42], i.e. 6.5 and 10 MPa strength in modes I and II, respectively, the corresponding fracture energies being 360 and 980 J/m^2. The powers m and n as defined in Equation (5.5) were set to $m = n = 2$, and tri-linear uniaxial stress-slip relations were employed. The wood was modelled as being a linear elastic orthotropic material with the engi-

neering constants of E_x=16800 MPa, E_y=560 MPa, G_{xy}=1050 MPa, and ν_{xy}=0.45. The elements not representing the bond line are 4-node isoparametric plane stress elements or triangular constant strain elements for mesh refining. The deformed beam at maximum load is shown in Figure 6.17.

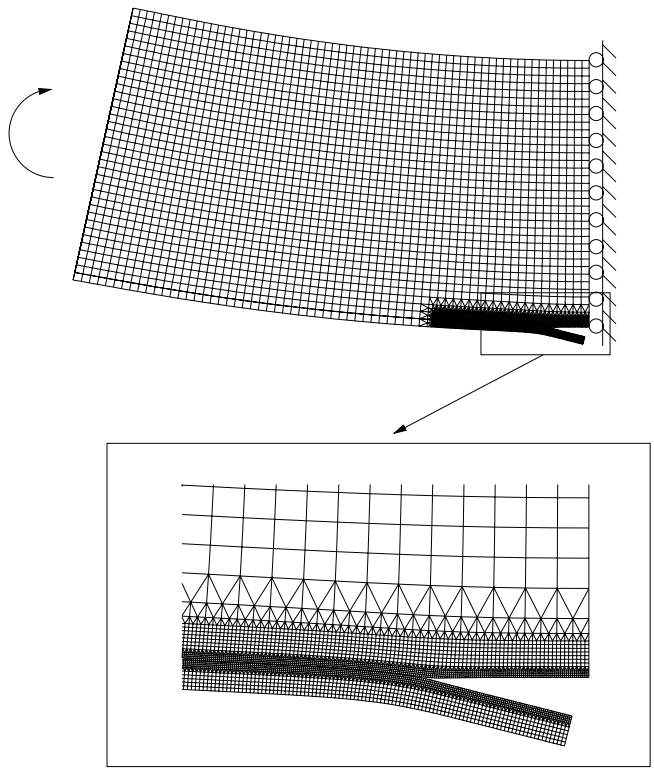

Figure 6.17. *The deformed beam at maximum load. The crack has extended 50–60 mm. The displacements are magnified by a factor of 30.*

The results of the five different lamination thickness simulations are shown in Figure 6.18. The five simulations are represented by circles, whereas the dashed lines represent results based on Equation (6.7) with $G_c = G_{Ic} = 360$ J/m^2 and $G_c = G_{IIc} = 980$ J/m^2. A major outcome of the simulations is that, as the lamination thickness decreases, the crack propagation is increasingly governed by mode II.

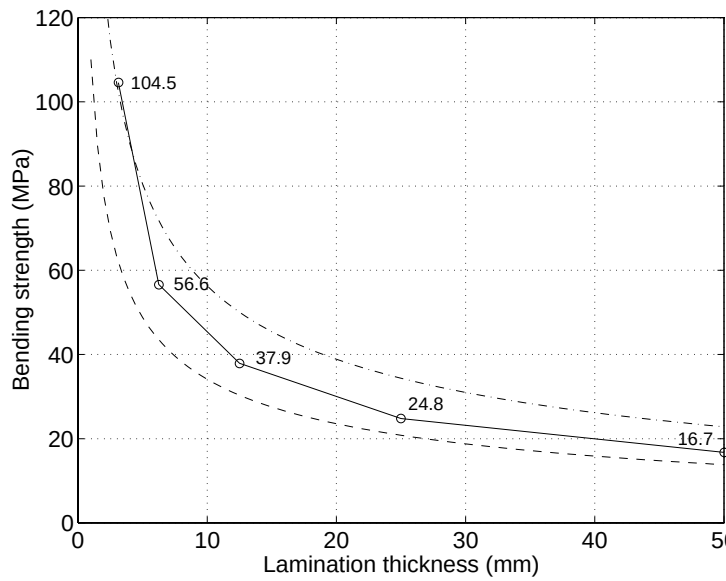

Figure 6.18. *Formal bending strength, $6M/(bh^2)$, versus lamination thickness for a laminated beam 450 mm in height. The circles represent results of FE-simulations. The dashed lines represent results based on Equation (6.7) for $G_c = G_{Ic}$ (dashed) and $G_c = G_{IIc}$ (dashed-dotted).*

Another way of presenting the results of the finite element analyses is shown in Figure 6.19, displaying the strongly nonlinear behaviour of the beam. This figure presents the formal bending stress in the outer lamination as a function of the position of the tip of the fracture process zone (as measured from the symmetry line). For all the analyses, the load reached a plateau-value. Since this corresponds to the propagation of a fully developed fracture process zone, constant in shape, LEFM can be expected to provide an accurate estimate of the peak load, provided the proper mixed-mode value of G_c is employed.

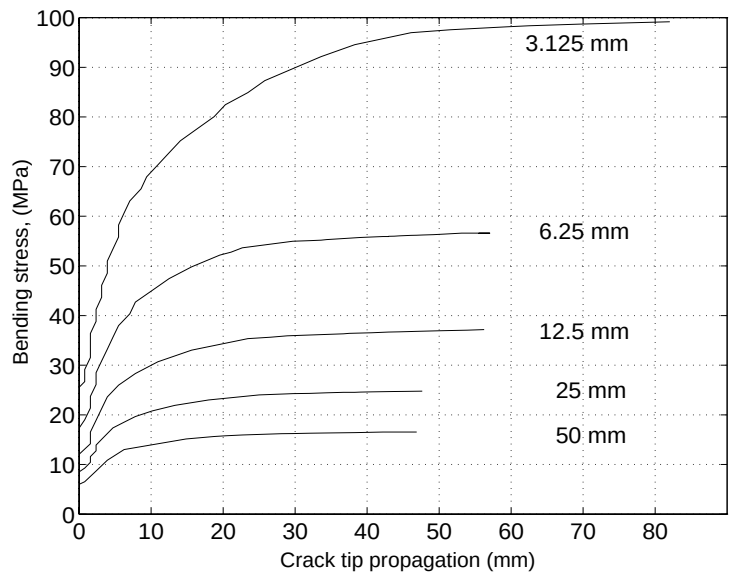

Figure 6.19. *Formal bending stress, $6M/(bh^2)$, versus crack tip position for various lamination thicknesses. The crack tip position is measured from the symmetry line, see Figure 6.16.*

Figures 6.20 and 6.21 show the stress distribution along the bond line of the outermost lamination at peak load for the cases of Δh being 12.5 and 3.125 mm, respectively. The 3.125 mm lamination gives a stress distribution that differs considerably from the distributions obtained for the thicker laminations. The thicker laminations have stress distributions very similar to that obtained for the case of Δh being 12.5 mm. The main difference is the size of the fracture process zone, which for the 3.125 mm lamination is approximately 48 mm long. For all the thicker laminations, the fracture process zone is approximately 25 mm long.

Figure 6.22 shows how the mixed mode state varies during crack propagation. The curves are given in terms of the mixed mode angle φ, as defined in Equation (5.4), versus the crack tip position. The value of φ is calculated at the peak shear stress position.

Finally, Figure 6.23 shows how the different contributions of mode I and mode II fracture depend on the lamination thickness. Again, it can be seen that a thin lamination yields almost pure mode II fracture.

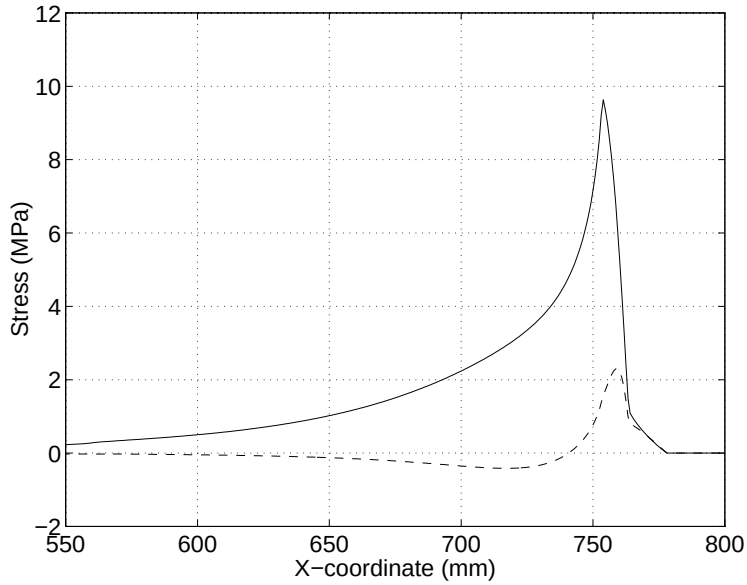

Figure 6.20. *Stress distribution along the bond line of the outermost lamination at peak load. The solid line corresponds to shear stress and the dashed to normal stress.* Δh *=12.5 mm.*

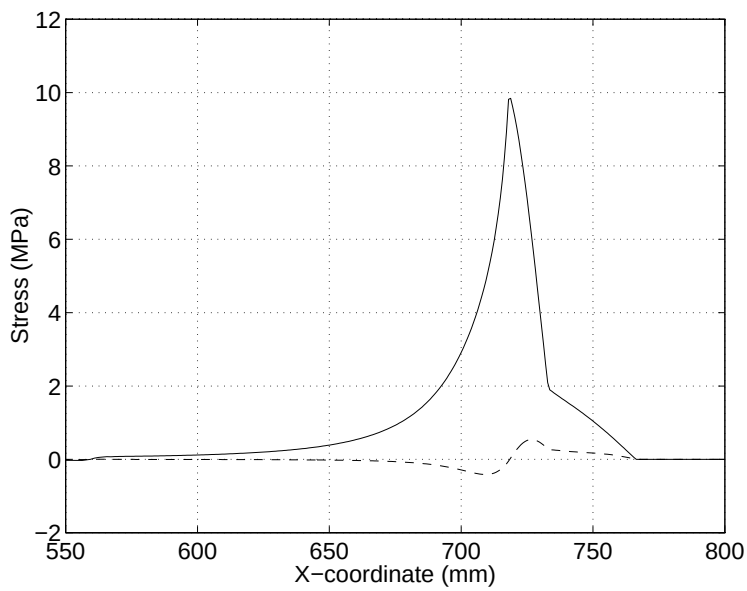

Figure 6.21. *Stress distribution along the bond line of the outermost lamination at peak load. The solid line corresponds to shear stress and the dashed to normal stress.* Δh *=3.125 mm.*

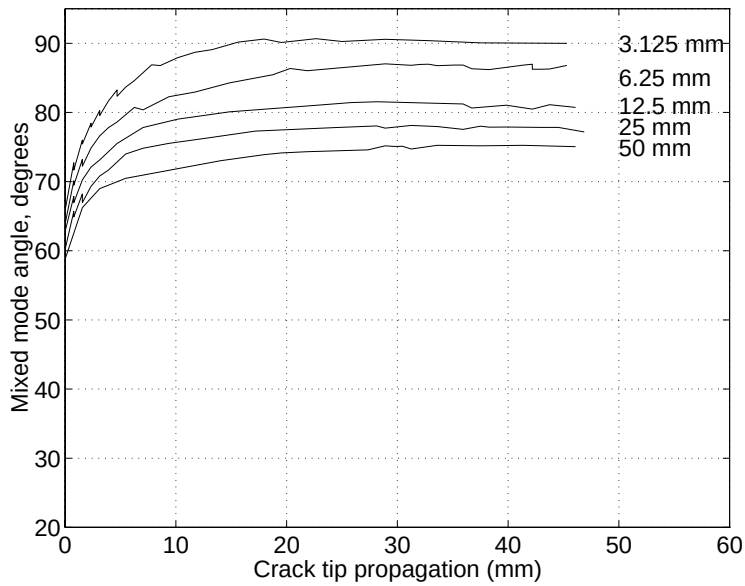

Figure 6.22. *Mixed mode angle φ as defined in Equation (5.4) versus crack tip position for different lamination thicknesses.*

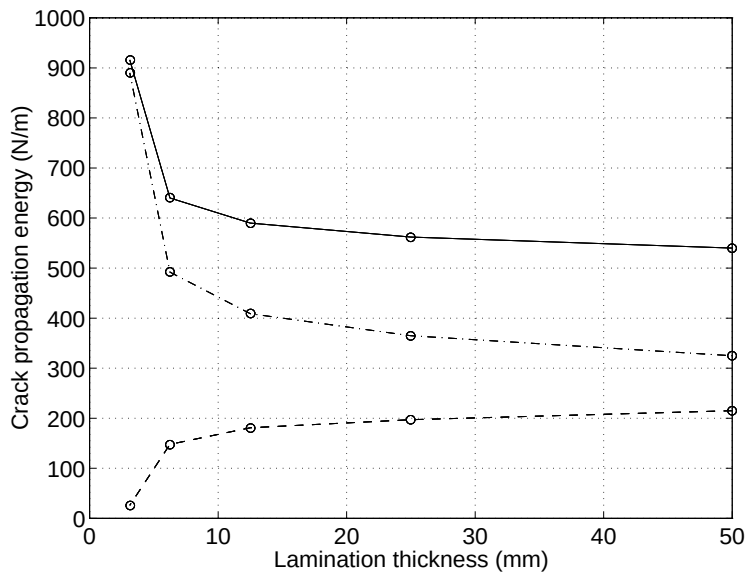

Figure 6.23. *Energy consumption for different lamination thicknesses at the propagation of a fully developed fracture zone (solid line). The dashed lines represent the contributions of mode I (dashed) and mode II (dashed-dotted), respectively.*

7. Concluding Remarks

7.1 Summary and conclusions

The use of laminated timber such as glulam makes it possible to overcome many of the disadvantages associated with the use of solid wood. Many of these disadvantages are related to size limitations and to the large variability in material properties. Such a phenomenon as the size effect, as explained by Weibull theory is well-known. Another phenomenon of interest, subject to many discussions in recent years, is the so-called laminating effect. The various studies presented in this report aimed at contributing to the development of partially new explanations of the above mentioned effects. Fracture mechanics provides the basis for these new explanations, both for the experimental and for the numerical investigations performed.

7.1.1 Experimental studies

The experimental programme involved testing the strength, the stiffness and the fracture mechanical properties of finger-joints and bond lines. The fracture mechanical properties were tested for three modes of deformation (shear, normal and mixed-mode) using three different adhesives: resorcinol-phenol (RP), 2-component polyurethane (PUR) and polyvinylacetate (PVAc). Since the bond lines tested were cut from finger-joints, the bond lines had an approximately 6° slope to the nominal grain direction. The tests aimed to record the complete stress–slip relation of the bond line. This was achieved for all three adhesives, although considerable difficulties were involved in testing the resorcinol adhesive due to its very brittle behaviour. The other two types of adhesive showed a much more ductile response, the PVAc-adhesive being the most ductile of the three adhesives tested. The PVAc-adhesive behaved in a clearly nonlinear way prior to peak stress. This was also the case for the PUR-adhesive, but was not noticeable at all for the RP-adhesive. In addition to the bond line tests, tests on finger-jointed laminations of nearly "structural size" were performed. These lamination tests were carried out in order to verify the bond line model by the use of finite element simulations of the tests.

The test results for the three adhesives showed little scatter and were found to be within three separate intervals. The small scatter in the results was probably due to the efforts made in the careful selection, production and matching of the specimens. Resorcinol-phenol is an adhesive much used for structural purposes. It also showed the highest strength of the three adhesives tested, the PVAc-adhesive being the weakest.

When a tensile test of a lamination specimen is performed, simultaneous bending deformations can occur. If these deformations are not restrained, as they are if the lamination is contained within a glulam beam, failure of the lamination will occur at a lower load level. In the tests performed here, the bending was constrained at the ends of the specimens through their being clamped to the testing machine. In addition, the bending deformations occurring were measured using strain gauges glued to the surface of the laminations. The lamination tests yielded values for the strength, evaluated as

(normal force)/(cross-section area), approximately 10% lower than the maximum stress actually occurring in the cross-section. Thus if the simultaneous bending moment occurring in the tensile tests is not taken into account when the strengths involved are evaluated, an apparent "laminating factor" of $k_{lam} = 1.10$, with k_{lam} defined as in Equation (2.3), will arise. The stresses in the different parts of the cross-section of the lamination were obtained by the use of strain gauges calibrated for centric tension and for pure bending.

7.1.2 Model verification

From the small-specimen tests, input data was available for performing numerical simulations of the behaviour of the different joints tested. Here, the nonlinear fracture mechanical bond line model of Wernersson [42], was employed, being implemented in an commercial FE-code, [22]. Verification of the method of evaluating the recordings obtained from the small specimen tests was done by simulating the small specimen tests themselves. To verify the applicability of the model to a complete finger-joint, several simulations of the lamination specimens were carried out. The tests of laminations with finger-joints glued with resorcinol yielded a mean value for the maximum formal stress of 56.6 MPa. The simulation of these lamination tests gave a strength of 79.9 MPa, which was a 41% overestimate. This overestimate can be mainly explained by size effect due to variability in strength. The small test specimen results showed the shear strength of the bond line to be very high (21.2 MPa) and it is not likely that the idealized situation in the numerical simulation is representative of the entire bond line in the finger-joint. The finger-joint has a total bond-line length of approximately 420 mm while the tests for bond line properties were carried out on specimens involving only 3 mm long bond lines. It should also be noted that a conventional linear elastic brittle finite element analysis, i.e. an analysis on the assumption of zero fracture energy, predicted the formal maximum stress at failure to be as low as 20 MPa, which is a 65% underestimate. If the bond line is modelled as being elastic-perfectly plastic the predicted formal maximum stress at failure would be approximately 125 MPa.

The simulations show that the model adopted is useful for the prediction of the load bearing capacity of finger-joints and also that, since the bond line is a very small part of the finger-jointed lamination, the response of the lamination is close to that of a perfect linear elastic member. This is the case if the test is viewed from a global perspective, in terms of load vs. total elongation. The bond line response is highly nonlinear, however, and the behaviour of the bond line after peak local stress is crucial for the overall strength performance of a lamination. Since, from a global perspective, the performance is linear elastic up to maximum load and the failure is sudden and brittle, it is easy to jump to the conclusion that the bond line behaves in the same way. In the present work it was clearly shown that such conclusions cannot be drawn. Simulations were performed for both centric tensile loading and tensile loading combined with the bending recorded during the tests. An outcome of these finger-joint simulations was that the load-bearing capacity of a lamination is determined by the maximum formal bending stress in the cross-section rather than by the mean stress. For the case of simultaneous bending in the lamination when a tensile test is performed, this yields an apparent *laminating effect* due to the method of evaluation.

7.1.3 Parameter studies

Parameter studies dealing with the load-bearing capacity of finger-joints were carried out, using the simulation of the RP-glued finger-joint as a reference case. These studies concerned the influence of various mechanical properties, the influence of small defects (bond line voids) and the influence of various stiffness variations in the wood in the vicinity of the finger-joint. One major outcome was that for a brittle adhesive such as the RP there is a large potential for increasing the finger-joint strength by increasing the fracture energy of the adhesive. Despite this, the fracture energy already present is very beneficial: for the reference values of material parameters it was found that already at approximately 25% of the global maximum load, peak stress was reached in the bond line element that was most stressed. This implies that a conventional brittle stress based failure criterion would underestimate the load-bearing capacity of the finger-joint by 75%. Study of the bond line voids showed that a RP-glued finger-joint is very sensitive to small defects. Even a single defect (void) 1 mm in length was found to reduce the load-bearing capacity of a finger-joint by approximately 10%. It is highly probable that, in practice, one or more defects of this size are present in most finger-joints. The influence of the stiffness being reduced in one or both of the two wood pieces that are finger-jointed was also examined. A reduction in the stiffness of the wood was found to lead to a reduction in the strength of the finger-joint. The results of the investigation also show that the strength of a finger-joint can be just as much influenced by only one of the pieces being of low stiffness as if the mean value of the stiffnesses is low. A 40% reduction in stiffness of the one half of the finger-joint would result in a reduction in the strength of 22% – 28%, whereas reducing the stiffness in both halves by the same amount would result in a reduction in strength of 18%. Indeed, for more severe reductions in stiffness, the strength should be primarily governed by the stiffness of the part that is least stiff. This is due to the fact that in the limiting case of one of the two halves being of zero stiffness, the strength would approach zero. In the case studied in which one half of the finger-joint was reduced in stiffness by 60%, the strength of the joint was found to be reduced by 41-42% (cf. Table 6.2). In the parameter study of brittleness, a 60% reduction in stiffness of the complete finger-joint resulted in a 32% reduction in the joint's strength. (cf. Figure 6.1 and Table 6.2). In the latter case, the strength reduction would be 37% according to LEFM, but 0% according to a conventional stress-based fracture criterion.

It was also found that a so-called arc length method such as the Riks' algorithm is useful for determining the complete load response of a finger-joint, at least in cases in which only a single finger and a short section of a lamination is modelled. The complete finger-joint response, in most cases characterized by snap-back behaviour, was calculated using boundary conditions corresponding to an inner finger. These boundary conditions yielded an approximately 10–15% overestimation of the strength for the more brittle adhesives (RP and PUR), whereas the highly ductile PVAc-adhesive was insensitive to the simplification in modelling.

7.1.4 Simulations of laminated beams

Simulations of laminated beam behaviour were also carried out. In one set of simulations, linear elastic analyses of laminated beams of low stiffness in a small part of the beam were performed. It is often claimed that a weak zone in a glulam beam, i.e. a zone of low stiffness and thus probably also of low strength, would not be subjected to the

most severe stresses, since a high stiffness acts as a magnet to stress. It is often assumed that the stress reduction in a zone of low stiffness is proportional to the reduction in stiffness, leading to the well-known piecewise linear stress distribution according to ordinary beam theory. However, if such a low stiffness zone is small compared with the beam length, which most certainly is the case for knots and finger-joints, the analyses presented show that the stress reduction is almost negligible.

A second set of laminated beam simulations involved a fracture mechanics study of the laminating effect. Simulations of an initially cracked laminated beam were performed. The laminated beam was assumed to be made up of several layers of equal thickness, the bond line of the outermost layer on the tension side of the beam being modelled using the nonlinear bond line model. A hand calculation formula based on LEFM and given by Petersson [32] was used to verify some of the results of the nonlinear analyses. These calculations showed one reason for the load-bearing capacity of an initially cracked laminated beam being higher in the case of thin laminations than in the case of thick, is that at crack propagation the fracture mode changes. For thinner laminations, the fracture mode reaches a pure mode II, and since this mode is generally associated with the fracture energy being much larger, the load-bearing capacity increases correspondingly.

7.2 Laminating effect

It was stated in Chapter 2 that the laminating effect found in laminated products traditionally has been explained as an effect of the following:

1. In a laminated beam the defects are smeared out resulting in a more homogeneous material than solid wood. The probability of a defect's having a serious influence on the strength of the beam is less than it is in a single lamination.

2. A single lamination tested in pure tension, will bend due to knots and other anomalies. This is due to the stiffness not being constant over the cross-section of the lamination. If the same lamination was contained in a glulam beam, the rest of the beam would prevent such bending.

3. If a lamination that is tested contains knots or other zones of low stiffness, a pure tensile test does not represent the true stress distribution found in a beam that is subjected to pure bending. The adjacent stiffer laminations adjacent to it would then take up a larger part of the tensile stresses.

The present study aimed at giving partially new explanations to this laminating effect. The results of the experimental and numerical investigations performed can thus be summarized:

1. The smearing out or dispersion effect found in glulam beams was not investigated in the present study.

2. The tensile tests of finger-jointed laminations showed that even for the case of a short specimen being clamped to the testing machine, an apparent laminating factor of approximately 1.10 existed.

3. The linear elastic analysis of a laminated beam of varying stiffness showed that the stress relaxation in a tension lamination that contains a low stiffness zone of small size, is negligible.

4. The nonlinear analyses of a laminated beam with an initial crack showed there to be a small laminating effect. According to the analyses, this effect is only of importance, however, for laminations thinner than 10 mm.

7.3 Future research needs

The present work centered on the fracture mechanical tests carried out on small specimens, together with verifying tests carried out on matched samples of finger-jointed laminations. The constitutive model used to characterize the bond lines is a rather straightforward approximation of the response of a bond line tested in a bi-axial test. In future work, efforts should be made to improve the constitutive modelling of the bond lines through including the consideration of nonlinearities prior to peak stress and in the case of compressive normal stress. Also including time dependent strength and deformation and extending the model so that possible unloading can be treated in a more realistic manner, is of interest. The present model is a nonlinear elastic model, corresponding to reversible performance during possible unloading.

In the future it would also be of considerable interest to include the modelling of defects in the wood material, such as knots and deviations in grain. The fracturing of the wood itself is also a feature not included in the present study, emphasis having been placed instead on the characterization of the bond line. With improved constitutive models of the bond line and more realistic modelling of the wood, it would be possible to study fracturing both of the bond lines and of the wood itself. In future studies, such modelling at the structural-size level, could be of major interest. The main objective could be to model the behaviour of complete glulam beams, taking into account the nonlinear responses of the finger-joints and of the inter-laminate bond lines. In addition, Monte-Carlo simulations of the position of finger-joints and of other defects, in order to further investigate the laminating effect and size effect, could be of considerable interest.

An interesting phenomenon is the effect of pre-stressing. Pre-stressing is probably introduced in the production of finger-joints as well as in the production of laminated beams and its influence on the load bearing capacities might be of importance.

Another topic not much discussed in the report is that of the level of material modelling. In the present work, the wood was treated as a linear elastic orthotropic material, the orthotropic directions coinciding with those of the lamination or of the beam, whichever was the case. In modelling the small test specimens, the differences in mechanical properties between earlywood and latewood were not taken into account. Besides earlywood differing from latewood with respect to stiffness and strength properties, the microstructural differences between the two may very well play a decisive role in the adhesion of the adhesive to the substrate.

A. Test Results From Finger-joint Tests

As indicated in Chapter 4, each of the large test specimens was equipped with 10 strain gauges, 8 of which were actually used in the evaluations. The 8 strain gauges, 4 on each half of the specimen, made it possible to determine the modulus of elasticity separately for each half of the 9 specimens included in the present study. Measurements with the strain gauges were made both during the two introductory elastic region tests and during the test to failure under clamped conditions. In addition to the strain measurements, data was available from the LVDTs used in the final test to failure under clamped conditions. The LVDTs were mounted over a measuring length of approximately 150 mm, one on each flat side of the specimen, cf. Figure 3.4. All of these test data are given in Tables A.1–A.4. Table A.5 gives the estimated section forces at peak load, together with the maximum measured mean stress.

Finally, the different densities of the finger-jointed laminations and the corresponding moisture content are given in Table A.6.

Table A.1. *Modulus of elasticity of finger-jointed laminations evaluated by strain gauges during introductory pure centric tension tests.*

Glue	Specimen	E_{left} *(MPa)*	E_{right} *(MPa)*
RP	G15a	15700	17400
	G15b	16900	18200
	G15c	19200	17100
PUR	G33a	15400	15100
	G33b	16700	14600
	G33c	15800	16000
PVAc	G13c	19500	16700
	G13d	17500	17400
	G14a	14400	12500
Mean:		16450	
COV:		10.5%	

Table A.2. *Modulus of elasticity of finger-jointed laminations evaluated by strain gauges during flatwise bending tests.*

Glue	Specimen	E_{left} *(MPa)*	E_{right} *(MPa)*
RP	G15a	15900	17000
	G15b	16400	16700
	G15c	18400	17000
PUR	G33a	16900	16300
	G33b	18100	16200
	G33c	18700	17300
PVAc	G13c	18700	16600
	G13d	18200	17200
	G14a	14700	12500
Mean:		16800	
COV:		8.9%	

Table A.3. *Modulus of elasticity of finger-jointed laminations evaluated by strain gauges during tensile tests to failure under clamped conditions. The evaluation was made at 5–15 MPa.*

Glue	Specimen	E_{left} *(MPa)*	E_{right} *(MPa)*
RP	G15a	15400	16900
	G15b	16000	17000
	G15c	19000	17000
PUR	G33a	15600	15400
	G33b	17600	15300
	G33c	17000	17000
PVAc	G13c	20000	16900
	G13d	17900	18000
	G14a	15000	12400
Mean:		16630	
COV:		10.2%	

Table A.4. *Modulus of elasticity of finger-jointed laminations evaluated LVDTs during tensile tests to failure under clamped conditions. The evaluation was made at 5–15 MPa.*

Glue	Specimen	*E (MPa)*
RP	G15a	15800
	G15b	18500
	G15c	17300
PUR	G33a	16800
	G33b	15400
	G33c	16500
PVAc	G13c	16900
	G13d	16100
	G14a	12400
Mean:		16190
COV:		10.4%

Table A.5. *Estimated section forces at test to failure under clamped conditions (N,M_{flat} and M_{edge}) and maximum nominal stress according to beam theory ($f_{t,est}$). The mean stress measured (f_t) is also given.*

Glue	Specimen	N	M_{flat}	M_{edge}	$f_{t,est}$	f_t
		(kN)	*(Nm)*	*(Nm)*	*(MPa)*	*(MPa)*
RP	G15a	31.2	4.1	-18.9	51.9	46.8
	G15b	38.7	4.7	-21.6	63.7	56.3
	G15c	34.8	1.5	-11.6	54.0	50.3
PUR	G33a	25.6	1.7	54.1	46.8	40.0
	G33b	30.5	1.8	-14.0	49.0	41.6
	G33c	29.7	-0.1	6.8	44.2	44.7
PVAc	G13c	21.4	-1.4	29.6	36.3	32.0
	G13d	22.3	-2.9	-5.8	36.1	33.6
	G14a	22.5	-2.6	-37.6	39.2	35.0

Table A.6. *Density, ρ, and moisture content, w, of the finger-jointed laminations.*

Glue	Specimen	$\rho(kg/m^3)$	w (%)
RP	G15a	520	12.4
	G15b	536	12.4
	G15c	518	12.5
PUR	G33a	524	12.4
	G33b	509	12.6
	G33c	540	12.4
PVAc	G13c	562	12.7
	G13d	547	12.6
	G14a	480	13.0
Mean:		526	12.6
COV:		5%	2%

Bibliography

[1] ASTM D3737-91 1991. *Standard method for establishing stresses for structural glued laminated timber (glulam).*

[2] Aicher, S., Klöck, W. *Spannungsberechnungen zur Optimierung von Keilzinkenprofilen für Brettschichtholz-Lamellen.* Bauen mit Holz Vol. 92(5), pp. 356–362, 1990.

[3] Aicher, S., Klöck, W. *Finger joint analysis and optimization by elastic, nonlinear and fracture mechanics finite element computations.* Proceedings 1991 International Timber Engineering Conference, London, UK 1991.

[4] Bender, D. A., Woeste, F. E., Schaffer, E. L., Marx, C. M. *Reliability formulation for the strength and fire endurance of glued-laminated beams.* Research paper FPL 460. U.S. Department of Agriculture, Forest Service, Forest Products Laboratory 1985.

[5] Blaß, H. J. et al. (ed.). *Timber Engineering STEP1. Basis of design, material properties, structural components and joints.* First edition, Centrum Hout, The Netherlands, 1995.

[6] Bodig, J., Jayne, B. A. *Mechanics of wood and wood composites.* Van Nostrand. New York 1982.

[7] Colling, F. *Einfluß des Volumens und der Spannungsverteilung auf die Festigkeit eines Rechteckträgers.* Holz als Roh- und Werkstoff 44, pp. 121–125, 1986.

[8] Colling, F. *Tragfähigkeit von Biegeträgern aus Brettschichtholz in Abhängigkeit von den festigkeitsrelevanten Einflußgrößen.* Berichte der Versuchsanstalt für Stahl, Holz und Steine der Universität Fredriciana, Karlsruhe 1990.

[9] Colling, F. *Biegefestigkeit von Brettschichtholzträgern in Abhängigkeit von den festigkeitsrelevanten Einflußgrößen. Entwicklung eines statistischen Modells.* Holz als Roh- und Werkstoff 48, pp. 269–273, 1990.

[10] Colling, F. *Biegefestigkeit von Brettschichtholzträgern in Abhängigkeit von den festigkeitsrelevanten Einflußgrößen. Einfluß der Trägergröße und der Belastungsart.* Holz als Roh- und Werkstoff 48, pp. 321–326, 1990.

[11] Colling, F. *Biegefestigkeit von Brettschichtholzträgern in Abhängigkeit von den festigkeitsrelevanten Einflußgrößen. Überprüfung des statistischen Modells mit Hilfe von Trägerversuchen.* Holz als Roh- und Werkstoff 48, pp. 391–395, 1990.

[12] Colling, F., Falk, R. H. *Investigation of laminating effects in glued-laminated timber.* Proceedings CIB-W18. Åhus, Sweden, 1993.

[13] Dinwoodie, J. M. *Timber its nature and behaviour.* Van Nostrand. Wokingham, 1981.

[14] Dinwoodie, J. M. *Wood. Natures cellular, polymeric fibre-composite.* The institute of metals. London, 1989.

[15] Ehlbeck, J., Colling, F. *Die Biegefestigkeit von Brettschichtholzträgern in Abhängigkeit von den Eigenschaften der Brettlamellen.* Bauen mit Holz Vol. 89(10), pp. 646–655, 1987.

[16] Ehlbeck, J., Colling, F., Wenz, J. *Prüfung der Tragfähigkeit von Keilzinkenverbindungen der Lamellen für Brettschichtholz.* Versuchsanstalt für Stahl, Holz und Steine. Universität Fredriciana, Karlsruhe, 1989.

[17] Falk, R. H., Solli, K. H., Aasheim, E. *The performance of glued laminated beams manufactured from machine stress graded norwegian spruce.* Norsk Treteknisk Institutt, Oslo, 1992.

[18] Foschi, R. O., Barrett, J. D. *Glued-Laminated Beam Strength: A Model.* Journal of the structural division, ASCE, Vol. 106, No ST8 pp. 1735–1754, 1980.

[19] Gehri, E. *Determination of characteristic bending values of glued laminated timber. EN-approach and reality.* Proceedings CIB-W18, Åhus, Sweden 1992.

[20] Gustafsson, P. J. *Fracture Mechanics Studies of Non-yielding Materials Like Concrete: Modelling of Tensile Fracture and Applied Strength Analyses.* Report TVBM-1007. Lund Institute of Technology, Division of Building Materials 1985.

[21] Hernandez, R., Bender, D. A., Richburg, B. A., Kline, K. S. *Probabilistic modeling of glued-laminated timber beams.* Wood and fiber science, Vol. 24(3), pp. 294–306, 1991.

[22] Hibbitt, Karlsson & Sorensen, Inc. *ABAQUS, Version 5.5.* Pawtucket, RI, USA 1995.

[23] Hillerborg, A., Modeer, M. and Petersson, P. E. *Analysis of crack formation and crack growth in concrete by means of fracture mechanics and finite elements.* Cement and concrete research, Vol. 6, pp. 773–782, 1976.

[24] Hoffmeyer, P., Bach, N. *Improvement of the load bearing capacity of glulam beams.* Nordiskt Träsymposium. Helsinki 1976. (In Danish).

[25] Johansson, C-J. *Glued-Laminated beams with Laminated Tension Laminations. Bending Tests on 14 Glued-Laminated Beams.* Chalmers University of Technology. Department of structural engineering. Division of steel and timber structures. Rep. no. Int.skr.S 75:1, 1975. (In Swedish).

[26] Johansson, C-J. *Strength of finger-joints for glued laminated timber.* Teknisk Rapport 1986:09. Borås 1986.(In Swedish).

[27] Johansson, C-J. *Strength of finger-joints for glued laminated timber. Determination of bending strength and tensile strength of finger-jointed laminations from five Swedish manufacturers.* Teknisk Rapport SP-RAPP 1983:10. Borås 1983.(In Swedish).

[28] Johansson, C-J. *Strength and stiffnes of glulam with lamellas of machine stress graded timber.* SP RAPPORT 1990:22. Statens provningsanstalt. Borås 1990. (In Swedish).

[29] Kollman, F. F. P, Côté, W. A. *Principles of wood science and technology. Vol. 1.* Springer Verlag. Berlin 1968.

[30] Larsen, H. J. *Strength of glued laminated beams. Part 5.* ISSN 0105-7421. Report no. 8201. Intituttet for Bygningsteknik. Aalborg 1982.

[31] Milner, H. R., Yeoh, E. *Finite element analysis of glued timber finger joints.* Journal of structural engineering. Vol. 117(3), pp.755–766, 1991.

[32] Petersson, H. *Fracture design criteria for wood in tension and shear.* Proceedings Pacific Timber Engineering Conference, Gold Coast Australia, 1994.

[33] Radovic, B., Rohlfing, H. *Untersuchungen über die Festigkeit von Keilzinkenverbindungen mit unterschiedlichem Verschwächungsgrad.* Forschungsvorhaben I.4-34701, FMPA, Stuttgart 1986.

[34] Selbo, M. L. *Effect of joint geometry on tensile strength of finger joints.* Forest Products Journal Vol. 13(9), pp.390–400, 1963.

[35] Serrano, E. *Calculation of the load bearing capacity of glulam beams.* Report TVSM-7088, Lund University, Division of Structural Mechanics, 1994. (In Swedish).

[36] Serrano, E. *Mechanical behaviour of fingerjoints analysed by fracture mechanics.* COST 508. Proceedings of the 1996 International Conference on Wood Mechanics, Stuttgart, Germany, 1996.

[37] Serrano, E., Gustafsson P. J., Larsen H. J., *Lamination Effect and Finger Joints Analysed by Fracture Mechanics.* Proceedings International Wood Engineering Conference, Vol. 4. New Orleans, USA, 1996.

[38] Serrano, E., Larsen H. J. *Influence of weak zones on stress distribution in glulam beams.* Proceedings CIB-W18/27-12-3. Meeting twenty-seven, Sydney, Australia, 1994.

[39] Solli, K. H. *Depth factor for Norwegian Glulam.* Norsk Treteknisk Institutt, Oslo 1994. (In Norwegian).

[40] Weibull, W. *A statistical theory of the strength of materials.* The Royal Swedish Institute for Engineering Research. Handlingar Nr. 151. Stockholm 1939.

[41] Weibull, W. *The phenomenon of rupture in solids.* The Royal Swedish Institute for Engineering Research. Handlingar Nr. 153. Stockholm 1939.

[42] Wernersson, H. *Fracture characterization of wood adhesive joints.* Report TVSM-1006, Lund University, Division of Structural Mechanics 1994.